Università
degli Studi di
Messina

Department of Chemical, Biological, Pharmaceutical and Environmental Sciences

Ph.D. Course in Applied Biology and Experimental Medicine
Curriculum: Pharmacological Sciences
XXXV CYCLE
S.S.D. CHIM/08

Computational and synthetic approaches for the development of new agents in the management of oncological and neurodegenerative diseases

Ph.D. Thesis of:

Federica Bucolo

Federica Bucolo

Supervisor:

Prof. Rosaria Gitto

Coordinator of Ph.D. course:

Prof. Nunzia Carla Spanò

2021/2022

UNIONE EUROPEA
Fondo Sociale Europeo

Ministero dell'Università e della Ricerca

PON RICERCA E INNOVAZIONE 2014-2020

TABLE OF CONTENT

Abbreviation list

Preface

Abstract

1 Focus on protein-protein interactions and protein aggregation in the development of new therapeutics ... 8

1.1 Mechanism of PPIs modulators ... 11

1.1.1 Type of PPIs modulators ... 13

1.2 Methods for analysis of PPIs and aberrant protein aggregation ... 15

1.2.1 Classification of PPI detection methods ... 15

1.2.2 Analysis of protein aggregation and its inhibition by small molecules ... 17

2 Multi-computational approach to explore MUC1-CIN85 interaction as promising biological target for anticancer therapy ... 19

2.1 MUC1 peptide ... 19

2.1.1 The tumor associated MUC1 ... 21

2.2 CIN85 ... 23

2.2.1 The high-expressed CIN85 in cancer cells ... 27

2.2.2 MUC1-CIN85 interaction ... 27

2.3 Results and discussion ... 28

2.3.1 Peptide docking and MD simulation of CIN85 dimer and MUC1 peptide ... 28

2.3.2 Computational Alanine Scanning of CIN85-MUC1 complex ... 31

2.3.3 Pharmacophore modelling and virtual screening ... 32

2.3.4 Molecular docking of peptide probes and related MD simulations and MM-GBSA Calculations ... 33

2.3.5 Comments and remarks ... 38

2.4 Material and methods ... 38

2.4.1 Protein preparation of CIN85 dimer and MUC1 peptide ... 38

2.4.2 Preparation of ligands ... 39

2.4.3 Receptor Grid Generation of CIN85 dimer and peptide docking ... 39

2.4.4 MD Simulations of CIN85 in Complex with MUC1 and peptide probes and MM-GBSA Calculations ... 39

2.4.5 CIN85 dimer-MUC1 complex residue scanning ... 40

2.4.6 Pharmacophore modelling and virtual screening ... 40

3 Discovery of new α-synuclein inhibitors as potential therapeutics against Parkinson's disease 41

3.1 The role of α-synuclein ... 43

3.1.1 Therapeutic strategies to inhibit α-syn aggregation ... 45

3.2 Result and discussion ... 50

3.2.1 Design and synthesis of a small set of new compounds bearing the pyridinyl-triazole scaffold ... 50
3.2.2 In vivo activity ... 53
3.2.3 Biological screening of derivatives 27-30 ... 56
3.2.4 Ligand-based approach to identify new molecular entities ... 57
3.2.5 In vitro screening of resulting thirty-four compounds ... 61
3.2.6 Computational analysis of the MeSC-4 binding mode ... 63
3.2.7 Design and synthesis of new derivatives of compound MeSC-4 ... 67
3.2.8 Comments and remarks ... 68
3.3 Experimental section ... 69
3.3.1 Chemistry ... 69
3.3.2 General procedure for synthesis of pyridinyl-triazole derivatives (28-32) ... 69
3.3.3 In vivo studies ... 71
3.3.4 General procedure for the synthesis of MeSC-4 derivatives ... 72
3.3.5 Ligand-based virtual screening procedure ... 73
3.3.6 Protein preparation of α-syn fibrils ... 73
3.3.7 Analysis of the potential binding sites ... 74
3.3.8 Molecular docking of MeSC-4 ... 75
3.3.9 Consensus docking and Prime MM-GBSA ... 75
3.3.10 In vitro studies ... 76
4 References ... 77

ABBREVIATION LIST

PPI	Protein-protein interaction	**VNTR**	Variable number of tandem repeats
CAS	Computational alanine scanning	**GalNAc**	N-acetylglucosamine
α-syn	α-synuclein	**STn**	Sialyl-Tn antigen
PD	Parkinson's disease	**ECD**	Extracellular domain
VS	Virtual screening	**TMD**	Transmembrane domain
HTS	High throughput screening	**CT**	Cytoplasmatic tail
BBB	Blood-brain-barrier	**TLR**	Toll-like receptor
NMR	Nuclear magnetic resonance	**TA-MUC1**	Tumor associated MUC1
MD	Molecular dynamics	**EGFR**	Epidermal growth factor receptor
RMSD	Root-mean square deviation	**HMFG1**	Human milk fat globule 1
SBDD	Structure-based drug design	**CIN85**	Cbl-interacting protein of 85 kDa
LBDD	Ligand-based drug design	**SH3**	Src Homology 3
DA	Dopamine	**RTKs**	Tyrosine kinases receptors
MAO-B	Monamino oxidase-B	**APCs**	Antigen-presenting cells
COMT	Catechol-o-methyltransferase	**NK**	Natural killer
TOM20	Outer membrane mitochondrial traslocase receptor	**DMSO**	Dimethylsulfoxide
HCA	Hydroxycinnamic acid	**SEA**	Sea urchin sperm protein enterokinase and agrin
SC-D	SynuClean-D	**MUC1-N**	N-terminal domain MUC1
Th-T	Thioflavin-T	**MUC1-C**	C-terminal domain MUC1
MPTP	1-methyl-4-phenyl-1,2,3,6-tetrahydropyridine	**TH**	Tyrosine hydroxylase
RT	Rotarod test	**DAT**	Dopamine active transporter
PT	Pole test	**MUC1**	Mucin 1

PREFACE

The PhD research project was focused on the identification of new chemical entities capable to interfere with specific proteins or selected protein-protein interactions (PPIs), that constitute valuable targets for development of pharmacological tools for treatment of several human diseases. In particular, Parkinson's disease and cancer progression are closely associated to specific proteins such as α-synuclein and MUC1-CIN85 involved in several physio pathological processes.

The research activity aimed to identify small molecules targeting selected proteins is reported in this thesis paper, which is organized into four chapters as follows

- **Chapter 1** provides the main features of PPIs reported in the literature, thus furnishing an overview about the biological target selected for the PhD research project; here, it is described the mechanism of PPIs modulators as well as the biochemical and computational methods useful to investigate these interactions. Furthermore, a focus on protein aggregation analysis techniques is also included.
- The first section of **Chapter 2** reviews the PPI named MUC1-CIN85, that is involved in the formation of tumor metastases, as an innovative target for new anti-tumor agents. In particular, the two partner proteins and their structural features, activity and role in tumor cell invasiveness were introduced. Then, the **Chapter 2** reports our investigation by applying different computational approaches to deeply investigate the MUC1/CIN85 interaction. This PhD research activity was carried out during the internship at the italian pharmaceutical company Sterling SPA in collaboration with the RiMED Foundation (Palermo, Italy); in details the research activity was carried out under the supervision of Dr. Ugo Perricone; these computational studies were also developed during the abroad period at the Pharmaceutical Chemistry Department of the University of Vienna under the supervision of Prof. Thierry Langer.
- Given the role of the neuronal protein α-synuclein (α-syn) in Parkinson disease, the **Chapter 3** focuses on the identification of novel α-syn aggregation inhibitors as potential therapeutics for the treatment of this neurodegenerative disorder. An overview of the role of α-syn in the pathogenesis of PD and the growing interest in modulating its amyloidogenic aggregation to halt the neurodegenerative process was presented. Subsequently, there were described our research efforts in designing and synthesizing of a small set of α-syn aggregation inhibitors starting from a ligand-based pharmacophore model. The synthesized compounds were subjected to an *in vitro* biochemical screening in

collaboration with Prof. Salvador Ventura (Institute of Biotechnology and Biomedicine, University of Barcelona), whereas the *in vivo* studies were performed by the research group of Prof. Rosanna di Paola (University of Messina). In the same chapter, a ligand-based approach for the identification of new chemical entities was reported. The virtual screening procedure selected several small molecules, that were purchased and subjected to an *in vitro* biochemical screening in collaboration with Prof. Salvador Ventura. The binding mode of the best active compound was investigated through molecular docking studies performed in collaboration with Prof. Laura De Luca (University of Messina).

ABSTRACT

Given the crucial role of several proteins in regulating pathophysiological processes, the research work carried out during the PhD was focused on the canonical MUC1/CIN85 protein-protein interaction as well as on the aberrant aggregation of the neuronal protein α-synuclein. The above-mentioned targets might offer valuable tools for the developments of pharmacological treatments in cancer progression and neurological disorders.

Moved by the purpose to identify new targets of pharmaceutical interest in cancer therapy, we focused our attention on the MUC1-CIN85 complex as a PPI implicated in the control of cancer progression and metastasis. For this reason, it was useful to start from the study of molecular contacts of MUC1 at CIN85 binding interface though a multi-computational approach, thus revealing new structural information relevant for the design of MUC1-CIN85 PPI inhibitors as potential anti-metastatic agents.

In parallel, we investigated the role of amyloid aggregation of misfolded α-synuclein in the pathogenesis of Parkinson's disease (PD). To date, inhibition of α-syn aggregation by small molecules has emerged as promising approach to block PD progression, thus providing new opportunities for drug discovery. Starting from previously identified α-syn aggregation inhibitors containing the chemotype 5-(4-pyridinyl)-1,2,4-triazole were optimized in terms of their *in vivo* efficacy. Our studies resulted in the identification of the ethyl 2-((4-amino-5-(pyridin-4-yl)-4H-1,2,4-triazol-3-yl)thio)acetate, that showed the ability to prevent MPTP-induced bradykinesia and to influence PD marker levels after administration of the same neurotoxin. In addition, we evaluated the prevention of the fibrillation process using light scattering and a Th-T binding assay; these compounds demonstrated a slight reduction in α-syn aggregation. To expand our knowledge about the chemical structural requirements exerting a blockade in the formation pf α-syn aggregates, we used the structures of two active α-syn inhibitors, SynuClean-D and ZPD-2, as query compounds for a ligand-based virtual screening (LBVS) on commercially available compound libraries using SwissSimilarity web-based tool. The selected compounds were analyzed in the Th-T fluorescence assay. Among them, the best active compound MeSC-4 displayed a similar inhibition profile compared to SynuClean-D and was used as a prototype for novel α-syn aggregation inhibitors. In addition, molecular modelling studies were performed to investigate the binding mode of MESC-4 through a consensus docking methodology.

Keywords: Protein-Protein interactions; α-synuclein; MUC1-CIN85; computer aided drug discovery; Parkinson's disease; cancer

CHAPTER 1

1 Focus on protein-protein interactions and protein aggregation in the development of new therapeutics

In the last decades, both physio-pathological protein-protein interactions and aberrant protein aggregation have earned an increasing interest in Medicinal Chemistry due to their role in modulating a huge number of cellular process.[1]

Several proteins undergo misfolding and failures in post-translational modifications that lead to the establishment of incorrect interactions and intramolecular aggregations. These events are massively implicated in various diseases including cancer, neurodegenerative diseases, inflammation, viral and bacterial infections.[2,3] The physical contacts involved in these dysfunctional events include specific and non-specific interactions: hydrogen bonding, van der Waals interactions and steric interactions, which have been hypothesised to play minor roles whereas electrostatic and hydrophobic interactions which possess an important role.[4] Under physiological conditions protein interactions and aggregations can occur in the modulation of many cellular processes, such as cell growth, DNA replication, transcriptional activation, translation, and signal transduction.[5]

It is well known that protein-protein interactions (PPIs) are often dysregulated in pathological conditions, thus offering a novel opportunity for the search for new drug therapies.[6] It has been estimated that there are 130000-650000 PPIs in the human organism, but only a small portion of these (~2%) had been considered as drug target.[7] The modulation of PPIs by molecules presents numerous challenges since the contact surfaces involved in PPIs are larger (1500-3000 Å2) than those of traditional molecular targets (300-500 Å2).[8] Moreover, these surfaces are usually flat and with a few druggable pockets accommodating small molecules. Therefore, compared with other targets such as enzymes and cell-surface receptors, PPIs do not possess physiological ligands that could be used as a starting point for the design of new substrates.[9] Another disadvantage of PPIs is related to their low druggability because some of them occur through phosphorylation. As a result, designing a small molecule that mimics the charged residue of a phosphorylated site is not an amenable strategy because it would display poor bioavailability.[10] Looking at all the above-mentioned aspects, PPIs have been treated as "undruggable" targets for decades.[1] Despite this, small-molecule modulators of PPIs were approved for clinical use in the 1990s, and the interest in

the development of new modulators of PPIs has been growing over the years (As shown in Figure 1).[8]

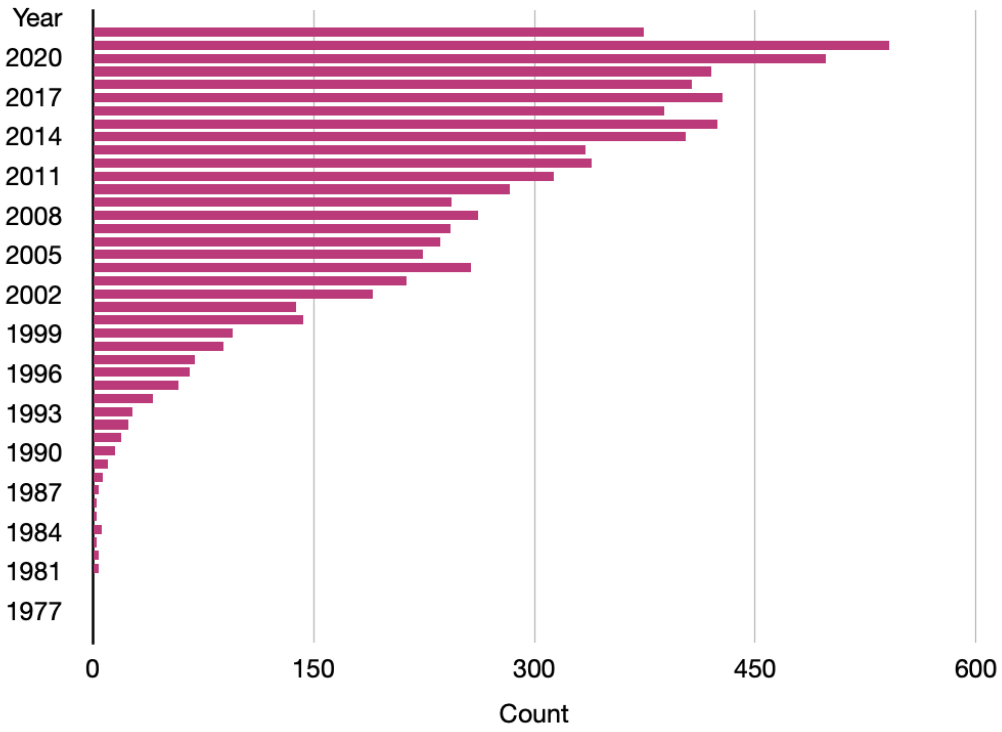

Figure 1. Graphical representation of published papers on PPI inhibitors over the past 20 years according to PubMed (https://pubmed.ncbi.nlm.nih.gov/).

Over the years, studies conducted on PPIs have led to some observations regarding the characteristics of the interface between the two protein partners. Despite the large binding surface area, mutational studies have shown that only one group of residues implicated in the interaction is responsible for the largest part of free energy of binding. These residues have been termed "hotspots" and account the best targets for small molecules.[11] An amino acid residue is generally named ‘hotspot’ if when its mutation to alanine, through scanning alanine mutagenesis, leads to an increase in Gibbs free energy higher than 2 kcal/mol. Therefore, a small molecule capable of interacting with hotspot residues could exert a blockade in the interaction between the two protein partners (Figure 2).[12]

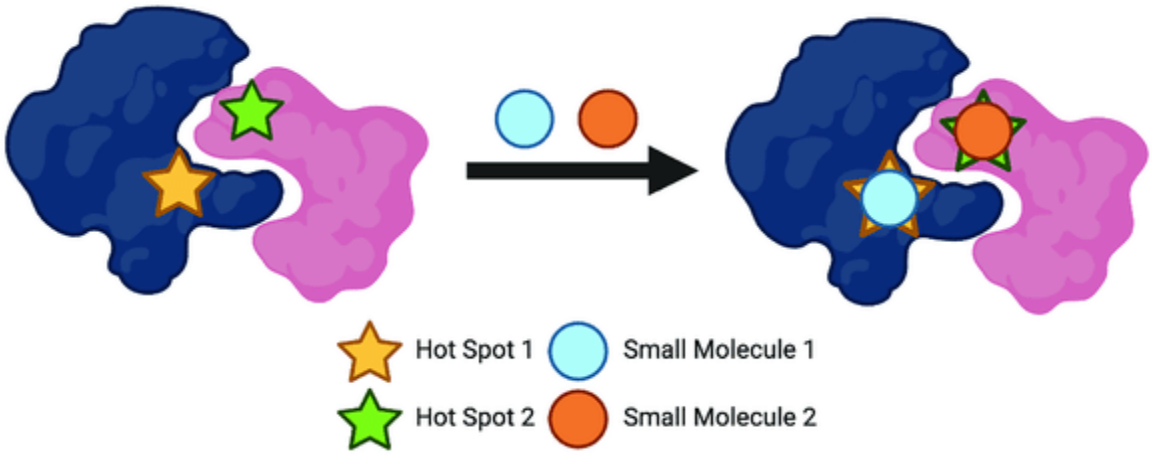

Figure 2. Representation of 'hotspots' used to target protein-protein interactions (PPIs). Image created with BioRender.com

The hotspot region is generally composed of a rim region, which is highly accessible and a core region, which is deeper. The rim is characterized by an aminoacidic composition similar to the rest of the protein surface whereas the core possesses aromatic residues.[13] The most frequently hotspot amino acids found in PPIs are Trp, Tyr and Arg. In particular, Tyr and Trp are involved in stacking and hydrophobic interactions with their aromatic side chain, moreover they could generate hydrogen bonds through the hydroxyl group and indole nitrogen atom. In contrast, the amino acid Arg, which is polar, can establish hydrogen bonds and salt bridges.[11] The amino acid composition of hotspots reveals that PPIs are mainly constitute by hydrophobic interactions, whereas hydrogen bonds and electrostatic interactions play a pivotal role.[5] Several studies revealed that hotspot residues are conserved and clustered in non-homogeneous regions on the surface.[14,15] The relevance of 'hotspots' has led to the development of computational tools for their prediction and the development of new drugs. For example, the ROBETTA server allows hotspot prediction through computational alanine scanning of PPIs.[16]

PPIs can generate obligate or nonobligate complexes. In details, obligate PPIs complexes are not stable on their own, whereas in the case of nonobligate PPIs, protein partners can exist in bound or dissociated form under various conditions.[11,17] Obligated associations are generally narrower, larger and more hydrophobic than nonobligated interactions, which are characterized by a more polar/charged interactions.[18] Moreover, PPIs can be classified into transient or permanent according on their half-life.[12] Indeed, in the first case the two partner proteins are associated and dissociated *in vivo*, whereas in the latter case the interactions are very stable, and the subunits generally exist in their complexed form.[19] The stability of a PPI is strongly dependent on

physiological conditions, shifts in protein expression and localization, or on the presence of molecules like GTP.[17] Furthermore, an interaction may be primarily transient *in vivo*, but become permanent under specific cellular conditions. Selecting a permanent PPI as a biological target is very difficult due to the matter that the successful approach to hinder this kind of interaction is to develop molecules capable to interfere during protein synthesis and the folding process.[12] Despite the above-mentioned obstacles that present PPIs as a challenging goal, progresses in structural biology, mutational studies, biophysical methods, and new computational techniques, as well as the development of high-throughput screening (HTS) methods for PPI inhibitors, have led to positive results with the identification of PPI modulators approved or included in clinical trials.

1.1 Mechanism of PPIs modulators

Inhibitors of PPIs can act by disrupting or stabilizing the binding between protein partners. The binding disruptors operate by blocking the interaction, while the stabilizers bind to the protein-protein complex, forming a ternary structure that represents an inactive conformation.[20,21] These two classes of PPI modulators can be also divided into orthosteric and allosteric inhibitors (Figure 3). In more details, orthosteric inhibitors link to PPI interfaces in a competitive manner. Allosteric inhibitors, on the other hand, interact with distinct sites to respect to the protein interface; inducing the target protein conformational changing that hinder the formation of the PPI.[22]

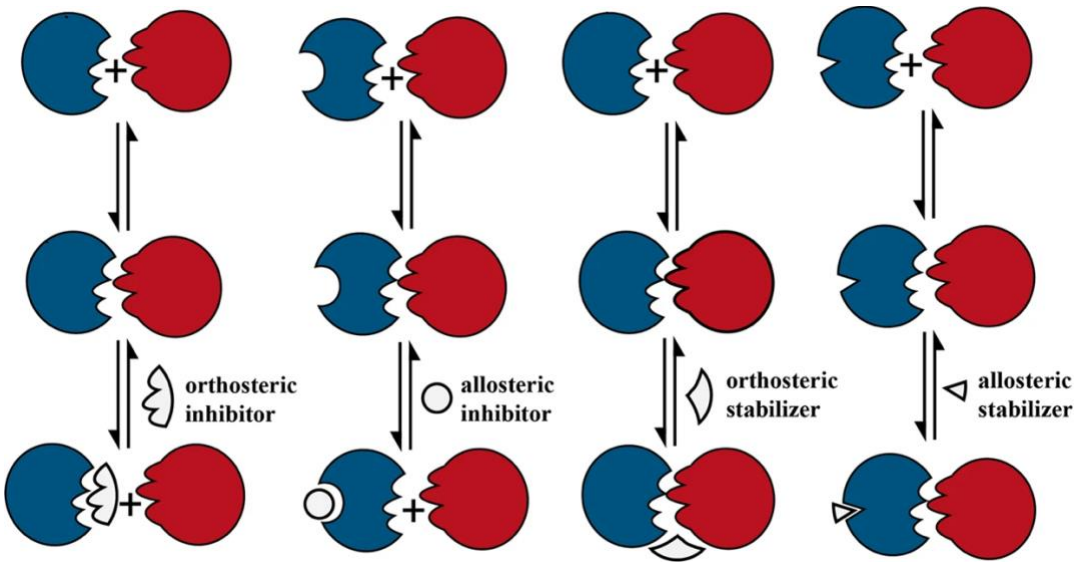

Figure 3. Orthosteric and allosteric mechanism of action of PPIs modulators. Image retrieved from Lu et al. 2020.

Most PPI modulators reported in the literature, belong to the class of orthosteric disruptors.[23]A successful example of this class of PPI inhibitors is ABT-199 (Venetoclax, **1**), approved by the FDA in 2016 for the treatment of chronic lymphatic leukaemia.[24,25] This small molecule binds the anti-apoptotic protein Bcl2, thus avoiding its interaction with its pro-apoptotic partner protein, facilitating tumor cell apoptosis. Allosteric inhibitors targeting PPIs possess several advantages, such as higher receptor subtype selectivity and a saturable effect. Amongst the allosteric modulators, BIO8898 (**2**), the synthetic small molecule fills an allosteric site of CD40L by blocking its binding to CD40 and thus inhibiting CD40L-dependent cell apoptosis *in vitro* assays. In fact, CD40 and CD40L are a complementary protein pair and belong to the tumor necrosis factor receptor superfamily. Moreover, CD40 and CD40L are largely expressed in T and B cells and blocking this interaction may has huge potential to treat the associated diseases (Figure 4).[26] In this case, the biggest challenge with this class of inhibitors is linked to the identification of suitable allosteric sites. To this end, various approaches have been used, such as HTS followed by crystallography, phage display always combined with crystallography and the study of interactions through different computational methods.[27]

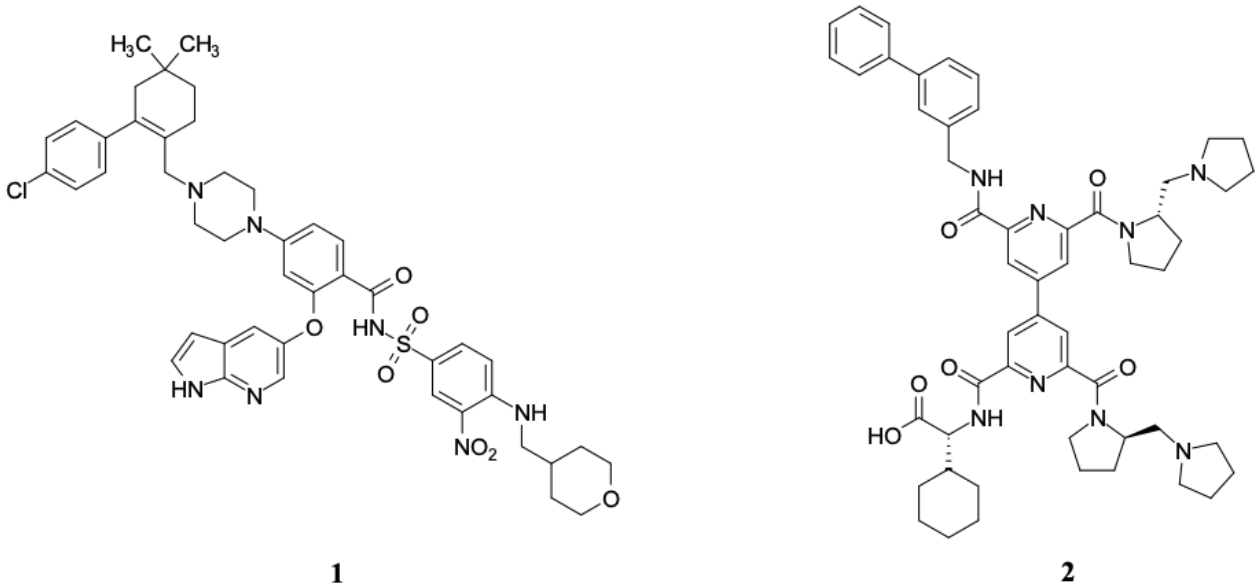

Figure 4. Structure of the orthosteric inhibitor ABT-199 (**1**) and allosteric inhibitor BIO8898 (**2**).

Furthermore, orthosteric and allosteric inhibitors display different pharmacological features; in general, allosteric modulators are more hydrophobic as they must bind allosteric sites that have a more hydrophobic character than the PPI interface, moreover, they possess a lower molecular weight and a structural rigidity. When the protein interfaces are small and possess simple conformations, the development of orthosteric modulators might be a useful strategy, whereas in the case of PPIs characterized by a large interface and more complex conformations, it is better to design small molecules as allosteric ligands.[23]

1.1.1 Type of PPIs modulators

PPIs modulators include various chemical species such as monoclonal antibodies, peptides and peptidomimetics, and small molecules. Monoclonal antibodies are usually competitive inhibitors binding an orthosteric site of the protein. The advantages of developing monoclonal antibodies for PPI modulation is related to their selectivity and affinity for the target.[3] Notwithstanding their higher specificity compared to traditional drugs, antibodies have different limitations, such as high production cost, and low oral bioavailability.[5] Peptides and peptidomimetics constitute another large group of substances studied as potential modulators of PPIs. Generally, peptides are designed based on amino acid residues present at the PPI interface, to mimic the natural interactions with the protein partner.[8] Some of these peptides have been designed as molecular probes with the purpose of studying PPIs or identifying and validating newer potential drug targets. From a pharmacological perspective, peptides also possess weak cell permeability and limited stability *in vivo*, being susceptible to the action of proteases.[28] To further optimize the pharmacokinetic properties of peptides, several chemical strategies have been applied, such as backbone modification, substitution of amino acids with non-standard residues and macrocyclization. In addition, macrocyclization restricts the peptide in its binding conformation, increasing proteolytic stability and enhancing cell permeability.[29] Regarding cyclization methods, the use of peptides with a hydrocarbon skeleton has emerged for the design of PPI inhibitors. Considering that helical motifs are common at most protein-protein interfaces, with this approach, it is possible to stabilize the α-helical secondary structure of a peptide by introducing an olefinic side chain at the α-carbon of a non-natural amino acid.[30] Hydrocarbon-stabilized peptides have demonstrated to be more stable and to have an improved membrane permeability.[31,32] This strategy has been successfully used in the development of PPI inhibitors for therapeutical applications.[33]

An exciting result was the identification of the double-selective peptide ALRN-6924 that block p53-Mdm2/Mdm4 interactions; it is currently being clinically evaluated for the treatment of hematology and solid tumors.[34]

Finally, PPI inhibitors include also small molecules. The development of PPI inhibitors with low molecular weight entities has been considered for years a difficult objective due to the large and flat protein-protein interface. However, if the hotspot residues that are usually concentrated in the middle of the binding interface and cover an area of 250-900 Å are considered, the interaction with a small molecule becomes possible.[9] In addition, proteins are dynamic systems with several conformational changes that could result in the formation of cavities or pockets capable of accommodating a small ligand. Different approaches such as nuclear magnetic resonance (NMR) and molecular dynamics (MD) simulation are useful to study protein structures in solution and their dynamic behavior.[11] As an example, a computational protocol was reported to identify transient pockets on the surface of three systems: BCL-XL, MDM2 and IL-2 in their apo-conformations. Since the native inhibitor binding site was not displayed in the unbound state, these crystal structures were subjected to MD simulation. Indeed, it was seen that the transient pockets opened up within 2.5 ps, and pockets with similar dimensions to those of known inhibitors were also revealed on the native binding site.[35] Small molecules possess many advantages, such as metabolic stability, low production cost, high bioavailability, and cell permeability.[8] Small molecules may be able to modulate PPI interactions by competing with the protein partner, either by occupying an allosteric site or by stabilizing the interaction mechanism.[21] An emerging procedure to inhibit PPIs has produced high-affinity inhibitors. This approach implicated that small molecules are resulting from the covalent modification of a nucleophilic residue, such as cysteine, methionine and lysine situated near the interface. Furthermore, inhibitors that covalently bind non-conserved residues exhibited a better selectivity than other similar members of the same protein family.[36] Small molecule modulators of PPIs have been identified by HTS of synthetic and natural compound libraries or by using *in silico* methods. They are generally distinguished by a higher molecular weight (>400 Da) and a stronger hydrophobicity than typical drugs, owing to the large and hydrophobic protein-protein interface.[37] Although some of them do not conform to Lipinski's rule of five, they have demonstrated good oral bioavailability. Of course, these small modulators of PPIs displayed more complex structures than the traditional compounds used as drugs. These considerations have pointed out the necessity to build databases of PPI modulators for screening characterized by greater complexity and chemical diversity than those used for traditional drug design. In this perspective, natural products offer an abundant resource of different chemotypes that constitute a good starting point for the construction, through chemical

modifications, of compound libraries for the identification of novel PPI modulators.[38] Although barriers to targeting PPIs with small molecules have been hurdled, several successful modulators have been developed, culminating with FDA approved small molecules for the treatment of cancer, dry eye syndrome, autoimmune diseases, and as immune suppressing agents.[39,40]

1.2 Methods for analysis of PPIs and aberrant protein aggregation

1.2.1 Classification of PPI detection methods

As seen above, PPIs are becoming a prominent topic for the discovery of new pharmacological targets and development of new therapeutic agents. Non-covalent contacts between the sidechains of protein amino acid residues are responsible for the possible misfolding, their assembly and the establishment of new PPIs. Several studies reported in the literature have revealed that proteins involved in the same cellular pathway are repeatedly found interacting with each other. Consequently, the role of PPIs is also important for deducing the function of proteins within the cell. Indeed, the functions of unidentified proteins can be predicted based on their interaction with another protein whose function is known. The detailed study of PPIs has brought additional knowledge about the molecular mechanisms of cellular processes.[41]

Methodologies for studying these interactions are divided into two broad categories: 1) *in vitro* or *in vivo* biochemical studies; 2) *in silico* methods. Biochemical assays for investigating protein interactions include affinity chromatography, co-immunoprecipitation, protein fragment complementation, phage display, X-ray crystallography, nuclear magnetic resonance (NMR) spectroscopy. *In silico* approaches include structure-based approaches, molecular dynamics simulations (MD) and mutagenesis studies such as computational alanine scanning (CAS), detailed below. The diagrammatic classification is shown in Table 1.

Approach	Method	Summary
Biochemical studies	Affinity chromatography	Highly responsive, able to detect weakest interactions in proteins
	Co-immunoprecipitation	Confirms interactions using a whole cell extract where proteins are present in their native form in a complex mixture of cellular components
	Protein fragment complementation (PCAs)	Used to detect PPIs between proteins of any molecular weight and expressed at their endogenous levels
	Phage display	Incorporation of the protein and genetic components into a single phage particle
	X-ray crystallography	Visualization of protein structures at the atomic level for the understanding of protein interaction and function
	NMR spectroscopy	Able to detect weak protein-protein interactions
Computational studies	Sequence-based approaches	Identification of PPI binding sites by employing information derived from conservation or sequence similarity of homologous proteins.
	Structure-based approaches	Predict protein-protein interaction if two proteins have a similar structure (primary, secondary, or tertiary)
	Molecular dynamics simulations	Characterization of binding site otherwise not detectable from the crystal structure
	Mutagenesis studies	Identification of hotspot residues through computational alanine scanning

Table 1. Summary of PPIs detection methods

- ***Structure-based methods***

Structure-based methods use the 3D structural coordinates of the target to identify potential ligand binding sites. The main limitation of this approach is that it requires the 3D structure of the protein. Structure-based procedures can be further classified into three types: geometry-based, energy-based, and pattern-based. Geometry-based approaches use geometric parameters, such as surface area, to identify cavities on the protein. Energy-based methods search for energetically favorable hotspots on the structure. Finally, model-based methods predict the putative binding site of the ligand from known protein models, based on the assumption that structurally similar proteins share similar activity. These approaches also include structure-based pharmacophore model, allowing to discover the necessary steric and electronic properties for molecular recognition in the ligand-receptor complex. Through the experimental structure of the complex, atomic coordinates and interactions with the ligand can be exploited to find so-called pharmacophoric features and to obtain information on the shape of the binding site.[42]

- ***Molecular dynamics simulation (MD)***

The process of ligand binding to a target macromolecule is dynamic, involving conformational changes in the protein structure. This overcomes the initial model of the 'lock and key' theory where a rigid receptor can accommodate a small molecule without undergoing any structural modification.[43] The molecular dynamic simulation (MD) is a computational method applied to calculate the time-dependent motion of molecules when interacting with a target. In fact, during MD simulation, consecutive configurations of the evolving system are generated, resulting in trajectories in which the positions and velocities of the particles are specified over time.[44]

- ***Computational alanine scanning (CAS)***

Computational alanine scanning (CAS) can be applied to a huge variety of protein complexes to understand their structural and energetic characteristics. This mutagenesis procedure consists of *in silico* site-directed mutation of a specific residue used to determine its contribution to the stability or function of the protein. Alanine is used for its methyl functional group, which is non-binding and chemically inert. The contribution of the single amino acid is calculated as the difference in free binding energy between wildtype and ALA mutant proteins for the formation of a protein-protein complex.[45]

1.2.2 Analysis of protein aggregation and its inhibition by small molecules

Pathological aggregation of proteins and peptides is a key event in several chronic and devastating neurodegenerative conditions. Analytical methods for investigating protein aggregation are important for mapping physio-pathological events and for the development of new therapies and better diagnostic tools. The assembly of aggregates occurs as a result of intermolecular interactions between proteins.[46] This aggregation can be regarded as non-canonical PPI which can also be analyzed using computational and biochemical methods. Furthermore, several mechanisms have been reported in literature whereby aberrant and misfolded forms of proteins, which generally undergoes aggregation, can interact directly with different protein partners thus generating new PPIs.[47]

Common methods used to study the formation and structural features of protein aggregates are classified according to their assembly state. Among these methods are NMR spectroscopy and X-ray crystallography techniques that are also used to resolve protein structure at the atomic level for conventional PPIs.[48] However, most methods used to explore protein aggregation characterize the

secondary structure. In fact, fibrils formed by protein aggregates, although have a different structure and appearance, are rich in β-sheets and are suitable for high-throughput screening assays offering the opportunity to identify, small aggregation-inhibiting molecules acting on these phases. A widely used approach is the dye Thioflavin T (ThT) which verifies the presence of fibrils as well as the examination fibrillation kinetics *in situ.* Moreover, protein aggregates can also be detected by light scattering, which simply monitors the increase in size of a protein when it undergoes aggregation and then fibrillation.[49] In detail, these two techniques are used for the evaluation of misfolded protein aggregates known as amyloid plaques, a characteristic feature of neurodegenerative diseases, both *in vitro* and *in vivo*.

- ***Thioflavin T fluorescence assay***

Thioflavin-T (ThT) is a benzothiazole salt obtained by methylation of dehydrothioluidine with methanol in the presence of hydrochloric acid. The dye is used to visualize and quantify the presence of misfolded protein aggregates called amyloids. When it binds to β-sheet-rich structures, it produces an increased fluorescence and a characteristic red shift in its emission spectrum.[50] Before binding to an amyloid fibril, ThT emits weakly around 427 nm. When excited, it emits a strong fluorescence signal at around 482 nm upon binding to amyloids. The benzylamine and benzothiazole rings are connected by a carbon-carbon bond. These two rings can freely rotate when the molecule is in solution. However, when it binds to amyloid fibrils, the rotation planes of the two rings become immobilized and thus the molecule can maintain its excited state.[51]

- ***Light scattering measurement***

Light scattering measurement concerns the study of the interaction between light and matter. Due to this interaction, light striking a set of particles (molecules, atom etc.) is partially 'deflected' in different directions than the incident light. In this process of scattering, in addition to the change in direction, there is also a change in frequency. The evaluation of scattered light in relation to intensity and wavelength often provides valuable information about the studied substance. Protein aggregation causes increased light scattering, while a reduction is observed in the presence of a ligand that blocks aggregation.[52]

CHAPTER 2

2 Multi-computational approach to explore MUC1-CIN85 interaction as promising biological target for anticancer therapy

The design of PPI modulators is a difficult challenge due to the structure of protein interface that lack well-defined binding sites for small molecules. However, it is possible to observe the opening of transient ligand binding sites by means of the dynamic nature of these interfaces, offering new opportunities for drug discovery. In this scenario, my research conducted on the modulation of the MUC1-CIN85 PPI is placed. As discussed below, this complex plays a key role in tumor invasion and metastasis formation and constitutes a valuable target for the development of novel agents to be used in cancer therapy.

2.1 MUC1 peptide

MUC1 is a transmembrane glycoprotein (molecular weight 300 to 600 kDA), it is physiologically expressed on the apical surface of epithelial cells of a wide range of tissue, including mammary gland, lung, stomach, esophagus, duodenum, pancreas, uterus, prostate, and hematopoietic cells, involved in both signal transduction and the formation of a protective barrier.[53] The MUC1 gene codifies for a single polypeptide chain which, after translation, is autoproteolytically cleaved at the GVSVV motif located in the SEA domain (sea urchin sperm protein enterokinase and agrin) thus generating the N-terminal domain (MUC1-N) and the C-terminal domain (MUC1-C) linked by stable H-bonds (Figure 5).[54]

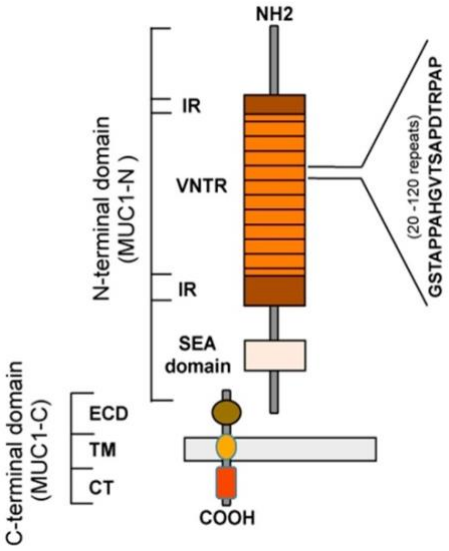

Figure 5. Schematic illustration of the N-terminal and C-terminal subunits of MUC1. The N-terminal domain comprises a variable tandem repeat number region (VNTR) that is largely glycosylated under physiological conditions. The C-terminal domain contains an extracellular domain, a transmembrane domain, and a cytoplasmic tail. The two subunits, N- and C-terminal, are connected by non-covalent interactions to the SEA domain.[54]

From a structural point of view, the N-domain is located on the membrane surface and is characterized by a variable number of tandem repeat regions (VNTRs), composed of a 20 amino acid sequence (PDTRPAPGSTAPPAHGVTSA) and being rich in proline, threonine, and serine residues.[55] These residues provide glycosylation sites which are highly glycosylated under physiological conditions, through O-glycosylation and N-glycosylation. O-glycosylation happens at hydroxylic residues Thr and Ser present in VNTRs and plays a pivotal role in the biological activity of MUC1. Indeed, the hyperglycosylation on the branches led to an oligomerization, that form a mucinous gel for the protection of epithelia from pathological agents, pH changes and dehydration. O-glycosylation occurs upon the addition of N-acetylglucosamine (GalNAc) to residues Thr and Ser by GalNAc transferases, which results in the formation of GalNAcαSer/Thr structures also known as Tn antigens. Thereafter, the GalNAc residues are subjected to further modifications carried out by different glycosyltransferases leading to the construction of different glycan substructure such as i) core 1 consisting of the addition of galactose (T or TF antigen), ii) glycan core 3 formed by the addition of GlcNAcβ1-3GalNAcα and iii) the Sialyl-Tn (STn) antigen obtained with the addition of sialic acid. Glycosylation proceeds by extension and chain termination occurs through the addition of carbohydrates such as sialic acid. N-glycosylation, on the other hand, happens at the level of Asn residues located in the degenerate sequence and is essential for folding, sorting, apical expression, and secretion of MUC1. The glycosylation process

thus protects the peptide structure from cleavage by proteolytic enzymes and clathrin-mediated endocytosis.[53] In contrast, the MUC1-C subunit is composed of an *extracellular domain* (ECD) with 58 amino acids, a *transmembrane domain* (TMD) containing 28 amino acids, and a *cytoplasmic tail* (CT) of 72 amino acids. This latter region contains seven Tyr residues, including 4 residues that can be phosphorylated by kinases, promoting signal transduction cascades.[56] Among the physiological functions of MUC1, the main relevant are lubrication and hydration of the cell surface and protection from microorganisms and proteolytic enzymes. [55]In addition, MUC1 plays an important role in the regulation of inflammatory responses by its CT domain. It has been reported that the CT domain acts as a negative modulator of Toll-like receptor (TLR) signaling. TLRs are receptors implicated in the response of the innate immune system, as they are responsible for the early recognition of pathogens, which then triggers the host's defensive responses. For example, infections caused by pathogens such as *P. aeruginosa* and respiratory syncytial virus generally result in the activation of TLRs, triggering the production of inflammatory mediators. Subsequently, upregulation of MUC1 follows and TLR signaling is inhibited in order to reduce inflammation. Furthermore, MUC1 is implicated in the regulation of the NLRP3 inflammasome complex, whose activation provokes the production of inflammatory cytokines and subsequently the recruitment of effector cells. Induction of the inflammasome complex requires activation of TLRs and the NF-kB pathway leading to upregulation of pro-IL-1β, pro-IL-18, pro-caspase-1 and inflammasome components. Consequently, MUC1 works as an inhibitor of the inflammasome pathway, decreasing the activation of TLRs and blocking the upregulation of inflammasome components. Recently, it was discovered that the expression of MUC1 during *Helicobacter pylori* infection in mice and *in vitro* suppresses the production of gastric IL-1 β and, as a result, it was observed a reduction of *H. pylori*-induced inflammation.[56]

2.1.1 The tumor associated MUC1

Tumor associated MUC1 (TA-MUC1) displays different biochemical features and cellular distribution than the protein under physiological conditions. In tumors, MUC1 is overexpressed and is found both on the surface and in the cytoplasm of epithelial cells, as they lose their cellular polarity.[57] In addition, the VNTRs of TA-MUC1 are hypo-glycosylated with truncated long-branched glycans that are often capped by sialic acid following the overexpression of α2,6- and α2,3-sialyl transferases; the above-mentioned transferases are responsible for the premature termination of the chain elongation process.[58] Several studies have shown that TA-MUC1 plays a

key role in the transcription of genes associated with tumor invasion, angiogenesis, cell proliferation, apoptosis, inflammation and drug resistance. In fact, the CT domain binds to the epidermal growth factor receptor (EGFR) and translocases into the nucleus initiating a cascade of signals that stimulate cell proliferation. In preclinical models, TA-MUC1 enhances metastasis formation by disrupting normal cell-cell and cell-matrix adhesion and activating cell-endothelium adhesion. In this regard, TA-MUC1 has been demonstrated to interact with the cell adhesion molecules such as ICAM-1 and E-selectin, promoting cell migration and vascular invasion.[53] Overexpression of TA-MUC1 has been related to a poor prognosis in colon, pancreatic, bladder and breast cancer.[59,60] Consequently, TA-MUC1 represents an attractive target for antitumor therapy owing to its expression on the surface of cancer cells. In particular, truncated glycans located in the VNTR act as antigens and can be recognized by antibodies, thus becoming an interesting immunotherapeutic-based strategy for cancer treatment. Various antibodies targeting different domains of MUC1 have been designed and some of them are the subject of clinical studies.[53,61] One of the antibodies studied is human milk fat globule 1 (HMFG1) which is a murine IgG1 antibody with light chain k that recognizes the PDTR epitope present in the VNTR of the extracellular domain of MUC1.[61] The radiolabeled form of HMFG1 with ^{90}Y was developed for the treatment of ovarian cancer. The humanized version of this antibody, AS1402, exhibited a good tolerability and safety profile in the Phase I study. In the Phase II study, it was co-tested with endocrine therapy; however, this co-treatment did not lead to positive results, despite observing no safety problems.[62] Among the antibodies we also mention TAB004 which is a humanized IgG1 mAB that has detected the STPPVHNV sequence located in the VNTR region of TA-MUC1. This immunoglobulin has been shown to be effective in targeting pancreatic cancer cells, but not normal cells. In addition, TAB004 has been shown to stop the anti-apoptotic activity of MUC1 and increase the antitumor effect of chemotherapeutic drugs.[63,64] Another anti-MUC1 monoclonal antibody is MUC1-014E, which targets a 19 amino acid intracellular sequence (RYVPPSSTDRSPYEKVSAG) of the MUC1-CT domain. This monoclonal antibody has been shown to detect isolated tumor cells of the signet-ring cell carcinoma and the non-solid type poorly differentiated gastric adenocarcinoma, suggesting that this antibody can be utilized for the detection of these cells, which are frequently present in a type of gastric cancer called gastric scirrhosis.[65] Moreover, monoclonal antibodies that interact with glycopeptide epitopes of TA-MUC1 have been reported, such as PankoMab. This is a murine IgG1 antibody, which targets the glycopeptide TA-MUC1. It showed high *antibody-dependent cellular cytotoxicity* (ADCC) activity and rapid internalization, thus emerging as a potential anti-cancer agent. Several chimeric and humanized forms of PankoMab have also been designed and are under clinical trials as

potential therapeutic and diagnostic tools.[66,67] Several cancer diseases can be induced by microbial infections; microbes interact with the host through glycosylated mucin proteins, inducing its alteration by glycosylation, and it has been seen that a prolonged period of interaction with the microbe can alter the glycosylation of MUC1 resulting in a rupture of epithelial barrier, then switches from anti to pro-inflammatory (Figure 6).[68]

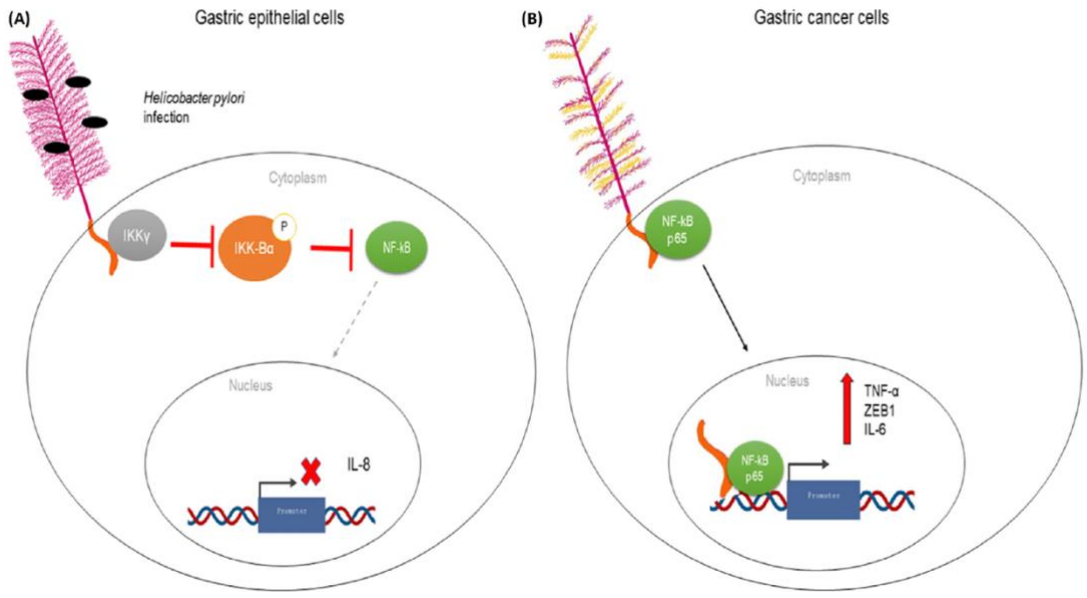

Figure 6. Schematic representation of pro-inflammatory role of MUC1. (A) During Helicobacter pylori infection, the cytoplasmic tail of MUC1 (orange) in gastric epithelial cells activates NF-kB (green) and suppresses proinflammatory signals. (B) In gastric cancer cells, the p65 subunit of NF-kB binds (green) to MUC1-CT (orange) and the complex localizes in the nucleus increasing the expression of proinflammatory cytokines. The MUC1 extracellular domain (MUC1-ED) in normal cells is hyperglycosylated (pink branches), but in cancer cells it is aberrantly glycosylated (yellow) and loses some residues. Image retrieved from Bose et al. 2020.

2.2 CIN85

CIN85 is the Cbl-interacting protein of 85 kDa and consists in a multifunctional adaptor protein involved in several biological functions. Adaptor protein is defined as non-catalytic peptides with one or more structural domain capable to bind other proteins or peptide thus generating multimeric complexes involved in signal transduction processes.[69] CIN85 is structurally constituted in the N-terminal portion of 3 Src Homology 3 (SH3), usually called SH3A, SH3B and SH3C, a central proline-rich region and a C-terminal coiled-coil (Cc) domain (Figure 7).

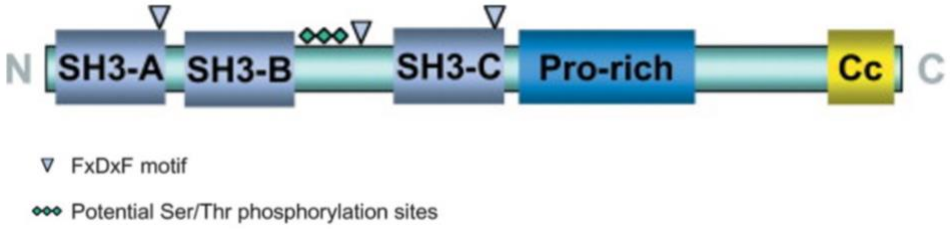

Figure 7. Schematic representation of CIN85 structure

The three SH3 domains bear a high similarity to each other compared to any other SH3 domain and establish their PPI by interacting with proline rich motifs. In addition, there is a region rich in Ser and Thr residues between the second and third SH3 domains that could be susceptible to phosphorylation. On the other hand, in the N-terminal domain, there are three FXDXF sequences that could provide a binding site for the AP2 adaptor protein of clathrin. As above-mentioned, the central Pro-rich region acts as a potential binding site for the other SH3 domains and is situated near the third SH3 domain. Finally, the C-terminal domain possesses a high propensity to produce coiled-coil structures that are implicated in the oligomerization of CIN85 leading to the formation of CIN85-associated multiprotein complexes.[70] These domains consist of approximately 60 amino acids, comprise of five β-strands arranged in two antiparallel β-sheets connected by three loops called RT, distal and n-Src and a short 3_{10} helix.[71] SH3 domains are well-known for binding proline-rich sequences containing the consensus motif PXXP, where X can be any amino acid. Due to the relatively small size of the detected sequence, the specificity of binding is achieved by the neighbouring residues.[72] Over the years, an increasing number of peptides have been discovered that bind SH3 domains with unusual binding motifs.[71]

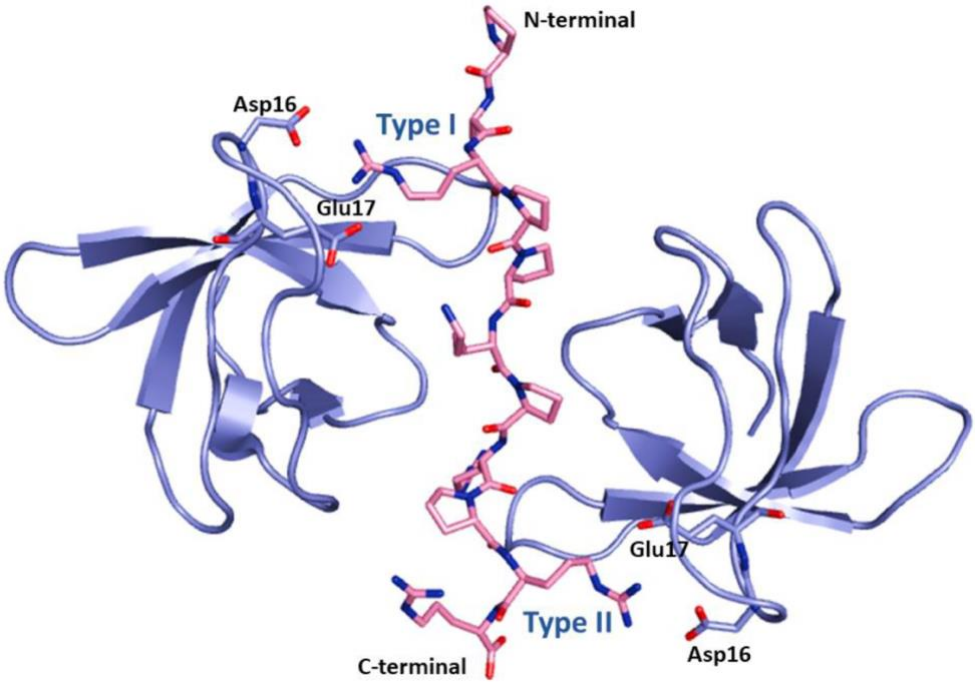

Figure 8. Crystal structure of CIN85 SH3A domain in complex with Cbl-b peptide. The SH3 domain is represented as blue cartoon and Cbl-b as pink-stick. The basic residue in the N-terminal part of peptide assumes the type I orientation on the hydrophobic pocket od SH3 domain and interact with Asp16 and Glu17. On the other hand, the basic residue in the C-terminal part of peptide interact with the same hydrophobic residues with a type II orientation.[73] (The image was created with PyMOL software).

The binding area of SH3 domains is largely conserved and contains hydrophobic residues such as Tyr, Phe, Pro and Trp, which are largely implicated in the binding of proline-rich sequences, as well as an acidic pocket that can create ionic interactions with basic residues adjacent to the PXXP motif.[74] These domains usually bind the protein partner with a stoichiometric ratio of 1:1, and those proteins with multiple SH3 domains can establish contacts with different ligands and thus enhance the affinity and specificity of the interaction.[73] However, several cases have been reported in the literature where the proline-rich motif simultaneously links two SH3 domains, forming heterotrimeric complexes.[75,76] After the ligand binds to the SH3 domains, it generally changes its conformation and adopts an extended, left-handed helix called the polyproline-2 helix (PPII).[77] Pro-rich sequences are able to interact in two orientations, *type I* and *type II*, depending on the position of the basic residues linked to the PXXP motif. In the type I orientation, basic residues from the N-terminal part to the binding motif can occupy the hydrophilic pocket, while in type II the same pocket can contains basic residues from the C-terminal part to the motif.[78] Specifically, the SH3 domains of CIN85 recognize an atypical PXXXPR motif present in the ubiquitin ligases c-Cbl and Cbl-b.[79] Through crystallographic studies of the interaction between the N-terminal SH3

domain (SH3A) of CIN85 and the Cbl-b peptide (RCSB PDB: 2BZ8); it was observed that there is formation of a heterotrimeric complex in which Cbl-b is sandwiched between two SH3 domains (Figure 8). Furthermore, one SH3 domain bound the Pro-rich peptide assuming a type I orientation, while the other SH3 domain binds in a type II orientation.[73]

In association with Cbl-b, CIN85 plays an important role in the organization and sorting of several receptor-activated tyrosine kinases (RTKs), including the *epidermal growth factor receptor* (EGFR)[69]. In particular, growth factor engages RTKs by provoking receptor autophosphorylation and phosphorylation of different substrates. Thereafter, activated RTKs move from the cell surface to the endosomal compartment, where they can be recycled to the plasmatic membrane or disposed for lysosomal degradation. These processes are modulated by different PPIs, receptor phosphorylation and ubiquitination. Cbl proteins, are implicated in ubiquitination as well as lysosomal degradation of various RTKs. This role of Cbl proteins on the modulation of RTK endocytosis occurs through the binding with CIN85. Specifically, Cbl links to phosphorylated RTKs and is itself phosphorylated. The formed Cbl-RTK complex interacts with the SH3 domains of CIN85, whose Pro-rich region is constitutively associated with endophilins. Endophilins act as regulatory proteins of clathrin-coated vesicles that are responsible for membrane invagination leading to endocytosis of RTKs.[70]

Furthermore, CIN85 is involved in CD2 receptor clustering and cytoskeletal polarity of the specialized junction between T cells and antigen-presenting cells (APCs), otherwise known as the *'immunological synapse*'. CD2 is an adhesion molecule found on the surface of T cells and natural killer (NK) cells. Under physiological conditions, it mostly interacts with CD58, another cell adhesion molecule located on APCs, and this interaction promotes T-cell activation. CD2's role in the immunological synapse is caused by its interaction with the SH3 domains of the adaptor proteins CIN85 and CD2AP, which is achieved through the proline-rich motifs present in the C-terminal tail of CD2. At the same time, the C-terminal region of CIN85 binds CAPZ, a capping protein that covers the upper end of actin filaments, thus creating a direct link between CD2 and the cytoskeleton. Thus, the binding of CIN85 and CAPZ supports the alignment of T-cell and APC membranes.[69,80]

2.2.1 The high-expressed CIN85 in cancer cells

High expression of CIN85 has been observed in invasive breast cancer cells, where this adaptor protein has been identified as a constituent of invadopodia, which are an actin-rich membrane protrusions that provide the ability to invade cancer cells. Two plausible mechanisms have been reported in the literature: a) CIN85 seems to be involved in invadopodia biogenesis by promoting the interaction between Cbl proteins and ASAP1/AMAP1 proteins; b) CIN85 promotes tumor cell invasiveness regards its interaction with TA-MUC1.[81]

2.2.2 MUC1-CIN85 interaction

Analogously to the PXXXPR motif found in Cbl and other effectors of CIN85, the VNTRs of MUC1 have highly conserved proline rich PDTRP motif which is detected by the SH3 domains of CIN85. However, both proteins are overexpressed in early and advanced clinical stages of breast cancer and co-localize in invadopode-like structures, resulting in increased invasiveness of cancer cells. Through in vivo studies on a B16 melanoma tumor metastasis model, it was observed that when CIN85-free melanoma cells, were inoculated into mice, they did not lead to any lung metastasis, while overexpression of MUC1 re-established the metastatic process. The formation of the MUC1-CIN85 complex depends on the rate of glycosylation of the VNTRs of MUC1. In particular, glycosylation decreases as the tumor progresses to more advanced stages. This, decreased glycosylation could increase the number of MUC1-CIN85 complexes, promoting the invasive capacity of cancer cells.[82] Indeed, alterations in the length of the sugar chains of VNTRs have been reported to contribute to the tumor progression and metastasis formation. [83,84,85] It was also observed through experimental studies, that in the presence of a MUC1 agonist peptide able to induce dimerization, the interaction between MUC1 and CIN85 was two times higher than in its absence, which prompted that CIN85 binds MUC1 forming a heterotrimeric complex, as observed for Cbl-b.[86] Unfortunately, to date, no crystallographic structure is available for the MUC1-CIN85 complex.

2.3 Results and discussion

2.3.1 Peptide docking and MD simulation of CIN85 dimer and MUC1 peptide

Computational studies previously carried out by the Laura De Luca and coworkers provided useful information for the design of new antitumor agents. The interaction models of MUC1 in complex with the dimeric and the monomeric forms of CIN85 revealed that the CIN85 dimer bound to MUC1 could establish a similar interaction pattern as found in the X-ray crystallographic structure of CIN85 SH3 domain in complex with Cbl-b peptide (RCBS PDB 2BZ8)[73]. The obtained heterotrimeric and dimeric complexes were subjected to two independent 50 ns MD simulations. The MD outputs showed that the most stable interactions in the heterotrimeric complex of CIN85 dimer with MUC1 agreed with the X-ray solved structure CIN85/Cbl-b. In addition, MM-GBSA calculations for each MD simulation, revealed that the formation of the heterotrimeric complex of MUC1-CIN85 is energetically most favored compared to the dimeric complex.

As a continuation of these studies, the present PhD research was focused on further exploration of possible interactions between CIN85 dimer and MUC1 peptide by different computational approaches. We decided to generate an interaction model of this complex by performing peptide docking of MUC1 VNTR to the CIN85 dimer and then MD simulation. For this purpose, we used a new crystal structure of SN-101 mAb in complex with MUC1 synthetic glycopeptide (RCSB PDB: 6KX1 at 1.77 Å resolution)[87] from Protein Data Bank. The protein partners of MUC1 were deleted, the peptide was prepared at pH 7.0 and docking was carried out using Glide software[88,89]. The calculations generated five protein-protein complexes whose showed docking scores ranged from -5.362 kcal/mol and -3.311 kcal/mol and all five poses showed to possess similar conformations to the natural PPII helix conformation held by the Cbl-b peptide (Figure 9). The analysis of the 2BZ8 complex and the MD results were used as a reference for running and validating the protein-peptide docking results.

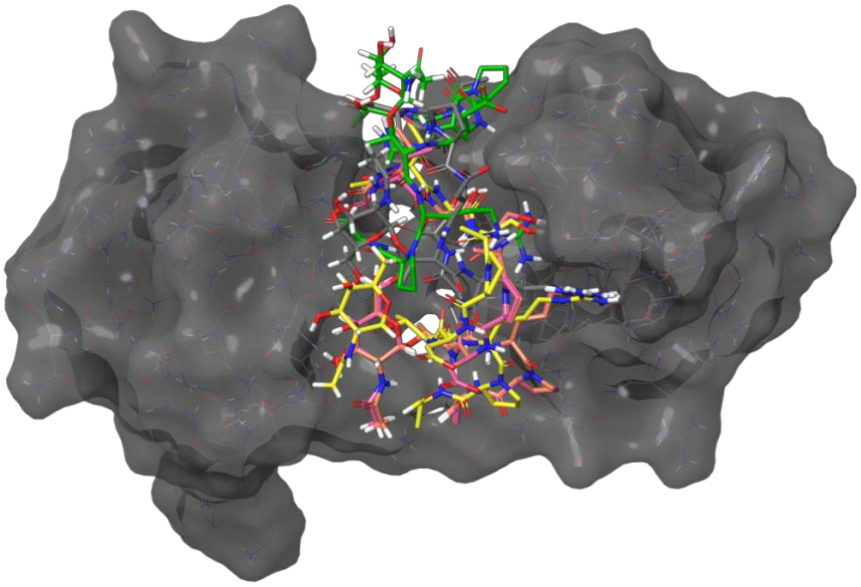

A

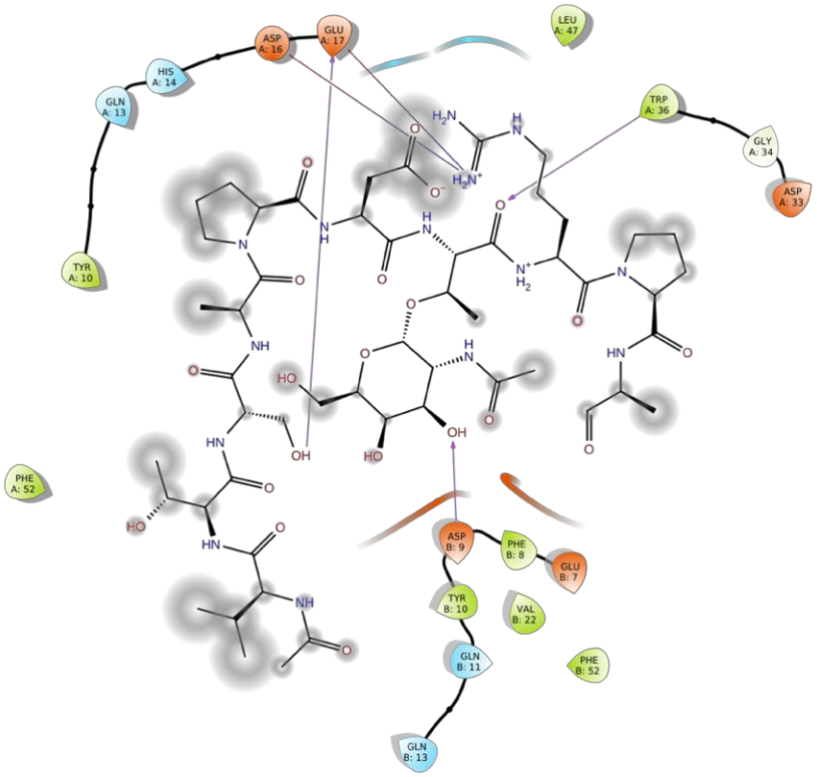

B

Figure 9. (A) Binding mode of all five poses of synthetic MUC1 VNTR glycopeptide retrieved from PDB 6KX1[87] to CIN85 dimer from PDB 2BZ8[73] (grey structure), **(B)** MUC1 VNTR peptide interactions with SH3 domains residues of CIN85.

As result, most of the CIN85-MUC1 peptide interactions from this docking study agreed with those identified from the PDB 2BZ8[73] where the key residues of CIN85 Asp16, Glu17 and Asn51 and Trp36 are involved in H-bonds and hydrophobic contacts. The residues Asp16 and Glu17 of an SH3 domain provided hydrogen bonds with MUC1 Thr2 and two salt bridge with Arg8. Trp36 of CIN85 created an H-bond with MUC1 Arg8, whereas Phe8, Tyr10 and Phe52 established a hydrophobic contact as shown in Figure 9.

To study the stability of the interactions, the complex selected from the output of the peptide docking was used to run MD simulations of 100 ns to identify the most frequent and stable interactions. The stability of the complex was verified by analyzing the RMSD graphs of the protein and ligand[90]. The analysis of the MD outputs confirmed that residues Glu17 and Trp36 of CIN85 established the most stable interactions with Arg8 of MUC1. Furthermore, residues Phe8, Phe52 and Asn51 of CIN85 formed hydrophobic contacts, whereas Asp16 of CIN85, one of the key residues from previous studies, was unable to provide stable and frequent contacts during the entire trajectory of MD simulation (Figure 10). To confirm the CIN85-MUC1 complex with the highest population for MD simulation, we conducted a trajectory clustering analysis using "Desmond Trajectory Clustering" from the Schrödinger suite. The resulting frames from trajectory were grouped according to RMSD to obtain a representative conformation of the system. The most representative structure of the cluster was selected and used for further studies.

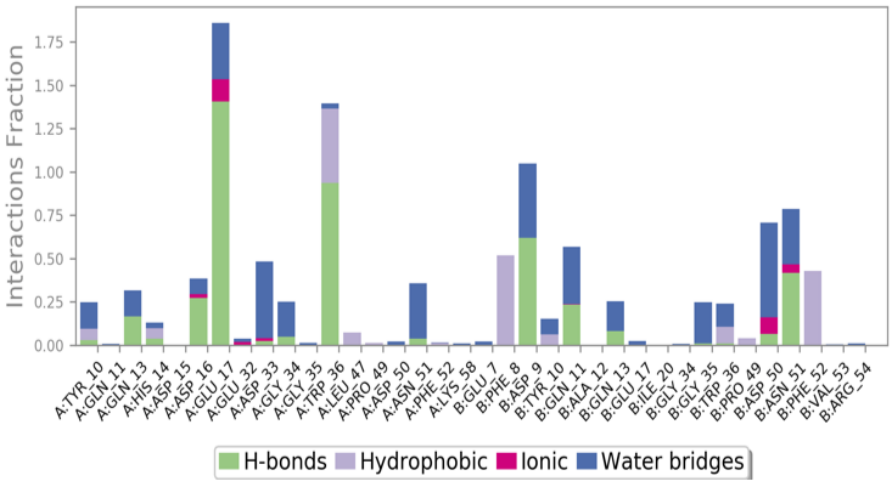

A

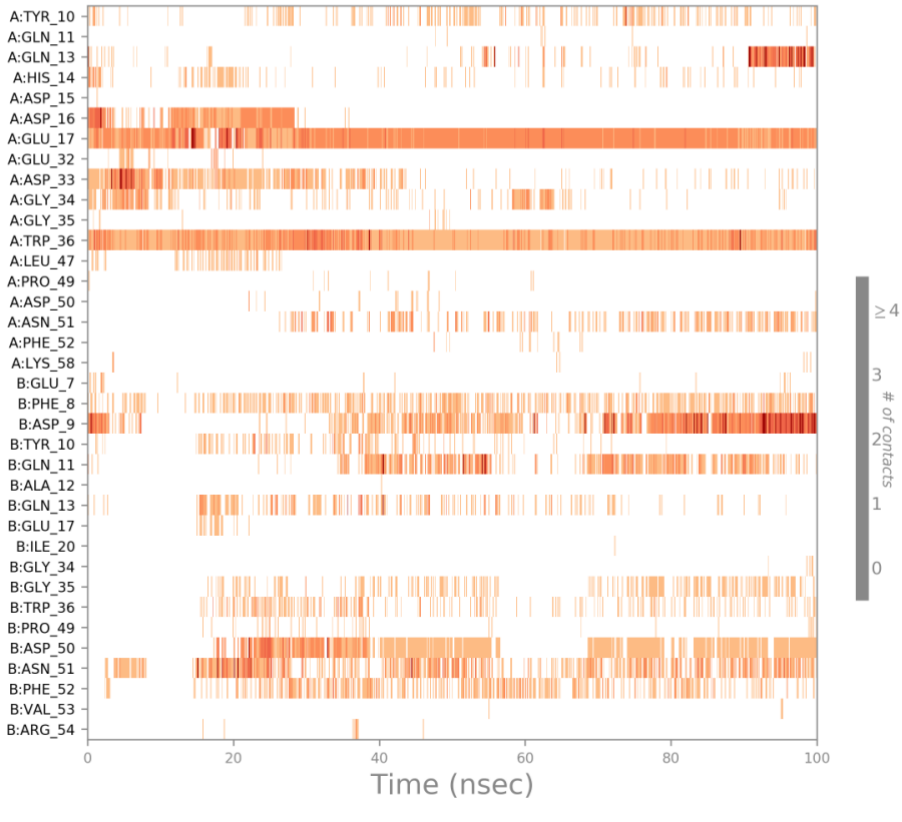

Figure 10. Schematic representations of the MD simulation of CIN85 dimer from PDB 2BZ8[73] in complex with MUC1 peptide from PDB 6KX1[87]. **(A)** Histogram plot highlighting the CIN85 residues involving in the interactions with MUC1. **(B)** Timeline representations of the interactions during the MD simulation.

2.3.2 Computational Alanine Scanning of CIN85-MUC1 complex

The study of alanine-scanning mutagenesis of protein-protein interfacial residues is a very useful process for the investigation of the binding mode of two proteins and for rational drug design. Based on the structural information from the literature about MUC1 peptide which shows in its sequence the motif PDTRP able to interact with the SH3 domain of CIN85, we decided to mutate all residues MUC1 synthetic glycopeptide. Starting from the cluster centroid retrieved from previously MD trajectory, we applied three different protocols from "Residue Scanning" tool of Schrödinger suite and the two webservices DrugScore^{PPI} (**http://www.dsppi.de**)[91] Robetta (https://robetta.bakerlab.org/)[92]. It is well known that low $\Delta\Delta G$ values indicate the unfavorable substitution of the amino acidic residue in alanine. As reported in Table 2, $\Delta\Delta G$ values retrieved from the three tools are all comparable such as Ser3, Thr2, Asp6, Thr7 except for the result for Arg8 obtained with Schrödinger, which deviate from average. These data showed that these amino acid residues of MUC1 are essential for interaction with the CIN85 dimer.

	Chain	Residues	ΔΔG
Schrödinger	C	ASP6	-4.23
	C	ARG8	19.48
	C	PRO9	2.17
DrugScore^{PPI}	C	VAL1	0.03
	C	THR2	0.22
	C	SER3	0.51
	C	ASP6	−0.22
	C	THR7	0.49
	C	ARG8	0.68
Robetta	C	ARG8	0.12
	C	THR2	-0.04
	C	SER3	-0.01
	C	THR7	0.23

Table 2. Alanine scanning results performed on MUC1 synthetic glycopeptide (PDB 6KX1[87]) through Schrödinger, DrugScore^{PPI}, and Robetta tools.

2.3.3 Pharmacophore modelling and virtual screening

In the second part of this study, the MD simulation results were used to generate a simple structure-based pharmacophore model to further explore the binding mode of the MUC1 peptide with the two SH3 domains of CIN85. To achieve this objective, a structure-based pharmacophore model was generated by using the software LigandScout V4.4[93]. As displayed in Figure 11, the obtained model was constituted by twelve features: four H-bond acceptors, four H-bond donors, three hydrophobic features and one positive ionizable feature. To perform virtual screening, we decided to prioritize the obtained features, thus simplifying the pharmacophore model; the evaluation of the importance of each feature was based on their presence in the previous studies such as the docking analysis, as well as the presence of these interactions in the MD simulation. Regarding H-bond features, we kept the H-bond acceptor of Ser3 and Thr7 and we removed the H-bond acceptor of 2-acetamido-2-deoxy-alpha-D-galactopyranose of MUC1 glycopeptide[87]. We also maintained

two H-bond donors of Ser3 and Arg8, two hydrophobic features of Ala4 and Thr7 and the positive ionizable feature of Arg8. Then, starting with the PXXXPR motif of MUC1[57], a similarity search was performed on the Scifinder (https://scifinder-n.cas.org/) platform and was created a library of peptide probes with a sequence of four/five amino acids analogues of MUC1. The use of peptide probes offered the advantage of exploring the PPI interface with compounds similar to natural peptide,[94] to investigate these interactions or to find additional ones and exploit them for the development of potential inhibitors.[95] The above-described structure-based pharmacophore model was used to screen this peptide library collecting 361 compounds, resulting in 43 hits and as result, we obtained twelve consensus compounds selected on the basis of the Pharmacophore Fit-Score, to perform the subsequent steps of our *in silico* study (Table 3).

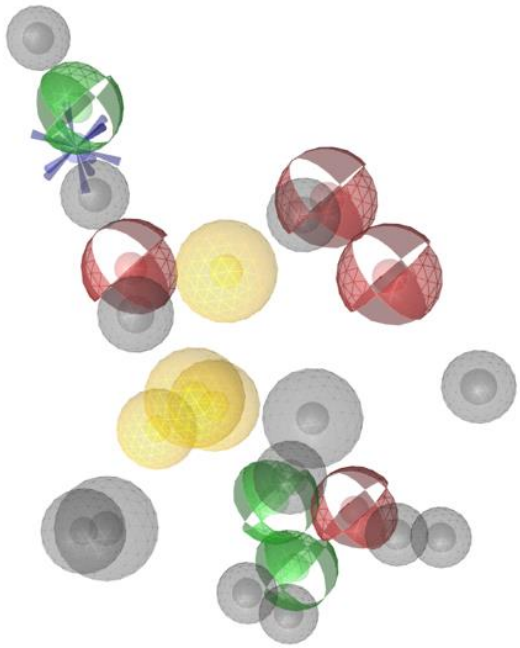

Figure 11. Structure-based pharmacophore model. The red spheres represent the H-bond acceptors, the green spheres represent the H-bond donors, the hydrophobic features are represented by the yellow spheres, and the blue star represents the positive ionizable feature.

2.3.4 Molecular docking of peptide probes and related MD simulations and MM-GBSA Calculations

The binding mode of the 12 hits selected through the virtual screening procedure was analyzed by molecular docking on CIN85 dime using Glide software from the Schrödinger suite[88 89]. Five poses for each peptide probes were generated and the poses with the best docking score were selected to run a 100 ns MD simulation per each peptide, using Desmond from Schrödinger suite[90]. In addition, to deeply explore the interaction stability between CIN85 and the selected peptides, MM-

GBSA calculations were run, using Prime from Schrödinger suite (Table 3)[96]. Through these calculations, one docked pose for each consensus peptide was selected according to the lowest $\Delta G_{binding}$ value (Equation 1).

$$\Delta G_{binding} = G_{complex} - G_{protein} - G_{ligand}$$

The analysis of the binding mode for each selected compound and the MD outputs pointed out that two consensus peptides were able to establish stable contacts with the CIN85 key residues previously encountered with MUC1 (Trp36, Asn51, Phe52, Asp16 and Glu17). As result, the peptide probe FM5 interacted with SH3 domains of CIN85 through four H-bond with Asn51 and Trp36 of both chains A and B and two π-cation interactions with Phe52 and Phe8 (Figure 12). The analysis of MD trajectory confirmed that residues Trp36 and Asn51 of both SH3 domain of CIN85 established the most stable interactions. Furthermore, residues Phe8, Phe52 and Asn50 of CIN85 provide stable and frequent contacts during the entire trajectory of MD simulation (Figure 13). Moreover, the peptide probe FM7 established H-bond with Gly17, Trp36 of both chains, a π-cation with Phe8 and hydrophobic interactions with Phe52 and Tyr10 (Figure 14). Also in this case, the analysis of MD outputs revealed that Trp36 and Asn51 of CIN85 SH3 domains, Glu7 and Phe8 of chain A give the most stable and frequent contact during the whole trajectory of MD simulation (Figure 15).

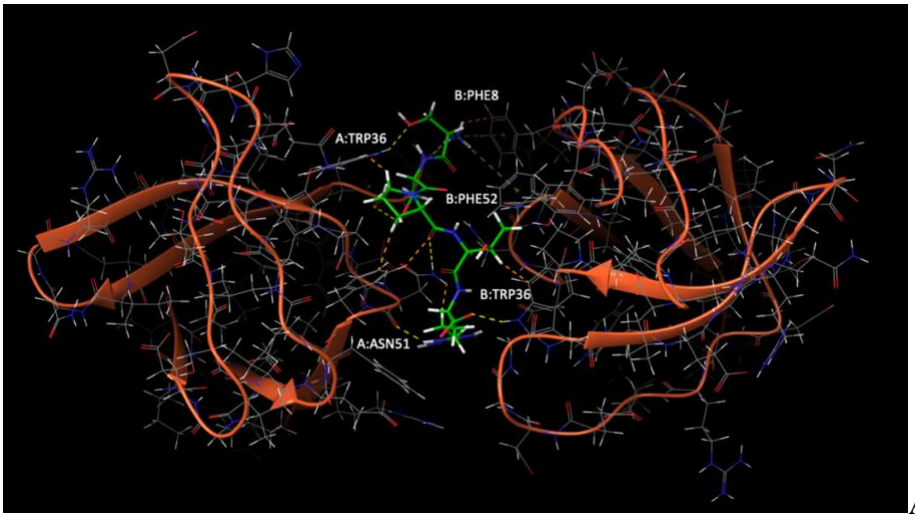

A

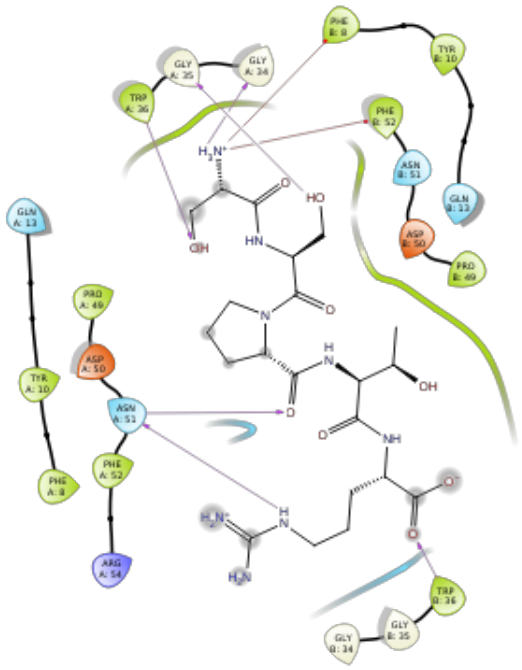

B

Figure 12. (A) Binding mode of peptide probe FM5 on CIN85 SH3 domains. **(B)** 2D depiction of the interactions with CIN85 SH3 domains.

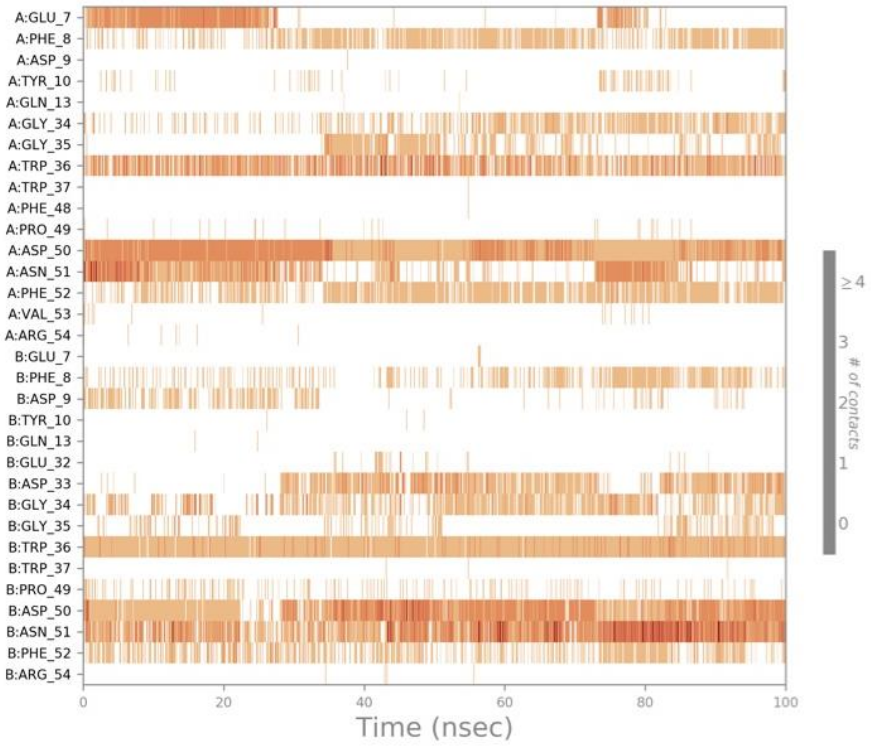

Figure 13. Timeline representations of the interactions during the MD simulation of CIN85 dimer from PDB 2BZ8 in complex with FM5 peptide.

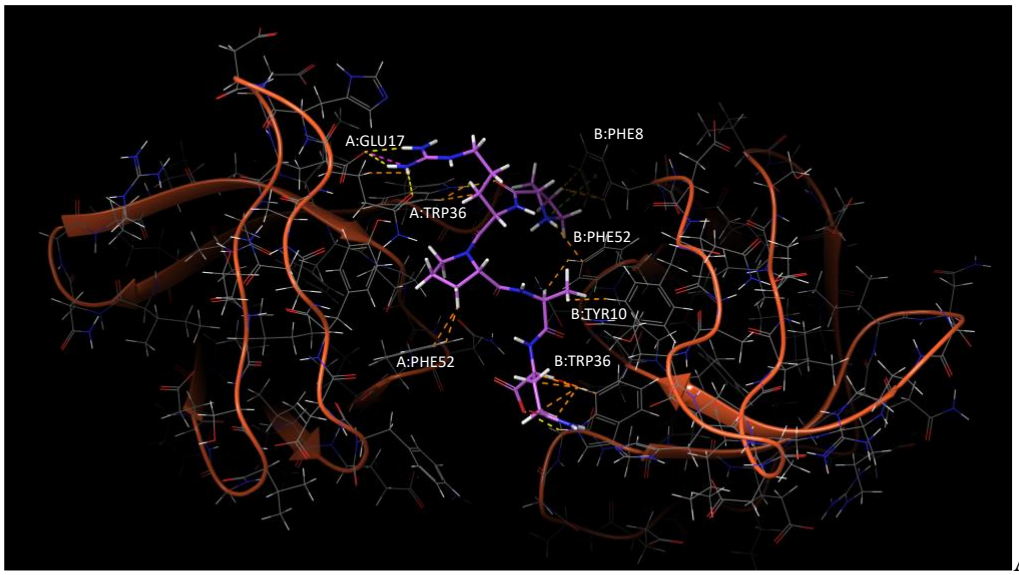

A

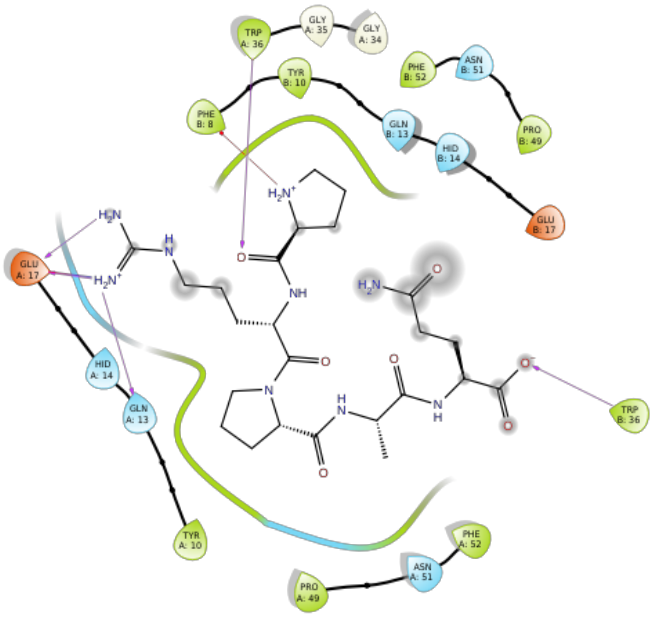

B

Figure 14. (A) Binding mode of peptide probe FM7 on CIN85 SH3 domains. **(B)** 2D depiction of the interactions with CIN85 SH3 domains.

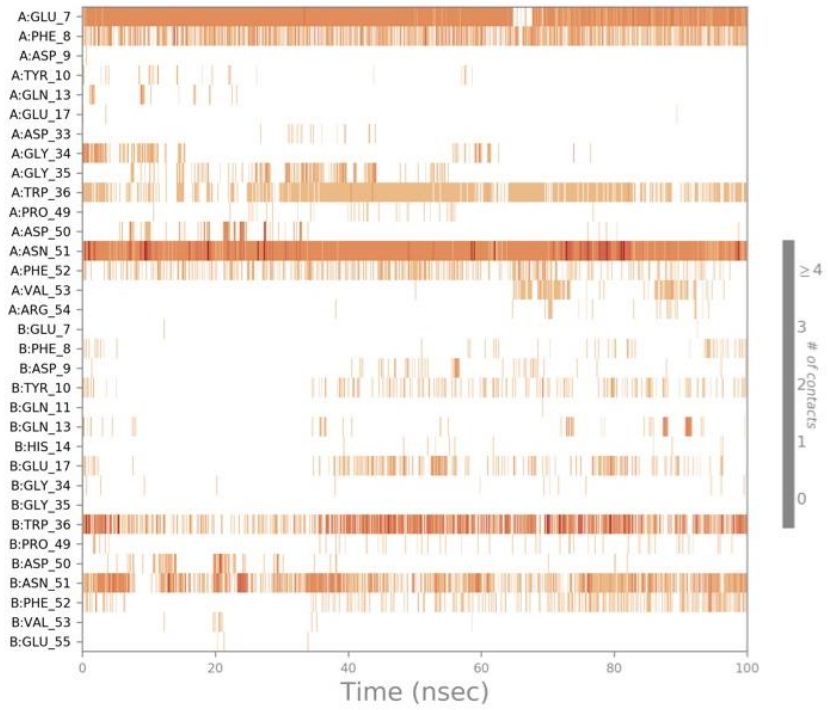

Figure 15. Timeline representations of the interactions during the MD simulation of CIN85 dimer from PDB 2BZ8 in complex with FM7 peptide.

Entry	Code	Docking score	Pharmacophore fit-score	ΔG bind kcals/mol
Glycine, N-[N-[1-(N-L-arginyl-L-threonyl)-L-prolyl]-L-seryl]- (9CI)	FM-1	-4.989	66.060	-53.58
L-Arginine, L-α-glutamyl-L-seryl-L-prolyl-L-alanyl-	FM-2	-5.841	65.850	-48.60
L-Arginine, N2-[1-[1-(N-L-threonyl-L-a-aspartyl)-L-prolyl]-L-prolyl]- (9CI)	FM-3	-4.949	65.180	-61.19
L-Arginine, L-prolyl-L-a-aspartyl-L-prolyl-L-alanyl-	FM-4	-7.012	66.670	-32.82
L-Arginine, L-seryl-L-seryl-L-prolyl-L-threonyl- (9CI)	FM-5	-5.640	75.650	-55.39
L-Aspartic acid, N- [1-[N-[N-(N2-L-prolyl-L-arginyl)-L-valyl]- L-seryl]-L-prolyl	FM-6	-5.926	66.230	-41.63
L-Glutamine, L-prolyl-L-arginyl-L-prolyl-L-alanyl-	FM-7	-5.611	66.240	-51.27
L-Proline, 1-[N2-[N-(N-L-prolyl-L-alanyl)-L-alanyl]-L-arginyl]- (9CI)	FM-8	-5.432	75.920	-51.44
L-Proline, L-threonyl-L-arginyl-L-prolyl-L-alanyl- (9CI)	FM-9	-6.110	65.460	-44.21
L-Serine, L-arginyl-L-prolyl-L-alanyl-L-prolyl-	FM-10	-6.327	65.710	-51.45
L-Serine, L-threonyl-L-arginyl-L-prolyl-L-alanyl-	FM-11	-6.989	75.940	-46.92
L-Threonine, L-prolyl-L-arginyl-L-prolyl-L-alanyl-	FM-12	-5.477	65.500	-54.82

Table 3. Data results from molecular docking on CIN85 dimer, virtual screening and MM-GBSA calculations.

2.3.5 Comments and remarks

The MUC1/CIN85 PPI represents a valuable pharmacological target for the development of novel antitumor agents. The current lack of a resolved structure of the complex hinders the design of potential inhibitors. The present protocol was designed to provide helpful insights for structure-based design of PPI modulators of MUC1-CIN85 as potential antimetastatic agents. By using peptide-based probes, our multi-computational approach offered essential structural information about this interaction. Firstly, we performed protein-peptide docking studies using a MUC1 peptide containing the PDTRP binding motif (RCSB PDB 6KX1)[87] and the dimeric SH3 domain of CIN85 (RCSB PDB 2BZ8)[73]. Subsequently, MD simulation of the CIN85/MUC1 complex was performed to deeply explore their stability. Furthermore, a structure-based pharmacophore model was created and was used to carry out a virtual screening of peptide probes MUC1 analogues. Finally, MD simulation and MM-GBSA calculations were performed for each selected peptide probes, revealing that the residues Trp36, Asn51 of CIN85 SH3 domains are involved into H-bond while Phe52 and Phe8 generated π-cation interactions. The best outcome of this computational study was to improve the knowledge about the key residues of the CIN85/MUC1 interaction for the development of selective and potent peptide-based compounds as inhibitors of this relevant PPI.

2.4 Material and methods

2.4.1 Protein preparation of CIN85 dimer and MUC1 peptide

The two PDB structures used in this work (RCSB: 2BZ8 and 6KX1) were previously downloaded from the Protein Data Bank, prepared, and optimized using the "Protein Protein preparation wizard"[97] from the Schrödinger suite (Schrödinger, LLC., New York, NY, USA, 2018, release April 2018). Firstly, binding orders were assigned for residues and then hydrogens were added. Additionally, was created zero-order bonds to metals with nearby atoms and disulfide bonds were created. Water molecules over 5 Å were removed from the het groups. For ligands, cofactors and metals, het states were generated at pH 7.0 ± 2.0 using Epik[98].

2.4.2 Preparation of ligands

The database of peptide probes was created starting from the PXXXPR motif of MUC1[57] and a similarity search (90-95%) was performed on Scifinder platform, including peptides with up to five amino acid residues as a filter. These ligands were prepared and optimised using "LigPrep" from the Schrödinger suite (Schrödinger, LLC., New York, NY, USA, 2018, release April 2018). For this purpose, was applied force field OPLS4 and then was generated possible states at target at pH 7.0 ± 2.0 using Epik[98]. The ligands were desalted, tautomers were generated and for stereoisomers was chosen to determine chiralities from 3D structure.

2.4.3 Receptor Grid Generation of CIN85 dimer and peptide docking

To execute peptide docking of the MUC1 peptide from PDB 6KX1 to CIN85 dimer, the receptor grid was created using PDB 2BZ8. Firstly, the binding region was defined by selecting the Cbl-b peptide and the option of a grid suitable for peptide docking was pointed out. The force field applied was OPLS4[99] and it was decided to write out at most five poses for all ligands including MUC1 peptide. Then, docking analysis were performed using the ligand docking tool from the Schrödinger suite[88, 89] and selected protocol was "SP-Peptide".

2.4.4 MD Simulations of CIN85 in Complex with MUC1 and peptide probes and MM-GBSA Calculations

MD simulations were run for different systems, CIN85 dimer-Cbl-b peptide, CIN85 dimer-MUC1 peptide and CIN85 dimer with each selected consensus peptide probes by using "Desmond" from the Schrödinger suite[90]. The systems were obtained from docking results and first tuned through "System builder" tool. The solvent model TIP3P and the orthorhombic box shape were selected[100]. The box side distances were set 10 Å for all ligands except for peptide probes FM9 and FM11 where the distances were set 13 Å. The system was neutralized by adding Na+ ions and then were run MD calculations of 100 ns per each trajectory. The number of atoms, pressure and temperature were maintained constant (NPT ensemble). The model systems were relaxed before simulation and OPLS3e force field was employed to parametrize the systems[99]. The obtained trajectory from CIN85 dimer-MUC1 complex was clustered according to RMSD employing "Desmond Trajectory

Clustering". Finally, the MD outputs of each selected consensus peptide probes were used to carry out MM-GBSA calculations through Schrödinger suite[101].

2.4.5 CIN85 dimer-MUC1 complex residue scanning

The resulted most representative structure of CIN85 dimer-MUC1 complex was used to perform point mutations through "Residue Scanning" tool of Schrödinger suite on MUC1 residues[102]. All residues were mutated to ALA and the predicted changes in binding affinity and stability were calculated according to Equation 1:

$$\Delta\Delta G_{binding} = \Delta G^{MUT}_{complex} - \Delta G^{WT}_{complex}$$

To combine results, the computational alanine scanning was also performed using DrugScore^{PPI} (**http://www.dsppi.de**)[91] and Robetta webservices (https://robetta.bakerlab.org/)[16] and the results were shown as the difference of binding free energy between for wild-type proteins and Ala mutans for protein-protein complex.

2.4.6 Pharmacophore modelling and virtual screening

LigandScout V4.4 software was employed for pharmacophore generation and virtual screening. The representative conformation of the system obtained from the clustering process was used as starting points for the construction of structure-based pharmacophore model. The virtual screening was performed by setting the option "Get the best matching conformation" as search mode.

CHAPTER 3

3 Discovery of new α-synuclein inhibitors as potential therapeutics against Parkinson's disease

The second part of my research work focused on protein aggregation underlying the onset of certain neurodegenerative diseases including Parkinson's disease (PD).

PD is a chronic and progressive neurodegenerative process linked to a loss of dopaminergic neurons in the *substantia nigra pars compacta* of the brain (SNpc).[103] Neurodegeneration results in a dramatic drop of dopamine (**3**, DA, Figure 16) levels in dorso-striatal synaptic connections, leading PD to the synaptopathy.[104]

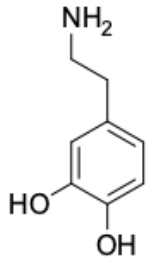

3

Figure 16. Structure of Dopamine (**3**, DA)

It is estimated that 7 to 10 million people worldwide are affected by PD. The most common risk factors in the incidence of this disease are genetic factors, such as age and gender (male individuals are more predisposed), and environmental factors such as exposure to herbicides and heavy metals.[105,106] DA deficiency leads to the typical motor symptoms of PD, such as bradykinesia, rigidity, resting tremor and postural instability. Post-mortem studies have revealed that several other regions of the central and peripheral nervous system are involved in the neurodegenerative process.[107] The involvement of these areas causes non-motor symptoms of PD, which include rapid eye movements, sleep disturbances, depression, olfactory dysfunction, and constipation. It has been seen that non-motor features usually occur before the onset of typical motor symptoms.[108,109] Although the main cause of PD is still highly controversial, studies conducted on the brains of PD patients have shown the common features as follow: the production of intracellular inclusions

called Lewy bodies, mainly composed of a misfolded intracellular protein named alpha-synuclein (α-syn).[110] Current therapeutic strategies are based on relieving motor symptoms and improving the quality of life of PD patients. Therefore, restoring DA levels is the most popular approach using the pro-drug L-Dopa **4**, which penetrates the blood-brain barrier (BBB) and then is converted to DA.[103, 111] It is combined with Carbidopa **5**, a peripheral decarboxylase inhibitor, to decrease some of its side effects, such as nausea, and to prevent its conversion into DA in the bloodstream, thereby providing more in the central nervous system.[103,112] Furthermore, the other treatments affect different target increasing DA concentrations such as dopamine receptor (e.g., ropinirole, **6**) or monoamine oxidase B (MAO B) (e.g., selegiline, **7**) and catechol-O-methyltransferase (COMT) (e.g., tolcapone, **8**; entacapone, **9**) (Figure 17).[112, 113] The side effects of the aforementioned drugs such as nausea, abdominal pains, dizziness, confusion and hallucinations, have been directed towards the exploration of new targets. The inhibition of α-syn aggregation could be considered a valid strategy for the discovery for new therapeutic agents, which could be able to reduce PD progression.[112,114]

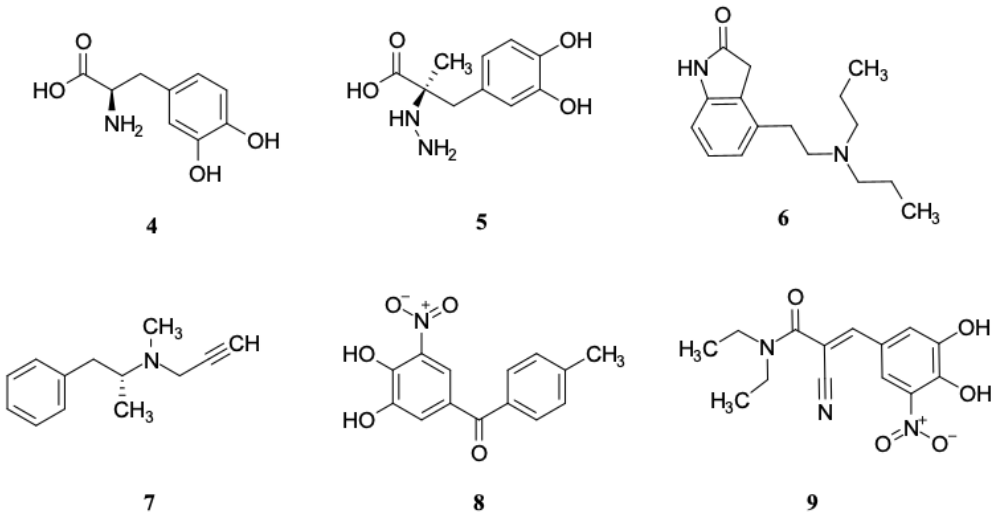

Figure 17. Chemical structures of well-known therapeutics for Parkinson's disease.

3.1 The role of α-synuclein

The α-synuclein (α-syn) is a small protein encoded by SNCA gene and localized in the pre-synaptic terminal.[104,115] α-syn is a physiologically soluble monomer, which by interaction with phospholipids assumes an alpha-helical structure.[116] In the misfolded state, aggregation of α-synuclein into amyloid fibrils causes the formation of neuronal pathological inclusions commonly noted as Lewis bodies and neurites located in both the neuron soma and axons (Figure 18).[117] This occurs through various mechanisms, such as an increase of membrane permeabilization, mitochondrial injury and oxidative stress.[118] Specifically, mitochondrial dysfunction in dopaminergic neurons, in turn, results in inflammatory activation, alteration of protein trafficking and degradation, and dysregulated cell signaling. Overexpression or decreased levels of α-syn have been found to be implicated in a regulatory pathway of neurotransmitter release, synaptic activity, and plasticity under physiological state. Thus, α-syn aggregates are also involved in the progression of pathology that coincides with the clinical progression of PD.[119] Recently, it was reported the mechanism for which oligomeric and post-translational α-syn directly interacts with the *outer membrane mitochondrial translocase receptor* (TOM20); it was demonstrated that α-syn prevents its association with the co-receptor TOM22, leading to the formation of the TOM complex, which is essential for the import of proteins at the mitochondrial level. The blockage of mitochondrial protein import by toxic α-syn species may be an important early factor contributing to dopaminergic neurodegeneration.[47,120] As a consequence, α-syn/TOM20 PPI may be an important target for therapeutic intervention. In addition, the misfolded extracellular α-syn exhibits a spreading mechanism similar to prions from neurons to glial cells.[121] Finally, this abnormal α-syn works as an antigen, prompting an immune-response strictly related with neuroinflammatory events.[122]

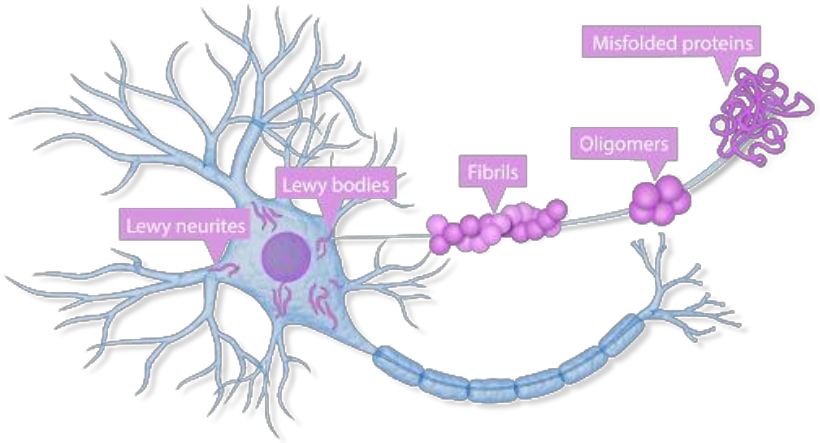

Figure 18. Representation of α-syn aggregation

The α-syn monomer is a small protein containing three domains: the N-terminal domain (aa 1-60), central NAC domain (aa 61-95) and C-terminal domain (aa 96-140)[108]. The N-terminal domain constitutes an amphipathic lysine-rich α-helix, which contains 11-aa repeats with a conserved motif KTKE/QGV, and it is responsible for α-syn unique binding capacity to vesicles and membranes (Figure 19).[123] Five missense mutations (A30P, E46K, H50Q, G51D and A53T) have been identified in this portion of the protein that are linked to familiar forms of PD and that contribute to an accelerated rate of α-syn fibrillation.[124,125] The central NAC domain of α-syn influences misfolding in β-sheet-rich amyloid aggregates. Finally, the C-terminal polar domain contains negatively charged residues, serine and tyrosine, which can be phosphorylated, leading to the regulation of membrane binding, aggregation and toxicity of α-syn.[126]

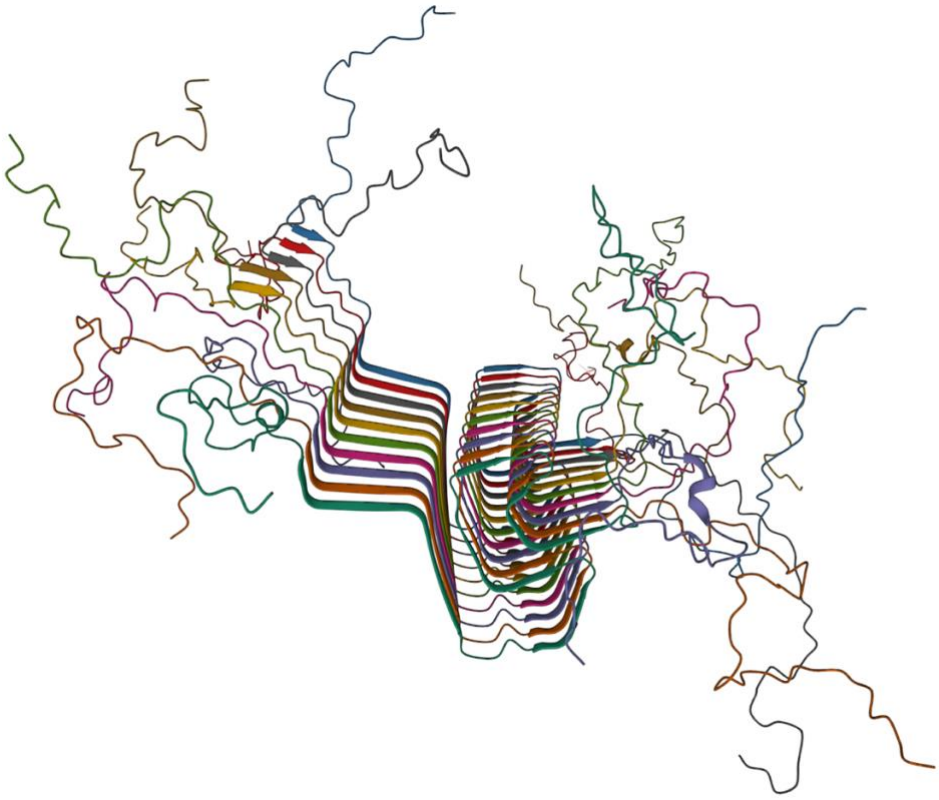

Figure 19. Structural mode of α-syn fibrils (PDB code 2N0A[127])

To date, many approaches that directly target α-syn have been explored, including gene silencing, immunotherapy and modulation of aggregation.[128] A discussion with a detailed description of the inhibition of α-syn aggregation will be presented in the following sections.

3.1.1 Therapeutic strategies to inhibit α-syn aggregation

- ***Gene silencing***

The expression of α-syn can be inhibited using a *small interfering RNA* (siRNA) that specifically targets α-syn mRNA. Through *in vivo* experiments, it has been reported that siRNA infusion can reduce α-syn levels in the hippocampus and cortical. However, this strategy is not selective towards α-syn in the brain and may induce similar effects in peripheral tissues, because α-syn is also located in the peripheral nerves and red blood cells.[129,130] A distinct approach to act on the α-syn expression is the administration of β2-adrenergic agonists. Epidemiological studies demonstrated that in patients treated with β2-adrenergic agonists for asthma, the onset of PD is lower, *in vitro* and *in vivo* studies demonstrated that these drugs lead to a decrease of α-syn expression mRNA through acetylation mechanism of lysine 27 of Histone 3.[131,132]

- ***Immunotherapy***

The active and passive immunotherapy might be employed as therapeutic strategy. Concerning the active immunization, the patient immune system is stimulated to produce antibodies against the target protein, whereas in the passive immunization the patient is directly treated with antibodies. The synthetic vaccine AFFITOPE® PD03A, developed by Affiris biotech company, consists in an α-syn mimicking peptide that led to an active immunization with a dose-dependent response.[130] Furthermore, two antibodies have been developed for passive immunization, the first one BIIBO54, a human derived antibody designed by Biogen, and the second one PRX002, a humanized monoclonal antibody created by Prothena. These two antibodies target α-syn aggregates hindering their spread. [128,130]

- ***Inhibition of α-syn aggregation***

Recently, it has been proposed that a promising therapeutic intervention could be realized by inhibiting or reversing aggregation using peptides or small molecules capable of interacting with the α-syn protein through different modalities and thus avoiding the formation of oligomers and subsequently amyloid fibrils.[126]

Regarding the development of peptides, the most important strategy is to mime the amyloidogenic sequence of α-syn. The use of peptides is characterized by a lot of advantages, like low toxicity,

low tissues accumulation, high selectivity, and good tolerability. Whereas the therapeutic applications of peptides are limited for their chemical and physical instability, their sensibility to proteolytic enzymes and the low penetration of biological membranes.[124]

Several synthetic peptides proved to inhibit the α-syn aggregation; the best results were found with peptides that reproduce the NAC sequence of α-syn. The mechanism of action is not very clear; it seems that these peptides might interact with the monomeric form of α-syn preventing the formation of toxic aggregates. There were also designed different cyclic-D, L- α-peptides, such as the hexapeptide CP-2 (**9**, Figure 20), which showed to be able to create supramolecular complex mimicking the structure and the function of amyloids and interact with NAC regions of α-syn.[133]

Finally, another class of peptide-based α-syn inhibitors, have been developed. They are small molecules (e.g. β-Harpin) with no homology with α-syn structure; there are evidences that they interact with hydrophobic areas at the protein interface, creating non-amyloid and non-toxic aggregates.[134]

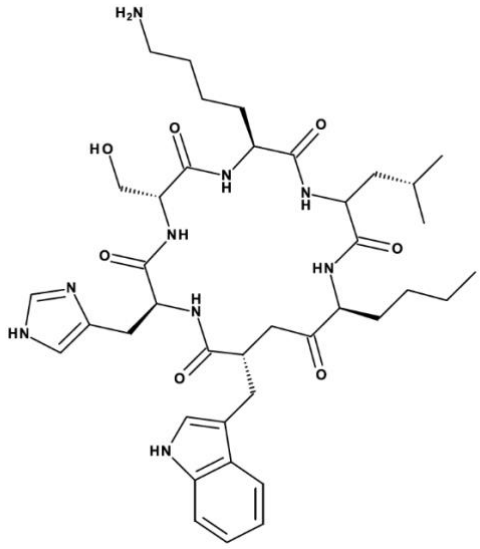

10

Figure 20. Structure of cyclic-D, L- α-hexapeptide CP-2

Up to date two major categories of small molecules have been recognized through *in vivo* screening assays; consisting in polyphenol and non-polyphenol compounds (Figure 21) from natural and synthetic sources. Among polyphenol compounds, structure-activity relationship studies have been demonstrated that the number of phenolics group and their position are crucial for the activity. Furthermore, the presence of the catechol moiety seems to be relevant for the inhibition of α-syn aggregation, as was observed in the case of the two COMT inhibitors tolcapone (**8**) and entacapone (**9**) and, also employed in the treatment of PD. Indeed, these two nitrocatechols in current therapy use have shown to inhibit the α-syn aggregation in the Th-T fluorescence assay.[135]

Among polyphenolic compounds, flavonoids are characterized by different biological properties like anticancer, antimicrobial and antioxidant activity. The flavone Baicalein (**11**), the main biological component of Chinese herbal medicine *Scutellaria Baicalensis*, has been shown to prevent the α-syn cytotoxicity, inhibiting the oligomerization of α-syn, thus blocking the fibrils formation.[136]

In the flavonoids chemical classes, quercetin (**12**) has also been demonstrated to successfully block the α-syn aggregation and to disassembly preformed fibrils.[135]

Curcumin (**13**) and hydroxycinnamic acid derivatives (HCA) are further polyphenolic compounds, which have been studied for their ability to act by blocking α-syn aggregation. The curcumin inhibits the formation of toxic α-syn aggregates, but it possesses low bioavailability; whereas the hydroxycinnamic acid derivatives (e.g. ferulic acid, **14**) represent an useful alternative due to their improved solubility in water.[123] Indeed, ferulic acid appears to interact with the oligomeric of fibril forms of α-syn, thus blocking the aggregation. The presence of the aromatic ring is essential to establish π-π and hydrophobic interactions with α-syn, which prevent the binding with other monomers.[137,138]

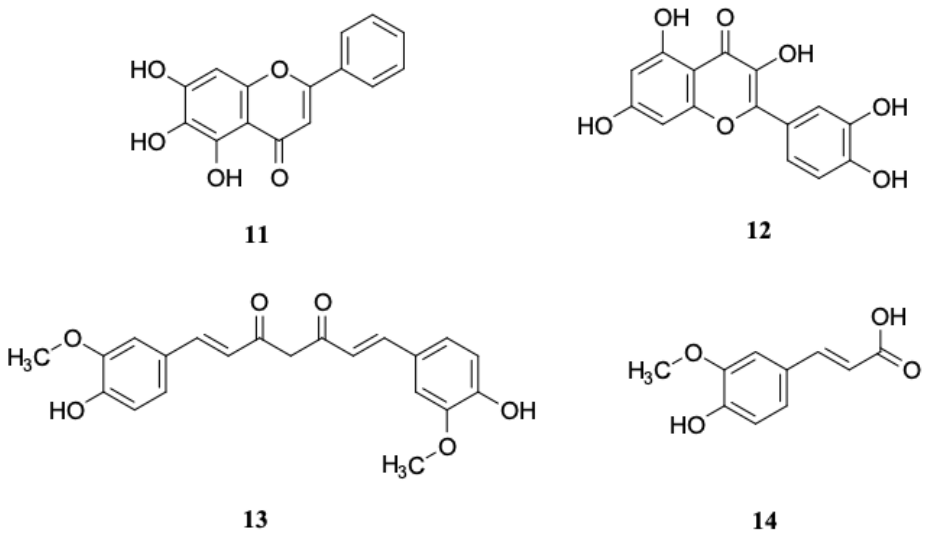

Figure 21. Structure of some polyphenol derivatives from natural source

Concerning non-polyphenol derivatives (Figure 22), inhibitory functions on the aggregation of α-syn were observed for mannitol (**15**), which proved to inhibit the formation of fibrils, by means of specific structure of α-syn oligomers. Several terpenoids, such as vitamin A (**16**) and β-carotene (**17**), have been shown to prevent α-syn fibrillation in a dose-dependent mode, due to their high hydrophobic character, which permits to interact with the hydrophobic NAC regions.[139,140] Through epidemiological studies, it has been demonstrated that coffee drinkers have a low risk of being affect by PD, because caffeic acid (**18**) possesses an anti-fibrillating ability in a dose-dependent manner against the aggregation of α-syn induced by treatment with the *selective serotonin reuptake inhibitor* (SSRI) escitalopram. In fact, it has been reported that the administration of escitalopram as an antidepressant could act as an environmental factor capable of producing structural alterations in α-synuclein that lead to the formation of aggregates and fibrils.[141] Cigarette smoking is also associated with a low incidence of PD, due to the ability of the alkaloid nicotine (**19**) to act on the monomeric form of α-syn. In detail the (+)-nicotine interacts with the N-terminal region, whereas the (-)-nicotine binds to both the C- and N-terminal domains.[142] By gathering structure-affinity relationship information, it was pointed out that the presence of aromatic rings and/or planar moieties could represent an important prerequisite for inhibitory activity.[123,143]

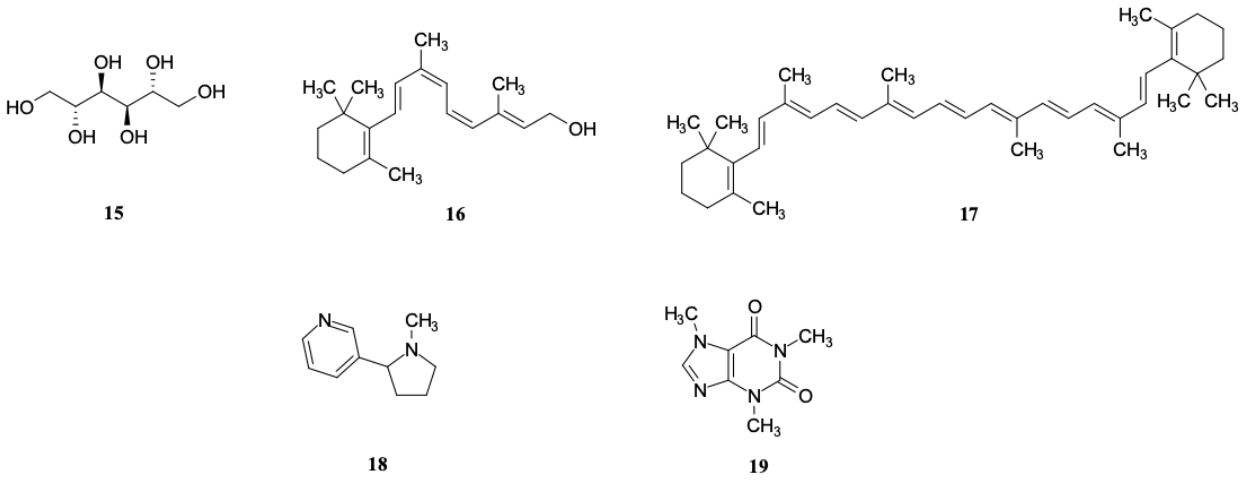

Figure 22. Structure of non-polyphenol compounds from natural source

However, several promising inhibitors from synthetic sources have been identified using innovative methods, including high-throughput screening (Figure 23).[144] The 3,5-diphenyl-pyrazole derivative Anle138b (**20**) has been identified as potent α-syn inhibitor, as it interacts with the oligomeric form of protein, both *in vitro* and *in vivo* and this mechanism of action proved to

reduce the accumulation of toxic species, neurodegeneration, and the PD progression in three different mouse models. This compound has been shown to have a good availability and to penetrate the *blood brain barrier* (BBB).[145] A phase 1b study of the compound Anle138b in 48 people with Parkinson's disease is currently underway. The study will assess safety, tolerability, and pharmacokinetics (Identifier: NCT04685265 see ClinicalTrials.gov). Furthermore, the 2-pyridone-based SynuClean-D (**21**) and 4-pyrimidinone-based ZPD-2 (**22**), have been denoted through a high-throughput virtual screening of a library containing 14000 molecules with different chemical scaffolds. The thioflavin-T assay (Th-T) displayed the ability of these two compounds to inhibit α-syn aggregation. All the compounds are marked by one or two aromatic rings, which probably provide contacts with the hydrophobic regions of α-syn, and by the presence of nitrile, trifluoromethyl and nitro groups, which could be implicated in the formation of H-bonds. Successively, the inspiring results from the *in vitro* and *in vivo* experiments of SC-D and ZPD-2, encouraged the researchers to develop analogs with the aim to obtain new entities as potential α-syn inhibitors useful for the treatment of PD.[146,147] For example, it was reported compound ZPDm (**23**), which could be considered the building block of ZPD2 as it shares the 2-nitro-4-(trifluoromethyl)phenyl moiety. This compound acts in the latest stages of the fibrillation process by disrupting large fibrillar species into shorter fibrils or amorphous agglomerate.[148] These efforts revealed that, in some cases, a single aromatic ring with appropriate molecular elements is the key to reducing α-Syn aggregation in *in vitro* models.[143] Indeed, another single-ring compound is 576755 (**24**), a quinone-based structure discovered by applying a new high-throughput strategy based on surface plasmon resonance with chemical microarrays. This compound showed a significant inhibitory effect in fibril and oligomer formation.[149]

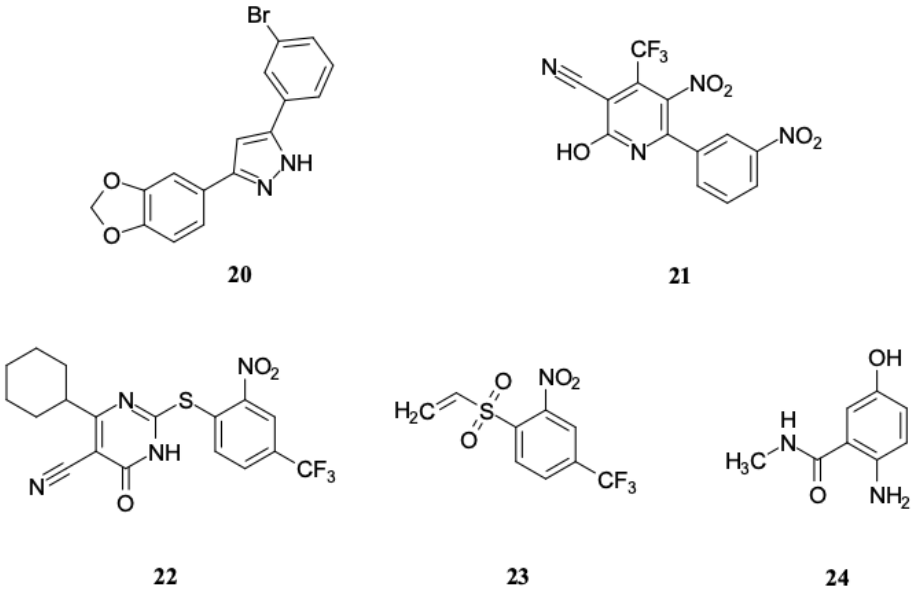

Figure 23. Structure of some synthetic α-syn aggregation inhibitors from synthetic sources

3.2 Result and discussion

3.2.1 Design and synthesis of a small set of new compounds bearing the pyridinyl-triazole scaffold

Based on the recognition that the aggregation prone NAC domain of α-syn (aa 61–95) is pivotal for the conformational transition to β-sheets secondary structure, recent research has been focused on the identification of novel α-syn aggregation inhibitors directed on the NAC domain of α-syn. From a set of 4-amino-5–(4-pyridinyl)-4H-1,2,4-triazole-derived compounds, we firstly discovered the 3-(cinnamylsulfanyl)-5-(4-pyridinyl)-1,2,4-triazol-4-amine (**25**), which was shown to reduce α-syn aggregation in *in vitro* assays. This pyridinyl-triazole based compound led to a decrease of Thioflavin-T (Th-T) fluorescence emission. Light scattering measurements were carried out at 300 nm at the endpoint of the reaction highlighting a diminution of 43% of aggregates in presence of compound **25.** Moreover, through *transmission electron microscopy* (TEM), this molecule showed a substantial reduction of the quantity of fibrils species. The docking studies revealed that compound **25** interact into a specific site situated between the N-terminal and the NAC domains. Subsequently, it was considered as 'lead compound' for the design of newer derivatives. In detail, the pyridinyl-triazole portion was retained, while the length of the linker connecting the sulphur atom to the phenyl ring was reduced. Among this first subset, the benzyl-derivative **26** showed to reduce of 33% the formation of Th-T positive structures and through light scattering measurements and TEM analysis, it displayed a decrease of aggregates and amyloid fibrils.[150] In addition, these pyridinyl-triazole derivatives have been shown to inhibit the metallo-enzyme tyrosinase (TYR, EC 1.14.18.1) involved in neuromelanin production. Indeed, it has been reported that neuromelanin in the human substantia nigra is closely related to the pathogenesis of PD (Figure 24).[151]

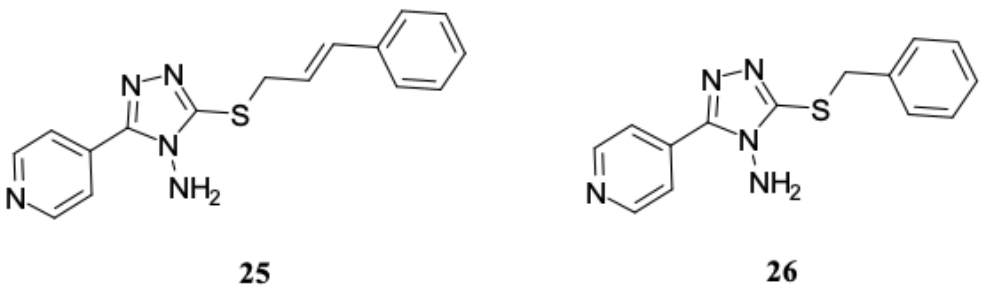

Figure 24. Structure of the lead compound 3-(cinnamylsulfanyl)-5-(4-pyridinyl)-1,2,4-triazol-4-amine (**25**) and the benzyl-derivative (**26**)

Searching for new small molecules having the ability to bind α-syn and exert inhibition of the aggregation, it has been previously reported a ligand-based pharmacophore model, built by means of LigandScout V3.4 software (Figure 25).[150]

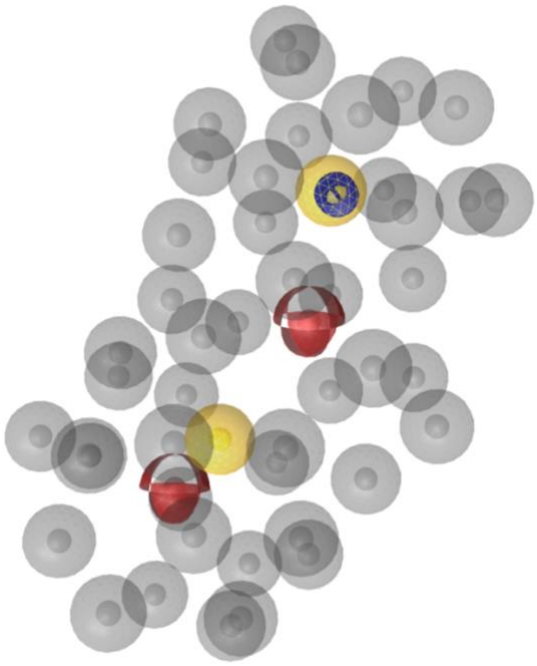

Figure 25. Ligand-based pharmacophore model. The red spheres represent the H-bond acceptors, the hydrophobic features are represented by the yellow spheres, and the blue circle represents aromatic features. Excluded volumes are represented by grey spheres.[150]

In details, model suggested for the α-syn aggregation inhibition: i) a salt bridge contact, ii) an uncommon π-anion interaction, iii) several hydrophobic and van der Waals interactions (Figure 26). Based on this pharmacophore model, we developed a further subset of compounds with the purpose of obtaining structural data for this series of compounds and improving the chemical and physical properties to improve absorption in *in vivo* assay.[150]

Specifically, we chose to maintain the 5-(4-pyridinyl)-1,2,4-triazol-4-amine chemotype and explored the eastern region of prototype **25** by depletion of the cinnamyl-fragment and insertion of small fragments. In particular, the new compounds were designed to study the impact of the introduction of small substituents capable of increasing H-bond donor/acceptor contacts as well as hydrophobic interactions in the sub-pocket coated by crucial NAC domain residues. Therefore, we analyzed the biological inhibitory effects on α-syn aggregation of the starting material 4-amino-5–(4-pyridinyl)-4H-1,2,4-triazole-3-thiol (**27**) and its corresponding three derived compounds **28-30** reported in Figure 26.[152]

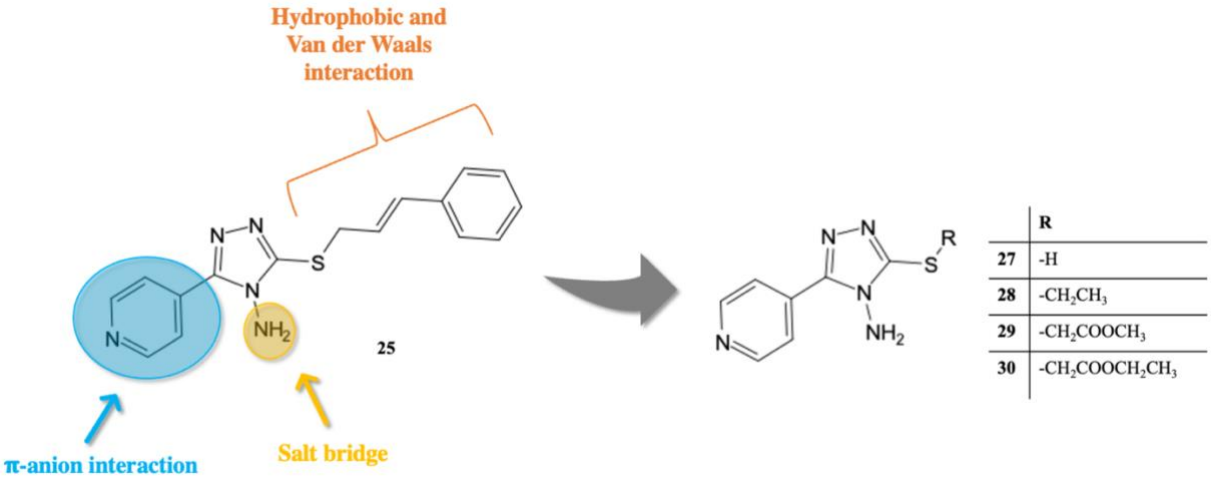

Figure 26. Newly designed compounds **27-30** bearing 5-(4-pyridinyl)-1,2,4-triazol-4-amine core

Compounds **28-30** were obtained by following a simple synthetic route described in Scheme 1. The 4-amino-5-(4-pyridinyl)-4H-1,2,4-triazole-3-thiol (**27**) was coupled with an opportune alkyl halide in alkaline medium at room temperature as previously reported by us. [150]

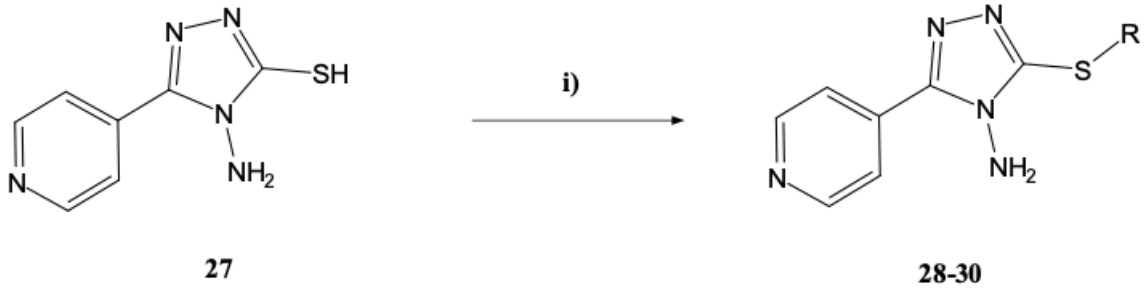

Scheme 1. Reagents and conditions: i) R-Br, NaOH, MeOH, rt

In addition, to obtain further structural information and to optimize pharmacokinetic and solubility properties, two additional compounds with a pyridinyl-triazole structure were synthesized, the carboxyl analog **31** and the piperidine amide derivative **32**. The evaluation of their *in vivo* biological profile after MPTP-induced damage is currently in progress as well as for compound **28** and **29**. The carboxylic derivative **31** was obtained through a simple hydrolysis reaction from the methyl ester **29** (Scheme 2). Compound **32** was prepared following two synthetic steps described in Scheme 3. Piperidine was coupled with 2-chloroacetyl chloride in alkaline medium heated at reflux. Then, the s-alkylation between the intermediate 2-chloro-1-(piperidin-1-yl)ethan-one and 4-amino-5-(4-pyridinyl)-4H-1,2,4-triazole-3-thiol (**27**) was carried out according to the previously reported method.[150]

All the synthesized compounds were structurally characterized through nuclear magnetic resonance (NMR) spectroscopy and melting point determination. All data are reported in experimental section.

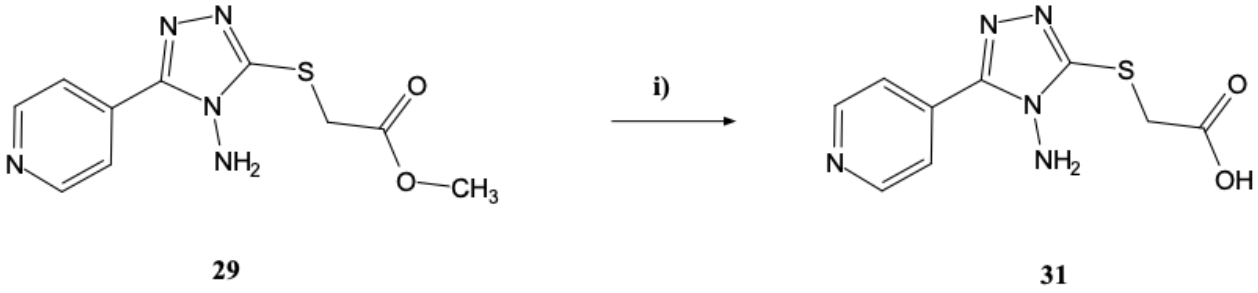

Scheme 2. Reagents and conditions: i) NaOH 0.5 M, reflux

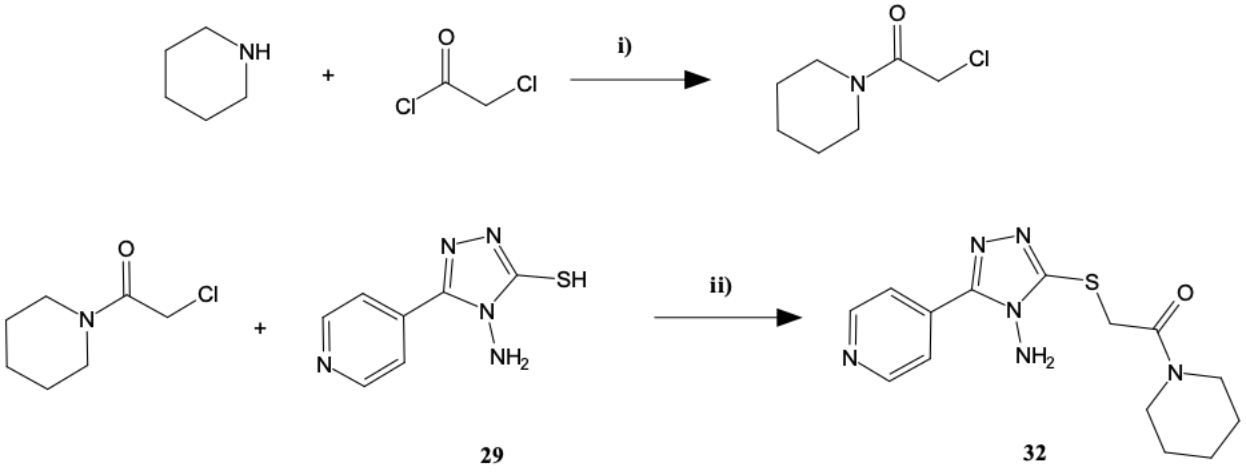

Scheme 3. Reagents and conditions: i) piperidine, 2-chloroacetyl chloride, triethylamine (TEA), MeOH, 0°C to rt; ii) 2-chloro-1-(piperidin-1-yl)ethan-one, NaOH, MeOH, rt

3.2.2 In vivo activity

Among the new synthesized compounds **28-30**, we choose to deepen the biological profile of ethyl 2-((4-amino-5-(pyridin-4-yl)-4H-1,2,4-triazol-3-yl)thio)acetate (**30**), as prototype of this series of potential neuroprotective agents, thus assessing its protective effect through behavioral measurements after the injection of 1-methyl-4-phenyl-1,2,3,6-tetrahydropyridine (MPTP). These studies were performed in collaboration with Prof. Rosanna Di Paola and coworkers. The studies were carried out following the experimental procedures that are detailed in experimental section. Specifically, to further explore the correlation between the degeneration of dopaminergic neurons MPTP-induced, and the recovery processes, we analyzed the motor activity 1 day prior and 8 days

after the MPTP induction. The data at time point 0 are not displayed as no significant differences were observed between the different groups.

With the Rotarod Test (RT), mice showed a significant motor disorder as indicated by a reduction in time spent on the apparatus and an increase in the number of falls. Treatment with compound **30** significantly reduced this motor dysfunction (Figure 27A). Moreover, the MPTP induced an important cataleptic effect in animals, especially at 8 days after MPTP injection, when the mice shown a significant rise of cataleptic symptoms. Importantly, the daily compound **30** administration significantly reduced the duration of MPTP-induced catalepsy (Figure 27B). In the Pole Test (PT), "total time" and "time to turn" significantly increased after MPTP injection compared with the Sham group. Compound **30** treatment at 10 mg/kg significantly reduced "total time" and "time to turn" suggesting that this compounds effectively prevents MPTP-induced bradykinesia (Figure 27C, C').

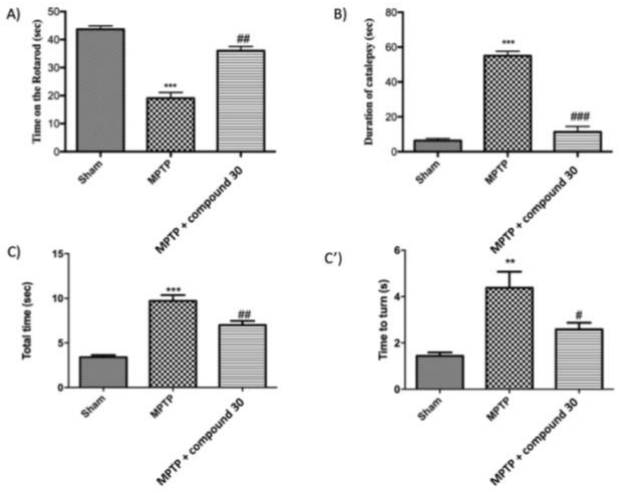

Figure 27. Effect of compound **30** on behavioral impairments induced by MPTP intoxication. (**A**) Rotarod test (RT) shown that at 8 days, mice exhibited a significant motor dysfunction as indicated by a decrease in time spent on the Rotarod apparatus. Compound **30** treatment relieved the motor dysfunction in mice. (**B**) Catalepsy test showed that compound **30** treatment reduced behavioral impairment induced by MPTP. (**C, C'**) Pole test (PT) displayed that at 8 days, mice exhibited a significant motor dysfunction as indicated by an increase in "Time to turn" and "Total time" spent to descend to the floor following injection of MPTP compared with the Sham group.

For compound **30** we also analyzed its ability to prevent MPTP-neurotoxin induced neurodegeneration. Among the alteration of PD-like markers, we examined the levels of *tyrosine hydroxylase* (TH), *dopamine active transporter* (DAT) and α-syn in the midbrain.

By immunohistochemical analysis, the expression of TH-positive neurons was significantly reduced 8 days after MPTP administration (Figure 28B, B', and D) compared to the Sham group

(Figure 28A, A', and D). Treatment with compound **30** enhanced the levels of this protein (Figure 28C, C', and D).

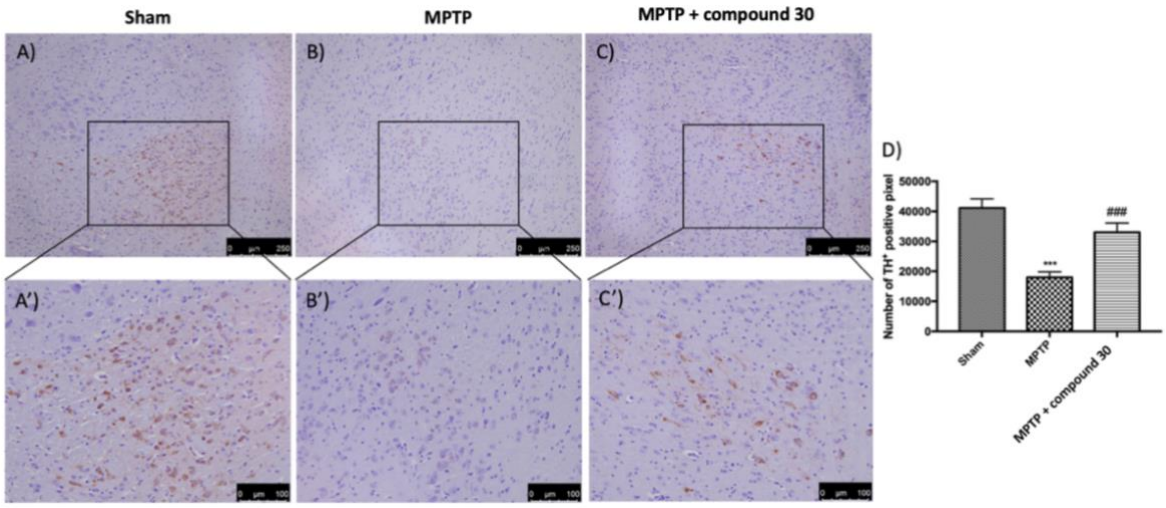

Figure 28. Effects of **30** on TH expression in midbrain of MPTP-treated mice. As results, compared to sham group (**A,A'**), the MPTP-treated mice exhibited loss of TH-positive cells (**B,B'**). Animals treated with compound **30** revealed an increase in TH expression (**C,C'**).

Subsequently, we confirmed the same results for DAT through Western blot analysis. In fact, it was observed that DAT expression significantly decreased after MPTP injection compared to the Sham group. Treatment with compound **30** led to an increase of DAT expression (Figure 29A, A').

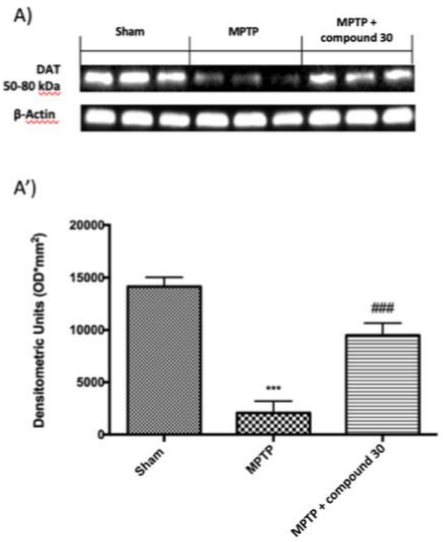

Figure 29. Effect of compound **30** treatment on DAT expression after MPTP-intoxication. Western blot analysis on midbrain region revealed a significant decrease in DAT in the MPTP group compared to sham animals. The treatment with compound **30** increased the DAT level (**A**).

Furthermore, it was observed a relevant immunoreactivity in MPTP-damaged mice (Figure 30B, B', and D) compared to sham animals with immunohistochemical analysis (Figure 30A, A', and D). On the other hand, compound **30** treatment significantly decreased α-synuclein expression in the midbrain after MPTP intoxication (Figure 30C, C', and D).[152]

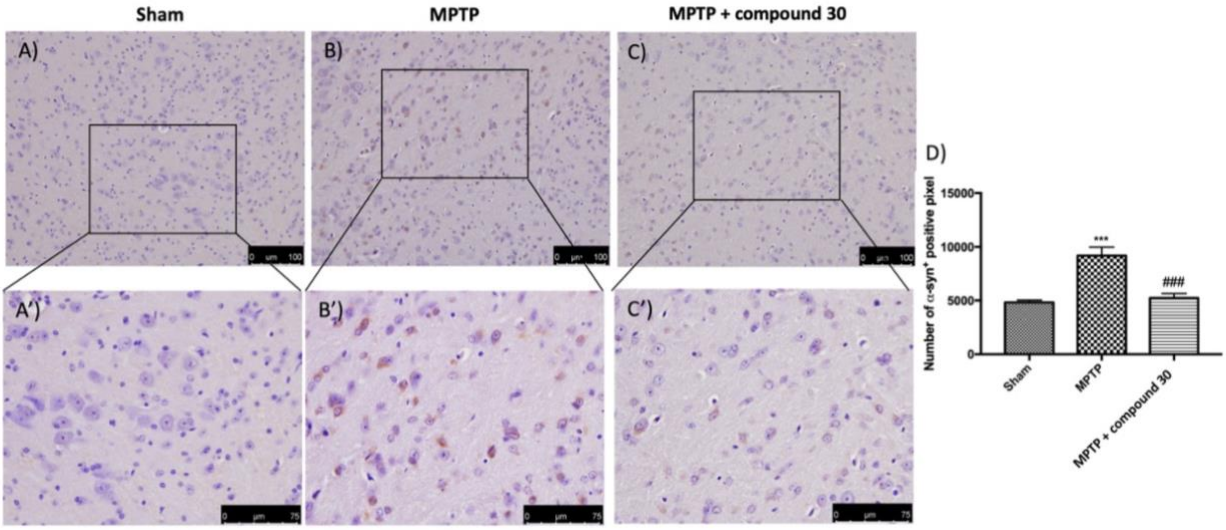

Figure 30. Effects of compound **30** on α-syn expression in midbrain of MPTP-treated mice. The positive staining for α-synuclein (**B,B'**) represented the MPTP-induced damage, compared with sham animals (**A,A'**). Compound **30** treatment appreciably reduced the α-synuclein staining (**C,C'**).

3.2.3 Biological screening of derivatives 27-30

Following the *in vivo* promising results demonstrated for representative compound **30**, we shifted our attention to evaluating its ability to reduce α-syn aggregation *in vitro*.

In collaboration with prof. Salvador Ventura from University of Barcelona we carried out the evolution of pyridinyl-triazole derivatives **27-30** by the same screening protocol previously applied using the potent inhibitor of α-syn aggregation SC-D. This compound was used as a reference molecule together the previously reported[150] benzyl derivative **26**.

We evaluated the kinetics of aggregation of 70 μM α-syn in the absence or presence of 100 μM of the tested compounds by following the increase in Thioflavin-T (Th-T) fluorescence (Figure 31A). Compounds **27** and **28** slightly accelerated the reaction, whereas the inhibitory effect of compound **30** was undistinguished from **26** (8 % reduction in Th-T signal), and compound **29** performed

slightly better (15 % reduction in Th-T signal). Light-scattering measurements at 300 nm at the end of the reaction indicated that **27**, **28**, **29**, and **30** decreased the aggregated α-syn levels in the solution (Figure 31B), with decrements of 44 %, 31 %, 18 %, and 18 %, respectively. The impacts of compounds **29** and **30** was comparable to **26** (21 %)[150]. The divergence between the influence of compounds **27** and **28** in Th-T and light scattering signals suggests that the aggregates formed in the presence of these molecules exhibit a higher affinity for Th-T, as they are probably richer in intermolecular β-sheet.

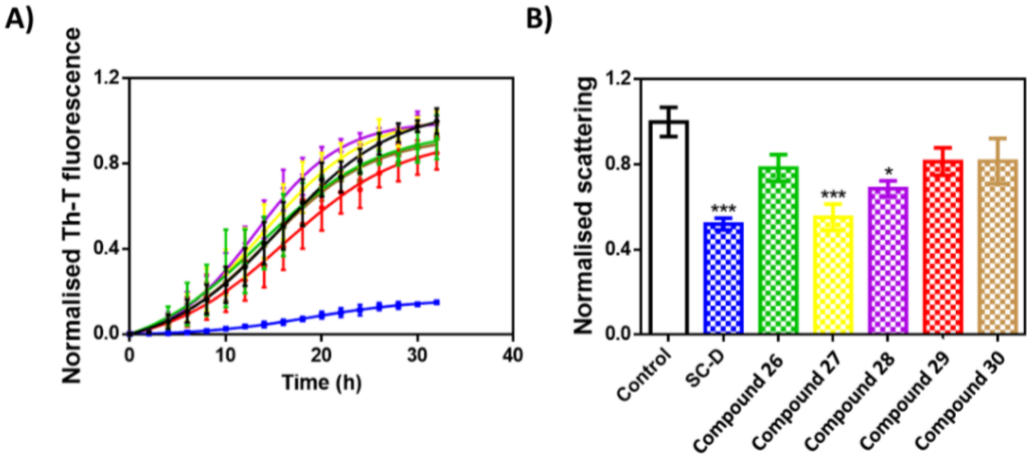

Figure 31. *In vitro* analysis of the capacity of the different compounds to inhibit α-Syn aggregation**.** (**A**) Aggregation kinetics of α-Syn in absence (black) or presence of 100 µM of compound **27** (yellow), compound **28** (violet), compound **29** (red) or compound **30** (brown) compared to previously described molecules **SC-D** (blue) and **26** (green). (**B**) Light-scattering measurements at 300 nm of end-point aggregates in absence (black) or presence of 100 µM of compounds **27-30**.

3.2.4 Ligand-based approach to identify new molecular entities

With the aim of extending our studies and identifying new scaffolds belonging to other chemical classes, we developed a computational protocol that provided new *'hit compounds*'.

Our research efforts were directed towards the identification new potential α-syn aggregation inhibitors structurally related to already reported active compounds. For this purpose, we used the web-tool SwissSimilarity by Swiss Institute of Bioinformatics to perform a similarity-based virtual screening (VS) procedure, which is a method based on the well-established premise that similar molecules may be predisposed to produce similar biological effects.[153] The free of charge SwissSimilarity platform (http://www.swisssimilarity.ch) can run a ligand-based virtual screening on large libraries of commercially available molecules including licensed drugs as well as bioactive compounds. The VS candidates are generally selected by applying two- and three-

dimensional research methods starting from a specific reference compound, according to the screening procedure information provided by the Swiss institute of Bioinformatics. [154, 155] In this case, two abovementioned inhibitors SC-D and ZPD-2 [146, 147] (see page 47, Figure 23) were chosen as reference structures, while the SPECS library, consisting of 326,000 commercially available small molecules, was selected for the search procedure. To evaluate the similarity between the reference molecules and the compounds included in the screening library, we applied three different virtual methods: FP2 fingerprints, Electroshape-5D and Spectrophores. The first one is a 2D similarity method which encodes linear molecular fragment paths up to 7 atoms into a 1024 bit string.[156] Instead, ElectroShape[157] and Spectrophores[158] are 3D similarity methods based on molecular shape complementarity; both methods do not require geometry alignment, allowing to make the VS process faster. In both methods, the molecular shape is described by 3D molecular parameters whose information is compressed into vectors.[155] The three methods were independently applied for each query molecule and the number of compounds achieved from each approach is reported in Table 4.

Query compounds	**FP2**	**Electroshape[a]**	**Spectrophores[b]**
SC-D	3	33	400
ZPD-2	2	400	400

Table 4. Number of hits obtained from the virtual screening runs employing SC-D and ZPD-2 as reference molecules [157a, 158b]

By using SC-D as query, the application of FP2 fingerprints resulted in the identification of three matches; whereas two matches were retrieved from ZPD-2 query compound. In contrast, the Electroshape method genereted thirty-three compounds whose Manhattan distance (MD) values varied from 0.861 to 0.707 in the case of SC-D reference compound. Instead, four-hundred hits, with a MD score ranging between 0.930 and 0.831 were achieved with the same approach starting from the inhibitor ZPD-2. In this case, we further filtered off the resulting hits according to the similarity score, selecting one hundred and seventy-eight molecules whose MD value was below 0.855. Finally, 400 hits were identified through the Spectrophore method for both compounds. The resulted hits fell in a similar range of MD values, that was comprised between 0.833 and 0.764 when using SC-D as reference and between 0.819 and 0.754 when using ZPD-2. Therefore, we applied the same MD cut-off value of 0.785 as pre-filter, resulting in thirty-nine compounds from ZPD-2 and one hundred eight hits from SC-D. A total of three hundred and sixty-three molecules

were selected from the LBVS runs for further evaluation. In particular, compounds with stereocenters or E/Z bonds whose configuration or geometry was not defined, were excluded. Regarding derivatives with similar scaffold, we selected compounds possessing highest similarity score. Finally, the residual molecules were filtered according to i) their drug-likeness characteristics measured by the Lipinsky rule of 5, ii) the absence of PAINS and iii) the commercial availability. The application of these filters resulted to the final selection of thirty-four compounds collected in Figure 32; among them, the first subset of twelve molecules (MeSC-1 – MeSC-12) was retrieved using SC-D as query molecule, while the second subset of twenty-two molecules (MeZP-1 - MeZP-22) was derived from ZPD-2. All candidates were purchased from SPECS supplier and tested in the Thioflavin-T fluorescence test and light scattering test to evaluate their ability to reduce α-syn aggregation as reported for SC-D and ZPD-2,[148, 159] that were used as reference compounds.

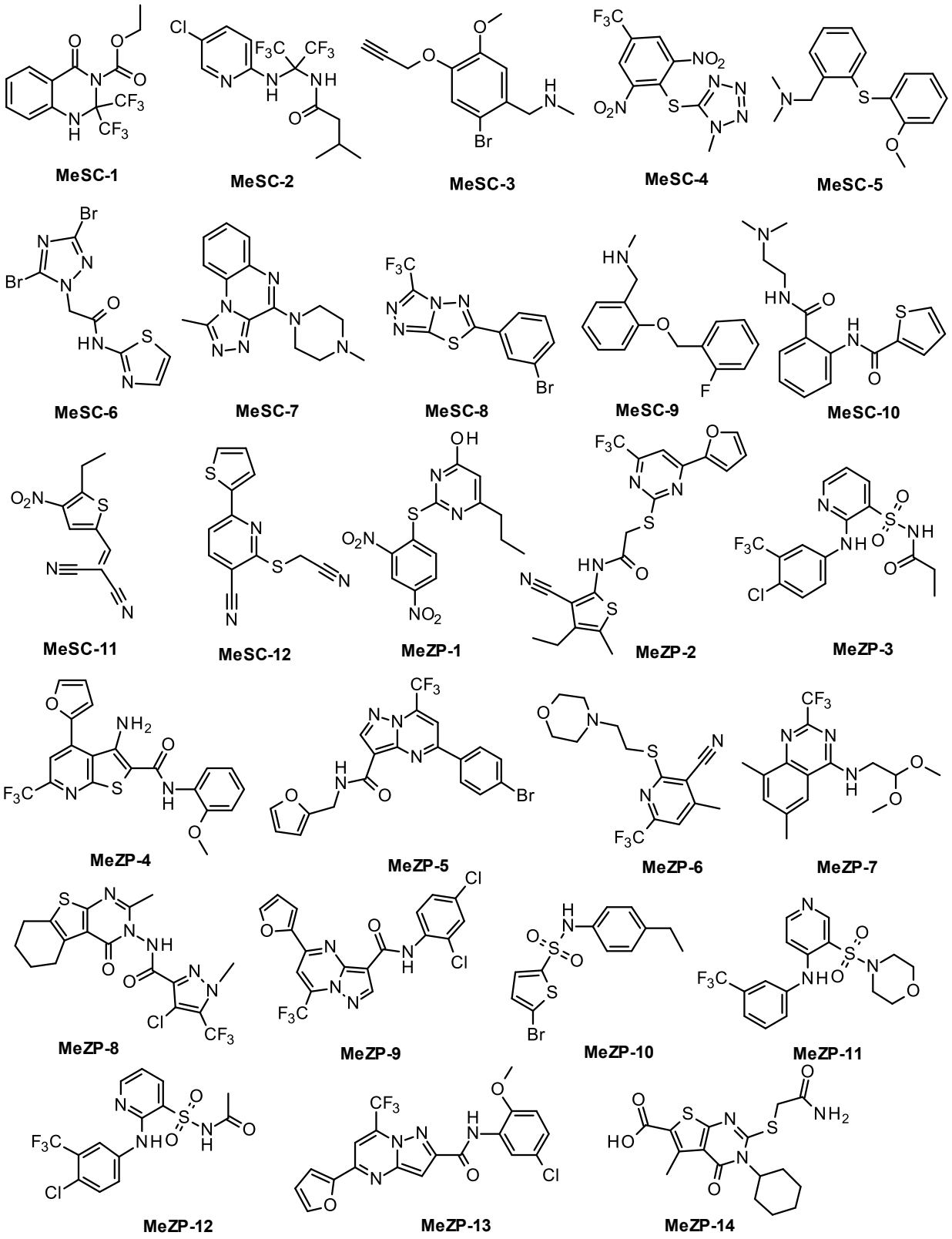

Figure 32. Chemical structures of compounds resulting from the VS employing as query SC-D (compounds MeSC-1 – MeSC-12) and ZPD-2 (compounds MeZP-1 - MeZP-22)

3.2.5 In vitro screening of resulting thirty-four compounds

To assess the inhibitory potential of the different compounds, we monitored the increase in Thioflavin-T (Th-T) fluorescence emission during the aggregation kinetics of 70 μM α-syn in the absence or presence of 100 μM of the molecules. The compound SC-D was used as a reference.

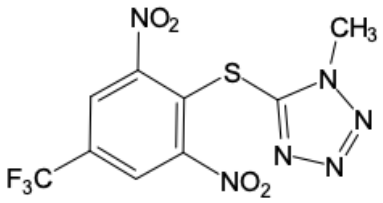

Figure 33. Chemical structure of best active compound MeSC-4

The 5-(2,6-dinitro-4-(trifluoromethyl)benzyl)-1-methyl-1H-tetrazole (MeSC-4, Figure 33) emerged as the best candidate, with a reduction of 69 % of Th-T fluorescence emission (Figure 34A). Moreover, the compound reduced the light-scattering by 20 % and 19 % at 300 and 340 nm, respectively (Figure 34B). In addition, also compound MeSC-12 showed to slightly reduce the Th-T fluorescence emission, while in the light-scattering measurement at 300 and 340 mn it exhibited a better profile than MeSC-4. Interestingly, compound MeSC-7 displayed the best results in the light-scattering analysis. Conversely, MeZP derivatives did not show a significant reduction of α-syn amyloid formation (Figure 35A). The best candidates of this subset, MeZP-1 and MeZP-16 reduced final point Th-T fluorescence by 26 and 32 %, respectively (Figure 35A). Regarding light-scattering, among all compounds, MeZP-1 significantly decreased the signal, around 50 and 58 % for 300 and 340 nm, respectively. Additionally, also compounds MeZP-14 and MeSC-20 presented interesting results with the reduction of light-scattering (Figure 35B). The absence of activity of MeZP-16 in the light-scattering assay may indicate the formation of alternative structures, such as amorphous aggregates. Overall, the *in vitro* screening exercise highlighted the MeSC-04 as the best molecule proving to be active as previously found for SC-D. Considering these results and the structural diversity of tested compounds, it was not possible to obtain information on *structure-activity relationship* (SAR).

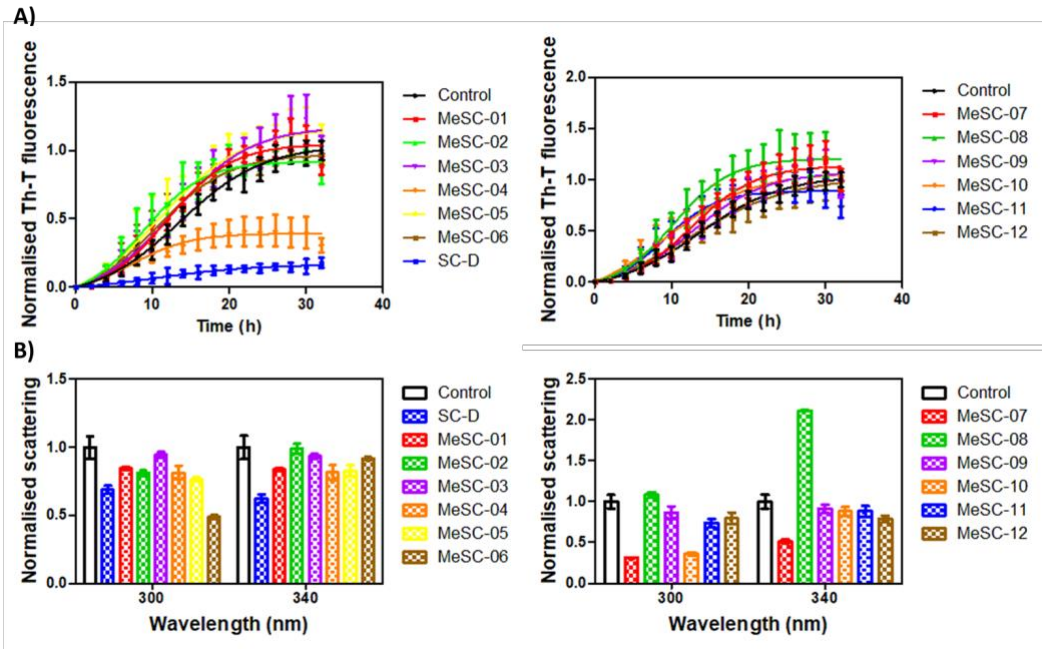

Figure 34. Inhibitory *in vitro* characterization of compounds MeSC-01 to MeSC-12. (A) Aggregation kinetics of α-Syn in the absence (black) or presence of 100 µM of the different compounds (colored) compared to SC-D (blue, left panel). (B) Light-scattering measurements at 300 and 340 nm of end-point aggregates in absence (black) or presence of 100 µM of the different compounds (colored) compared to SC-D (blue, left panel).

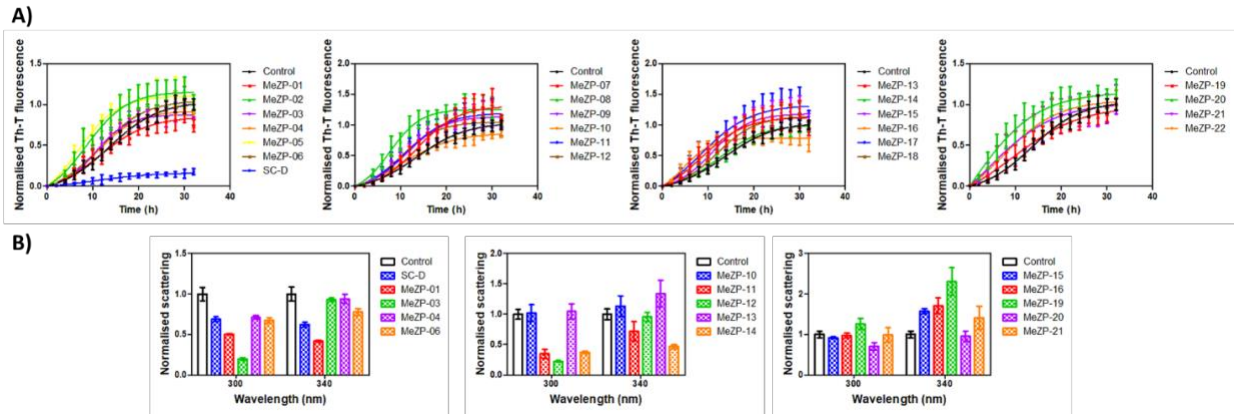

Figure 35. Inhibitory in vitro characterization of compounds MeZP-01 to MeZP-22. (A) Aggregation kinetics of α-Syn in the absence (black) or presence of 100 µM of the different compounds (colored). SC-D was used as reference (blue, left panel). Th-T fluorescence is plotted as a function of time. (B) Light-scattering measurements at 300 and 340 nm of end-point aggregates in absence (black) or presence of 100 µM of the different compounds (colored). SC-D was used as reference (blue, left panel).

3.2.6 Computational analysis of the MeSC-4 binding mode

To improve our knowledge about the binding mode of MeSC-4, for successful design guidance, additional computational studies were performed to carry out ligand pocket analysis and molecular docking. Several programs were developed to identify binding pockets or allosteric sites, classified according to the different type of algorithm used (docking-based, grid-based, and geometry-based algorithms). fPocket, SiteMap and FTMap were employed to estimate the druggability of α-syn fibrils for two three-dimensional structures available in the PDB databases (RCSB PDB: 2N0A[127] and 6FLT[160]). Different key amino acid residues, defined hot spots, were identified and clustered to obtain two ensemble consensus sites, namely site A and site B (Figure 36). Moreover, Table 2 describes all residues that constitute the two detected druggable binding sites.

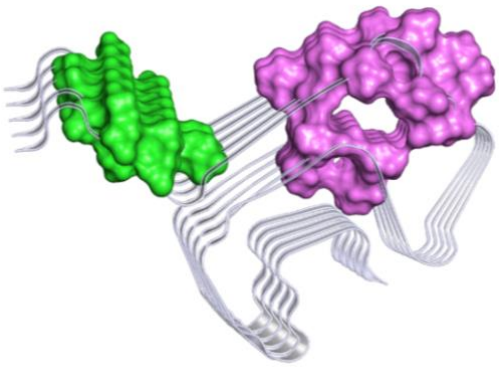

Figure 36. Two consensus druggable binding site: site A (magenta) and site B (green). The images were prepared by Pymol.[161]

The results obtained were compared with the data found in the literature.[146, 162-164] The comparative analysis displayed that site A resulted in high agreement with the previous described binding site of SC-D (Figure 37).[165] In detail, as displayed in Table 5 the amino acids Ala53, Val55, Thr59, Glu61, Thr72 and Gly73 were shown to be important for the interaction.[146] In addition, the amino acid residues Thr54, Ala56, Thr59, Glu61, Gly73, Val74 and Thr75 of chain B-C-D of Site A have recently been noted as key residues for Van der Waals and π-alkyl interactions between ulvan, a complex sulfated polysaccharide from green alga, and α-syn (Figure 38).[162] Furthermore, the site B was considered in a study of different putative binding sites on α-syn fibrils by molecular blind docking of small molecules and called as site 3/13, due to the fact that that the site 3 is contained in site 13 (Lys43, Lys45, Val48, and His50).[163] In addition, the binding of some derivatives of styryl aniline was studied and SAR analysis, further rationalized by molecular docking studies,

showed that H-bonds and cation-pi interactions with Lys43, Lys45 and Lys58 of chain B-C-D are decisive for binding. All these described residues are part of our site B (Figure 39).[164]

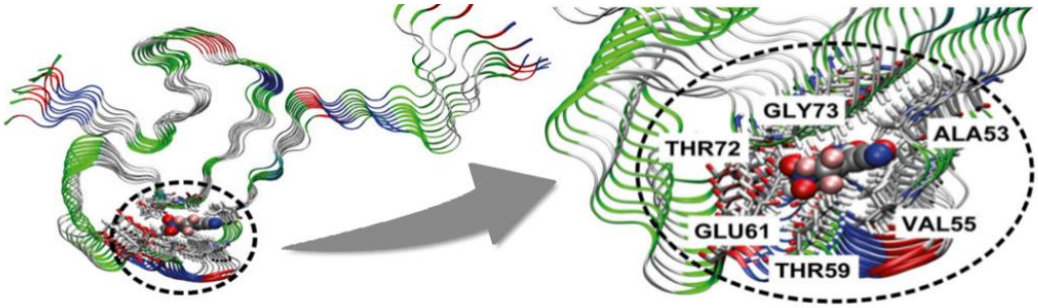

Figure 37. Binding mode of SC-D/fibrils interaction (PDB: 2N0A). Image retrieved from Pujols et al. 2018.

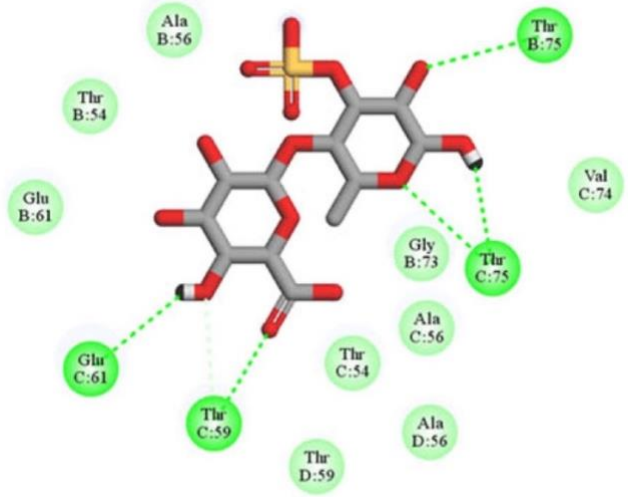

Figure 38. Binding mode of ulvan unit B_{3s} on α-syn pentamer. Light green spheres represent Van der Waals and π-alkyl interactions, while dark green spheres indicate H-bond (PDB: 6FLT). Image retrieved from Wang et al. 2022.

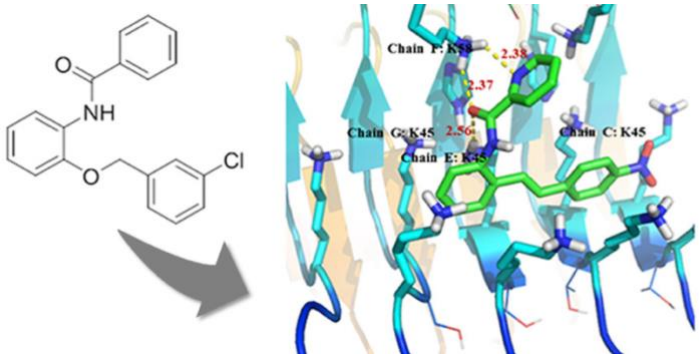

Figure 39. Binding mode styryl alanine derivative on α-syn aggregates (PDB: 6FLT). Lys43, Lys45 and Lys58 are involved into H-bond and cation-pi interactions. Image retrieved from Bian et al. 2021.

Putative binding sites	Residues
SITE A	VAL52A; ALA53A; THR54A; VAL55A; ALA56A; GLU57A; LYS58A; THR59A; LYS60A; GLU61A; VAL70A; VAL71A; THR72A; GLY73A; VAL74A; THR75A; THR92A; GLY51B; VAL52B; ALA53B; THR54B; VAL55B; ALA56B; GLU57B; LYS58B; THR59B; LYS60B; GLU61B; GLN62B; THR64B; VAL66B; VAL70B; VAL71B; THR72B; GLY73B; VAL74B; THR75B; ALA76B; THR92B; HIS50C; GLY51C; VAL52C; ALA53C; THR54C; VAL55C; ALA56C; GLU57C; LYS58C; THR59C; LYS60C; GLU61C; GLN62C; THR54C; VAL66C; ALA69C; VAL70C; VAL71C; THR72C; GLY73C; VAL74C; THR75C; ALA76C; THR92C; GLY93C; GLY51D; VAL52D; ALA53D; THR54D; VAL55D; ALA56D; GLU57D; LYS58D; THR59D; LYS60D; GLU61D; GLN62D; THR64D; VAL70D; VAL71D; THR72D; GLY73D; VAL74D; THR75D; ALA76D; THR92D; GLY51E; VAL52E; ALA53E; THR54E; VAL55E; ALA56E; GLU57E; LYS58E; THR59E; LYS60E; GLU61E; VAL70E; VAL71E; THR72E; GLY73E; VAL74E; THR75E.
SITE B	VAL40A; GLY41A; SER42A; LYS43A; THR44A; LYS45A; GLU46A; VAL48A; TYR39B; VAL40B; GLY41B; SER42B; LYS43B; THR44B; LYS45B; GLU46B; GLY47B; VAL48B; VAL49B; HIS50B; TYR39C; VAL40C; GLY41C; SER42C; LYS43C; THR44C; LYS45C; GLU46C; GLY47C; VAL48C; VAL49C; HIS50C; TYR39D; VAL40D; GLY41D; SER42D; LYS43D; THR44D; LYS45D; GLU46D; GLY47D; VAL48D; VAL49D; HIS50D; GLY41E; SER42E; LYS43E; THR44E; LYS45E; GLU46E; VAL48E; VAL49E; HIS50E.

Table 5. List of all the residues constituting the identified binding sites defined to include residues within 15 Å of any centroid of Fpocket results for protein 2N0A.

After validating the results obtained from the analysis of putative binding sites, the binding mode of compound MeSC-4 was investigated. In order to select one of the two fibril crystal structures as target for docking studies, we evaluated their quality by Ramachandran plot through PROCHECK.[166] The evaluation data indicated that 2N0A was the preferred structure with 85.1% of residues in the most favored region. Molecular docking studies were performed using three different software, such as Autodock V4.2.6,[167] Glide-v9.3[88, 168] and Gold 2020.3.0[169] on both abovementioned putative binding sites A and B. For each software, the first 10 clusters were selected according to docking value and submitted to a consensus docking methodology to get clusters populated by poses generated by different software with a Root-Mean-Square Deviation (RMSD) value just below 2.0 Å. Therefore, hierarchical clustering using the rms_analysis tool of any clusters was found at site B. Consequently, it was assumed that MESC-4 could only bind Site A on α-syn fibrils. Then, MM-GBSA free energy calculations were carried out to obtain quali-

quantitative estimations of the binding free energies of different MESC-4 poses retrieved from molecular docking studies. The pose with lowest free energy was selected to evaluate protein-ligand interactions through Maestro. In detail, the compound MeSC-4 bound to site A through Van der Waals and H-bond interactions with residues from Ala53 to Val74. In addition, MESC-4 also showed the formation of H-bond interactions between Gly73 of chain A and the tetrazole ring and H-bond between Thr59 of chain C and nitro-group. Finally, additional Van der Waals interactions were observed from the amino acids Ala53, Val55, Thr59, Glu61, Gly73, Val74 (Figure 40). Interestingly, these data were congruent with the network of interactions suggested for SC-D docked into the NAC domain of α-syn fibrils.

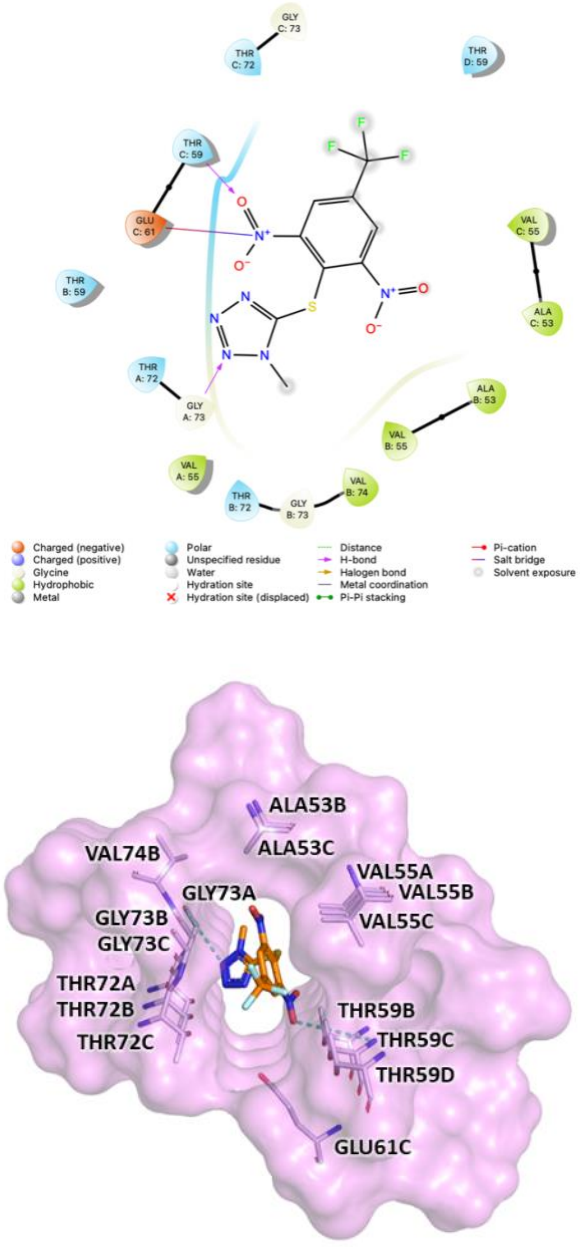

Figure 40. Binding mode of compound MESC-4. The image is created by PyMOL software.

3.2.7 Design and synthesis of new derivatives of compound MeSC-4

Prompted by the above reported findings, the compound MeSC-4 was considered as a lead compound for the design of a new set of potential α-syn aggregation inhibitors. The structural modifications on MeSC-4 were directed to improve its chemical-physical properties.
Using a rational approach, four different molecules were designed and synthesized as described in Figure 41.

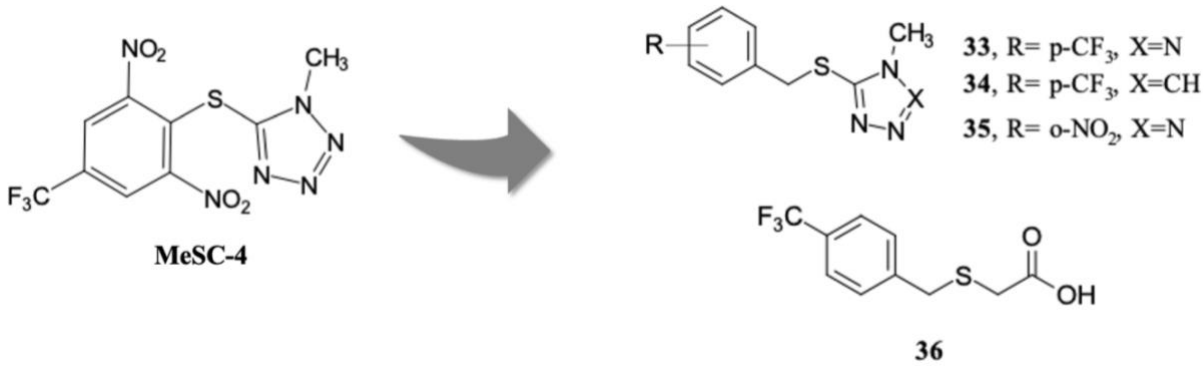

Figure 41. Structural modification on lead compound MeSC-4 to achieve the benzyl thioether derivatives **33-36**

In detail, we replaced the phenyl thioether fragment with a benzyl thioether one, thus extending the linking moiety. For compounds **33** and **35**, we retained the tetrazole ring with the methyl substituent. In the case of compound **36**, we modified the tetrazole portion, with the carboxyl group. However, for compound **34**, we replaced the tetrazole with a triazole, thus removing a nitrogen atom from the cyclic structure. Regarding the substituents on the aromatic ring, in order to assess whether the two nitro groups and the CF_3 group are essential for biological activity, in the design of compounds **33-34** and **36** we decided to keep CF_3 in para to the aromatic ring, while for compound **36** we removed p-CF_3 by replacing it with an -NO_2 in ortho position.

Compounds **33-35** were obtained by following synthetic pathway A described in Scheme 4. The 1-methyl-1H-1,2,3,4-tetrazole-5-thiol (X=N) for compounds **33** and **35** and 4-methyl-4H-1,2,4-triazole-3-thiol (X=CH) for compound **34** ware coupled with an opportune benzyl bromide in alkaline medium at room temperature as previously reported by us.[150] Compound **36** was obtained following the synthetic pathway B described in Scheme 4. The ethyl-2-sulfanylacetate was combined with 4-(trifluoromethyl)benzyl chloride in alkaline medium for K_2CO_3 at room temperature. The reaction environment led to basic hydrolysis, resulting in the corresponding carboxylic derivative. The resulting compounds were sent to Prof. Ventura's research group for *in vitro* biological screening, in order to obtain further data on their pharmacological activity and

potential use as drugs. Unfortunately, these compounds proved to be no active agents through Thioflavin-T (Th-T) fluorescence emission assay and light-scattering measurements.

These results suggested that some structural modifications such as the introduction of benzyl moiety instead of phenyl one negatively affected the recognition process with α-syn fibrils. Moreover, the presence of two -NO_2 and the -CF_3 groups on aromatic ring found in MeSC-4, SC-D and ZPD-2 proved to be essential for biological activity.

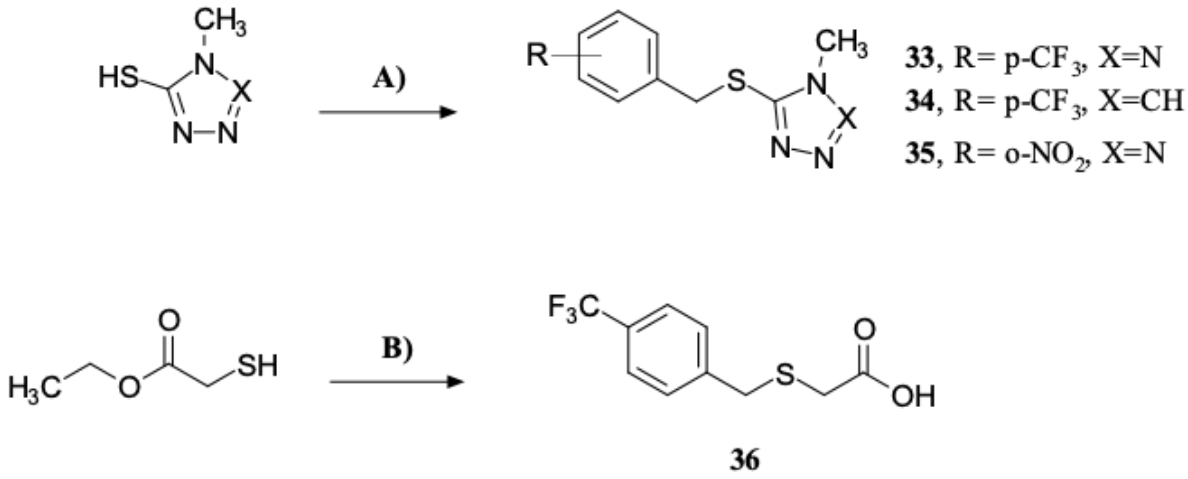

Scheme 4. Reagents and conditions: A) suitable benzylchloride, 1-methyl-1H-1,2,3,4-tetrazole-5-thiol or 4-methyl-4H-1,2,4-triazole-3-thiol, NaOH, MeOH, rt; B) 4-(trifluoromethyl)benzyl chloride, ethyl-2-sulfanylacetate, K_2CO_3, MeOH, rt.

3.2.8 Comments and remarks

Overall, these studies indicated that the inhibition of α-syn aggregation by new small molecules represents a useful approach against neurodegenerative disorders in the medicinal chemistry field.

We explored the 5-(4-pyridinyl)-4*H*-1,2,4-triazole scaffold, given its promising activity previously reported.[150] In detail, the new studies evidenced that in the immunohistochemical assays compound **30** proved to increase levels of TH and DAT in the midbrain of animals treated with neurotoxin MPTP; furthermore, this molecule demonstrated to reduce the α-syn expression in the same test. Moreover, motor deficit in MPTP-treated mice has been reduced by compound **30**. This compound demonstrated to affect fibrillization in *in vitro* assay.[152]

By applying an *in silico* procedure, we have identified the 5-(2,6-dinitro-4-(trifluoromethyl)benzyl)-1-methyl-1*H*-tetrazole (MeSC-4) as a potent *in vitro* α-syn aggregation inhibitor, which could represent a 'lead compound' for the development of new inhibitors in PD

therapy. MeSC-4 showed the same inhibitory activity of SC-D in the preliminary Th-T fluorescence assay. These results provided interesting information for developing a small series of new compounds, thus expanding our knowledge of the SAR of the NAC domain. The performed structural modifications made on MeSC-4 to refine its physicochemical properties and bioavailability in the central nervous system, did not produce biologically active compounds in the Th-T fluorescence and light-scattering assays. However, the collected structure-activity relationship data, indicated the minimum structural requirements of MeSC-4 that should be maintained in a future design.

3.3 Experimental section

3.3.1 Chemistry

All reagents were purchased from commercial suppliers (Merck KGaA and Thermofisher Scientific Inc.) and were used without further purification. For the determination of melting points of synthetized compounds, a Buchi B-545 apparatus (BUCHI Labortechnik AG Flawil, Switzerland) was used; we determined melting points with a permissible error range uncorrected by calibration. The purity of synthetized compounds was determined by combustion analysis (C, H, N) (Carlo Erba Model 1106-Elemental Analyzer); the results confirmed a ≥95% purity. Thin-layer chromatography was performed on Merk TLC plates (Silica gel 60 F254, 10 x 15). Chromatograms were visualized by UV light or by staining with iodine vapor and ninhydrin solution. ^{1}H-NMR and ^{13}C-NMR spectra were measured in dimethylsulfoxide-d$_6$ (DMSO-*d*$_6$) or deuterochloroform ($CDCl_3$-*d*) with a Varian Gemini 500 spectrometer (Varian Inc. Palo Alto, California USA) and chemical shifts are quoted in δ (ppm) and coupling constants (*J*) in Hertz. All exchangeable protons were confirmed by addition of D_2O.

3.3.2 General procedure for synthesis of pyridinyl-triazole derivatives (28-32)

Pathway A: The 4-amino-5-(4-pyridinyl)-4H-1,2,4-triazole-3-thiol (**27**, 250 mg, 1.29 mmol) were dissolved in MeOH (5 mL) with NaOH (51 mg, 1.29 mmol) and the suitable alkyl halide (1 molar equivalent). The S-alkylation was performed according to the experimental procedure previously reported to obtain desired final compound **28-30**.[150,152] The structural chemical assignment for

compounds **28** and **30** has been confirmed by means ^{1}H-NMR spectra and their spectral data were in good agreement with those that are already reported in literature.[170,171]

Pathway B: The methyl 2-((4-amino-5-(pyridin-4-yl)-4H-1,2,4-triazol-3-yl)thio)acetate (**29,** 150 mg, 0.56 mmol) was added to a 0.5 M NaOH solution and the reaction was stirred under reflux for 1 hour. The precipitate was filtered, dried with anhydrous Na_2SO_4 and recrystallized from Et_2O/EtOH to obtain the carboxylic derivative **31**.

Pathway C: Piperidine (0.173 mL 1.76 mmol) and 2-chloroacetyl chloride (0.140 mL ,1.76 mmol) were dissolved in methanol (5 mL) and triethylamine (293 mL, 2.11 mmol) was added. The reaction was kept at 0°C for about 30 minutes and then at room temperature. Subsequently, the collected intermediate was dissolved in MeOH (5 mL) and reacted with 4-amino-5-(4-pyridyl)-1,2,4-triazol-3-thiol (**27**, 250 mg, 1.29 mmol) and NaOH (51 mg, 1.29 mmol) to obtain compound **32** according to the experimental procedure previously reported.[150,152]

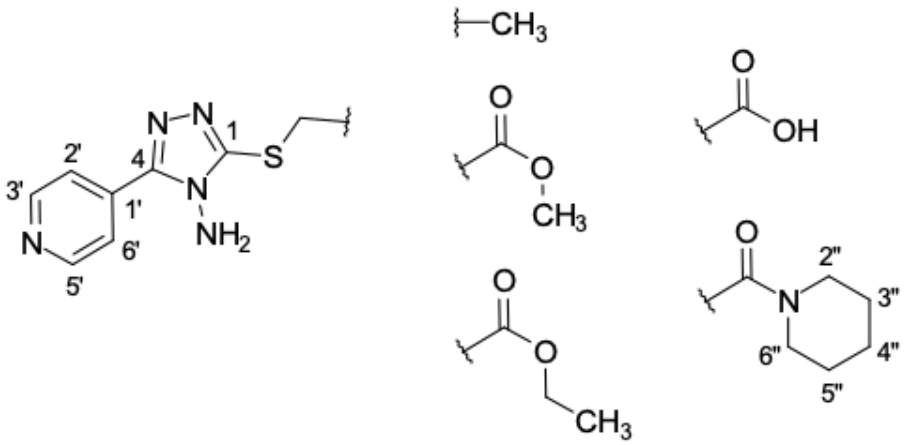

- ***3-(Ethylthio)-5-(pyridin-4-yl)-4H-1,2,4-triazol-4-amine (28)***

CAS number: 901096-40-0; Yield: 72.5%; white powder; m.p.: 125-127°C; ^{1}H-NMR (500 MHz, DMSO-d6): (δ) 1.36 (t, J= Hz, 3H, CH_3), 3.16-3.21 (m, 2H; CH_2), 6.21 (bs, 2H, NH_2), 7.99-8.01 (m, 2H, Ar-H2'and 6'), 8.71-8.72 (m, 2H, Ar-H3'and 5'); Anal. for ($C_9H_{11}N_5S$): C, 48.85%; H, 5.01%; N, 31.65%; Found: C, 48.70%; H, 5.16%; N, 31.50%

- ***Methyl 2-((4-amino-5-(pyridin-4-yl)-4H-1,2,4-triazol-3-yl)thio)acetate (29)***

CAS number: 150535-95-8; Yield: 38%; white powder; m.p.: 190-192 °C; ^{1}H-NMR (500 MHz, DMSO-d6): (δ) 3.66 (s, 3H, CH_3), 4.12 (s, 2H; CH_2), 6.31 (bs, 2H, NH_2), 7.96-7.97 (m, 2H, Ar-H2'and 6'), 8.71-8.72 (m, 2H, Ar-H3'and 5'); ^{13}C NMR (126 MHz, DMSO-d_6) (δ) 33.20 (CH_2), 52.92 (CH_3), 121.74 (C2', C6'), 134.28 (C1'), 150.57 (C3', C5'), 152.59 (C4), 154.85 (C1), 169.39

(C=O); Anal. for ($C_{10}H_{11}N_5O_2S$): C, 45.27%; H, 4.18%; N, 26.40%; Found: C, 45.42%; H, 4.03%; N, 26.55%

- ***Ethyl 2-((4-amino-5-(pyridin-4-yl)-4H-1,2,4-triazol-3-yl)thio)acetate (30)***

CAS number: 39875-99-5; Yield: 55%; white powder; m.p.: 180-82 °C; ^{1}H-NMR (500 MHz, DMSO-d6): (δ) 1.18 (t, J= 7.05 Hz, 3H, CH_3), 4.10 (s, 2H; CH_2), 4.11 (q, J= 7.05 Hz, 2H, CH_2), 6.34 (bs, 2H, NH_2), 7.96-7.97 (m, 2H, Ar-H2'and 6'), 8.70-8.71 (m, 2H, Ar-H3'and 5'); Anal. for ($C_{11}H_{13}N_5O_2S$): C, 47.30%; H, 4.69%; N, 25.07%; Found: C, 47.15%; H, 4.84%; N, 24.92%.

- ***2-((4-amino-5-(4-pyridin-4-yl)-4H-1,2,4-triazol-3-yl)sulfanyl)acetic acid (31)***

CAS number: 150536-07-5; Yield: 90%.; yellow powder; m.p.: 235-236 °C; ^{1}H-NMR (500 MHz, DMSO-d6): (δ) 2.1 (*s,* 2H, CH_2), 4.1 (*s,* 2H, NH_2), 8.02 (*d, J*= 6.04 Hz*,* 2H, Ar-H2'and 6'), 8.75 (*d, J*= 6.04 Hz*,* 2H, Ar-H3'and 5'), 12.9 (*bs*, 1H, OH). ^{13}C-NMR (126 MHz, DMSO-d_6): (δ) 44.25 (CH_2), 121.5 (C2', C6'), 133.04 (C1'), 147.3 (C4), 150.03 (C3', C5'), 150.2 (C1), 167.65 (CO). Calc.Anal. for $C_9H_9N_5O_2S$: C, 43%; H, 3,6%; N, 27,9%. Found: C, 43.3 %; H, 3.7%; N, 27. 5%.

- ***2-((4-amino-5-(4-pyridin-4-yl)-4H-1,2,4-triazol-3-yl)sulfanyl)-1-(1-piperidil)etanone (32)***

CAS number: 786671-63-4; Yield: 18%; white powder; m.p.: 181-182 °C; ^{1}H-NMR (500 MHz, DMSO-d6): (δ) 1.44 (*m*, 2H, CH_2-4"), 1.57 (*m*, 4H, CH_2-3" e 5"), 3.45 (*m*, 4H, CH_2-2" e 6"), 4.29 (s, 2H, CH_2), 6.31 (s, 2H, NH_2), 8.01 (*d*, *J*= 6.11 Hz, 2H, Ar-H2' and H6'), 8.73 (*d*, *J*= 6.11, 2H, Ar-H3' and H5'). ^{13}C-NMR (126 MHz, DMSO-d_6): (δ) 23.8 (C4"), 25.2 (C3", C5"), 36.0 (CH_2), 42.5 (C2", C6"), 121.3 (C2'-6'), 134.0 (C1'), 150.1 (C3'-5'), 151.8 (C1), 154.6 (C4), 165.0 (CO). Calc.Anal. for $C_{14}H_{18}N_6OS$: C, 52,8%; H, 5,7%; N, 26,4%. Found: C, 53.2 %; H, 5.5 %; N, 26.2 %.

3.3.3 In vivo studies

The *in vivo* experiments on neurodegenerative diseases with compound **30** at a dose of 10 mg/kg, after a preliminary dose–response study, were performed according to the experimental procedure reported.[152]

3.3.4 General procedure for the synthesis of MeSC-4 derivatives

The thiol derivatives, 1-methyl-1H-1,2,3,4-tetrazole-5-thiol, 4-methyl-4H-1,2,4-triazole-3-thiol and the ethyl-2-sulfanylacetate (1.29 mmol) were dissolved in methanol (5 mL) and was reacted with NaOH (51 mg, 1.29 mmol) and the corresponding benzyl chloride (1.29 mmol) according to the experimental procedure previously reported to retrieved the benzyl thioether derivatives **33-36**.[150,152]

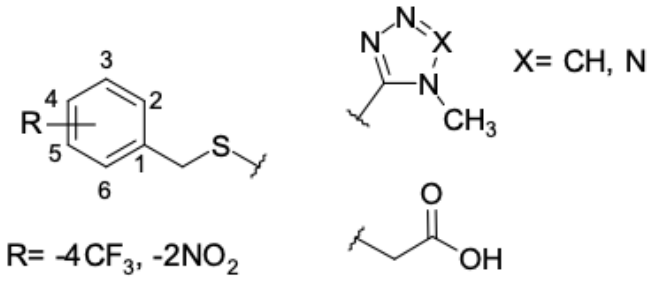

- ***1-Methyl-5-[[4-(trifluoromethyl)phenyl]methylsulfanyl]tetrazole (33)***

Yield: 30%; white powder; m.p.: 81-82 °C; ^{1}H-NMR (500 MHz, DMSO-d6): (δ) 3.87 (s, 3H, CH_3.), 4.61 (s, 2H, CH_2), 7.64 (d, J= 8.3 Hz, 2H, Ar-H2 and H6), 7.69 (d, J= 8.3 Hz, 2H, Ar-H3 and H5). ^{13}C-NMR (126 MHz, DMSO-d6): (δ) 33.6 (CH_3), 35.8 (CH_2), 124.0 (d, J_{C-F}= 271.4 Hz, CF_3), 125.3 (q, J_{C-F}= 3.8 Hz, Ar-C3 and C5), 128.1(d, J_{C-F} = 31.9 Hz, Ar-C4) 129.8 (Ar-C2-6), 141.8 (Ar-C1), 152.9 (C-tetrazole). Calc. Anal. for $C_{10}H_9F_3N_4S$: C, 43.80%; H, 3.30%; N, 20.40%. Found: C, 43.78%; H, 3.32%; N, 20.42%.

- ***4-Methyl-3-[[4-(trifluoromethyl)phenyl]methylsulfanyl]-1,2,4-triazole (34)***

Yield: 13%; white powder; m.p.: 48-49 °C; 1H-NMR (500 MHz, $CDCl_3$-d): (δ) 3.31 (s, 3H, CH_3), 4.32 (s, 2H, CH_2), 7.34 (*d*, *J*= 8.4 Hz, 2H, Ar-H2 e H6), 7.42 (*d*, *J*= 8.4 Hz, 2H, Ar-H3 e H5), 8.06 (s, 1H, CH, triazole). ^{13}C-NMR (500 MHz, $CDCl_3$-d): (δ) 30.9 (CH_3), 37.4 (CH_2), 124.0 (d, J_{C-F}= 272.4 Hz, CF_3), 125.7 (Ar-C3 e C5), 129.4 (Ar-C2 e 6), 130.1 (Ar-C4), 145.3 (CH-triazole), 149.8 (C-triazole). Calc. Anal. For $C_{11}H_{10}F_3N_3S$: C, 48.3%; H, 3.7%; N, 15.4%. Found: C, 48.0%; H, 4.0%; N, 15.0%.

- ***1-Methyl-5-[[2-nitrophenyl]methylsulfanyl]tetrazole (35)***

Yield: 90%; white powder; m. p.: 86-87 °C; ^{1}H-NMR (500 MHz, DMSO-d_6): (δ) 3.86 (*s*, 3H, CH_3), 4.79 (*s*, 2H, CH_2), 7.57-7.62 (*m*, 1H, Ar-H4), 7.69-7.74 (*m*, 2H, Ar-H5 e H6), 8.09 (*d*, *J*= 8.78 Hz, 1H, Ar-H3). ^{13}C-NMR (126 MHz, DMSO-d_6): (δ) 33.7 (CH_3), 34.3 (CH_2), 125.2 (Ar-

C3), 129.6 (Ar-C4), 132.1 (Ar-C6), 132.6 (Ar-C5), 135.2 (Ar-C1), 147.7 (Ar-C2), 153.0 (C-tetrazole). Calc. Anal. For $C_9H_9N_5O_2S$: C, 43.0%; H, 3.60%; N, 27.90%. Found: C, 43.02%; H, 3.59%; N, 27.92%.

- ***2-[[4-(Trifluoromethyl)phenyl]methylsulfanyl] acetic acid (36)***

Yield: 12%; white powder; m. p.: 226-227 °C; ^{1}H-NMR (500 MHz, DMSO-*d*$_6$): (δ) 2.87 (*s*, 2H, CH_2), 3.80 (*s*, 2H, CH_2), 7.52 (*d*, *J*= 8.1 Hz, 2H, Ar-H2 e H6), 7.63 (*d*, *J*= 8.1 Hz, 2H, Ar-H3 e H5). ^{13}C-NMR (126 MHz, DMSO-*d*$_6$): (δ) 34.7 (CH_2), 36.9 (CH_2), 124.4 (*d*, $J_{C\text{-}F}$ = 272.3 Hz, CF_3), 125.0 (*q*, $J_{C\text{-}F}$ = 3.8 Hz, Ar-C3-5), 172.6 (C=O), 144.4 (Ar-C1), 129.6 (Ar-C2-6), 127.2 (*q*, $J_{C\text{-}F}$ = 32.1, Ar-C4). Calc. Anal. For $C_{10}H_9F_3O_2S$: C, 48.00%; H, 3.60%. Found: C, 48.02%; H, 3.58%.

3.3.5 Ligand-based virtual screening procedure

To find new chemical entities that might be structurally similar to the two selected α-syn inhibitors SynuClean-D and ZPD-2, a ligand-based virtual screening (LBVS) was carried out. In more details, we adopted a similarity-based search web-tool, SwissSimilarity (http://www.swisssimilarity.ch)[154] for screening molecules from SPECS database (https://www.specs.net). Three different methods were independently employed to evaluate the similarity between the query molecules and those contained in the search database: FP2 fingerprints, Electroshape and Spectrophore. While the first one is a 2D approach, the latter is based on the 3D structure of the molecules. The hits obtained by the LBVS runs were ranked according to a similarity score corresponding to the Tanimoto score for the FP2 fingerprints, and to the Manhattan-based distance for Spectrophores and Electroshape approaches. Both scores can assume values between 0 and 1. A value of 0 indicates totally dissimilar molecules, while a value equal to 1 implies identical compounds.

3.3.6 Protein preparation of α-syn fibrils

The structure of *α*-syn fibrils (RCSB PDB: 2N0A) was modified via Pymol (https://pymol.org), and the amino acids between Leu38 and Val95 were retained. The PDB 6FLT was modified by retaining only the chains of one monomer (chains A; C; E; G; I). Then, we performed the alignment of 6FLT on 2N0A to obtain overlapping results through the software Pymol.

To get information about the flexibility of the selected structures, the RMSD values were calculated by Schrödinger 2021-4 considering the C-alpha compared with the reference protein structure 2N0A. Therefore, the RMSD value of 5.89 Å was obtained for 6FLT.

3.3.7 Analysis of the potential binding sites

To determine the different cavities on the α-syn fibrils, three programs FTMap, fPocket and SiteMap were used.

The FTMap web server (https://ftmap.bu.edu) is an open-source mapping server that provides direct information about binding hot spots, druggability, and fragment-based drug discovery. The method distributes 16 small organic probe molecules of various shapes, sizes, and polarities on a macromolecule surface to define hot spots through conformational and spatial searches, clustering procedures, and evaluation the probe's interaction energy over a dense grid using an empirical energy function including a continuum electrostatic term. Hot spots are smaller regions of proteins capable of contributing significantly to the binding of a drug to the binding site, and their strength describes the druggability of the site.[172]

SiteMap is a module implemented in Schrodinger capable of identifying potential binding sites and predicting their druggability. SiteMap uses the interaction energies between the grid probes and the protein to search for favorable binding sites. To classify each site, there is a series of physical descriptors that are used. These include (i) the size of the site calculated from the number of site points, (ii) the degree of closure by the protein, (iii) solvent exposure, (iv) the tightness between the site points and the protein, (v) the hydrophobic and hydrophilic character of the site, and (vi) the ability with which a ligand is capable to donating or accepting hydrogen bonds. Finally, an overall SiteScore is calculated using a linear combination of terms based on the above factors.[173]

fPocket (version 2.0) is an open source program capable of detecting potential binding sites using Voronoi tessellation and sequential clustering steps. The method employs α-spheres to analyze the protein surface. An α-sphere is a sphere in contact with four atoms on its boundary, containing no inner atom inside. For a protein, very small spheres are found on the inside of the protein, while large spheres are found on the outside. Clefts and cavities coincide with spheres of intermediate radii.[174]

fpocket is based on three main steps. During the first step the whole set of alpha spheres is determined from the protein structure and a pre-filtered set of spheres is obtained. The second step

involves identifying groups of spheres close to each other so as to identify pockets and remove all clusters of low interest. The last step involves estimating the properties of pocket atoms, for the purpose of score each pocket.[175]

3.3.8 Molecular docking of MeSC-4

The binding mode of MESC-4 was investigated using three different software using the 3D coordinates of the NMR structure of the fibrils of the protein α-syn (RCSB PDB: 2N0A). In this study, docking procedures were carried out: Autodock 1.5.7, Glide with Extra precision method (XP) and GOLD with the ChemScore fitness function. In addition, in the analysis conducted through GOLD, the "allow early termination" command was deselected, and poses that had an RMSD value of less than 0.75 Å were clustered. All setting parameters have been kept by default. For all the docking protocol, the binding cavity was defined to include all residues within 10 Å of the centre. For each site, centroid coordinates were calculated from fPocket outputs using Discovery Studio Visualizer. In detail, the centroid of coordinates x=115.647963, y=142.554128 and z=-35.965229 was used to define site A, while a box having centre coordinates x=92.100174, y=140.774522 and z=-19.706261 was used to delineate site B.
The structure of MESC-4 was built and minimized according to the Ammp calculation method implemented in Vega ZZ and was subjected to 100 runs in each molecular docking analysis.[176]

3.3.9 Consensus docking and Prime MM-GBSA

The 10 top-ranked docking poses obtained from the three different docking programs were selected and subjected to a hierarchical clustering procedure. The RMSD value of each docking pose compared with the others was calculated using rms_analysis software from the suite Gold. The group_average method was used as a hierarchical clustering algorithm and the poses were corresponding if they had an RMSD value less than 2.0 Å. Therefore, only clusters populated by the poses generated by at least two molecular docking software were selected. Subsequently, the poses belonging to the most populated cluster were submitted to binding free energy calculation by Molecular Mechanics-Generalized Born Surface Area (MM-GBSA) computational method performed using the Prime MM-GBSA module of the Schrödinger suite. This method combines molecular mechanics energy and continuum solvation models. Although the MM/GBSA method cannot predict experimental binding free energies with absolute accuracy, it is a very efficient

method for producing a good ranking of experimental values.[177] In this analysis, the VSGB solvation model and OPLS4 as force field were used to perform MM-GBSA calculations.

3.3.10 In vitro studies

Aggregation and α-synuclein inhibition *in vitro* assays using ThT fluorescence and light scattering measurements were performed in accordance with the reported experimental procedures.[150,152]

4 References

(1) Mabonga, L.; Kappo, A. P. Protein-protein interaction modulators: advances, successes and remaining challenges. *Biophys Rev* **2019**, *11* (4), 559-581. DOI: 10.1007/s12551-019-00570-x.

(2) Stevers, L. M.; Sijbesma, E.; Botta, M.; MacKintosh, C.; Obsil, T.; Landrieu, I.; Cau, Y.; Wilson, A. J.; Karawajczyk, A.; Eickhoff, J.; et al. Modulators of 14-3-3 Protein-Protein Interactions. *J Med Chem* **2018**, *61* (9), 3755-3778. DOI: 10.1021/acs.jmedchem.7b00574.

(3) Ryan, D. P.; Matthews, J. M. Protein-protein interactions in human disease. *Curr Opin Struct Biol* **2005**, *15* (4), 441-446. DOI: 10.1016/j.sbi.2005.06.001.

(4) De Las Rivas, J.; Fontanillo, C. Protein-protein interactions essentials: key concepts to building and analyzing interactome networks. *PLoS Comput Biol* **2010**, *6* (6), e1000807. DOI: 10.1371/journal.pcbi.1000807.

(5) Zinzalla, G.; Thurston, D. E. Targeting protein-protein interactions for therapeutic intervention: a challenge for the future. *Future Med Chem* **2009**, *1* (1), 65-93. DOI: 10.4155/fmc.09.12.

(6) Arkin, M. R.; Tang, Y.; Wells, J. A. Small-molecule inhibitors of protein-protein interactions: progressing toward the reality. *Chem Biol* **2014**, *21* (9), 1102-1114. DOI: 10.1016/j.chembiol.2014.09.001.

(7) Voet, A.; Berenger, F.; Zhang, K. Y. Electrostatic similarities between protein and small molecule ligands facilitate the design of protein-protein interaction inhibitors. *PLoS One* **2013**, *8* (10), e75762. DOI: 10.1371/journal.pone.0075762.

(8) Ran, X.; Gestwicki, J. E. Inhibitors of protein-protein interactions (PPIs): an analysis of scaffold choices and buried surface area. *Curr Opin Chem Biol* **2018**, *44*, 75-86. DOI: 10.1016/j.cbpa.2018.06.004.

(9) Wells, J. A.; McClendon, C. L. Reaching for high-hanging fruit in drug discovery at protein-protein interfaces. *Nature* **2007**, *450* (7172), 1001-1009. DOI: 10.1038/nature06526.

(10) Fry, D. C. Protein-protein interactions as targets for small molecule drug discovery. *Biopolymers* **2006**, *84* (6), 535-552. DOI: 10.1002/bip.20608.

(11) Metz, A.; Ciglia, E.; Gohlke, H. Modulating protein-protein interactions: from structural determinants of binding to druggability prediction to application. *Curr Pharm Des* **2012**, *18* (30), 4630-4647. DOI: 10.2174/138161212802651553.

(12) Chène, P. Drugs targeting protein-protein interactions. *ChemMedChem* **2006**, *1* (4), 400-411. DOI: 10.1002/cmdc.200600004.

(13) Sable, R.; Jois, S. Surfing the Protein-Protein Interaction Surface Using Docking Methods: Application to the Design of PPI Inhibitors. *Molecules* **2015**, *20* (6), 11569-11603. DOI: 10.3390/molecules200611569.

(14) Wang, H.; Liu, C.; Deng, L. Enhanced Prediction of Hot Spots at Protein-Protein Interfaces Using Extreme Gradient Boosting. *Sci Rep* **2018**, *8* (1), 14285. DOI: 10.1038/s41598-018-32511-1.

(15) Keskin, O.; Ma, B.; Nussinov, R. Hot regions in protein--protein interactions: the organization and contribution of structurally conserved hot spot residues. *J Mol Biol* **2005**, *345* (5), 1281-1294. DOI: 10.1016/j.jmb.2004.10.077.

(16) Kortemme, T.; Kim, D. E.; Baker, D. Computational alanine scanning of protein-protein interfaces. *Sci STKE* **2004**, *2004* (219), pl2. DOI: 10.1126/stke.2192004pl2.

(17) Nooren, I. M.; Thornton, J. M. Diversity of protein-protein interactions. *EMBO J* **2003**, *22* (14), 3486-3492. DOI: 10.1093/emboj/cdg359.

(18) Keskin, O.; Gursoy, A.; Ma, B.; Nussinov, R. Principles of protein-protein interactions: what are the preferred ways for proteins to interact? *Chem Rev* **2008**, *108* (4), 1225-1244. DOI: 10.1021/cr040409x.

(19) Villoutreix, B. O.; Kuenemann, M. A.; Poyet, J. L.; Bruzzoni-Giovanelli, H.; Labbé, C.; Lagorce, D.; Sperandio, O.; Miteva, M. A. Drug-Like Protein-Protein Interaction Modulators:

Challenges and Opportunities for Drug Discovery and Chemical Biology. *Mol Inform* **2014**, *33* (6-7), 414-437. DOI: 10.1002/minf.201400040.

(20) Fischer, G.; Rossmann, M.; Hyvönen, M. Alternative modulation of protein-protein interactions by small molecules. *Curr Opin Biotechnol* **2015**, *35*, 78-85. DOI: 10.1016/j.copbio.2015.04.006.

(21) Jin, L.; Wang, W.; Fang, G. Targeting protein-protein interaction by small molecules. *Annu Rev Pharmacol Toxicol* **2014**, *54*, 435-456. DOI: 10.1146/annurev-pharmtox-011613-140028.

(22) Lu, H.; Zhou, Q.; He, J.; Jiang, Z.; Peng, C.; Tong, R.; Shi, J. Recent advances in the development of protein-protein interactions modulators: mechanisms and clinical trials. *Signal Transduct Target Ther* **2020**, *5* (1), 213. DOI: 10.1038/s41392-020-00315-3.

(23) Ni, D.; Lu, S.; Zhang, J. Emerging roles of allosteric modulators in the regulation of protein-protein interactions (PPIs): A new paradigm for PPI drug discovery. *Med Res Rev* **2019**, *39* (6), 2314-2342. DOI: 10.1002/med.21585.

(24) Garner, T. P.; Lopez, A.; Reyna, D. E.; Spitz, A. Z.; Gavathiotis, E. Progress in targeting the BCL-2 family of proteins. *Curr Opin Chem Biol* **2017**, *39*, 133-142. DOI: 10.1016/j.cbpa.2017.06.014.

(25) Birkinshaw, R. W.; Gong, J. N.; Luo, C. S.; Lio, D.; White, C. A.; Anderson, M. A.; Blombery, P.; Lessene, G.; Majewski, I. J.; Thijssen, R.; et al. Structures of BCL-2 in complex with venetoclax reveal the molecular basis of resistance mutations. *Nat Commun* **2019**, *10* (1), 2385. DOI: 10.1038/s41467-019-10363-1.

(26) Silvian, L. F.; Friedman, J. E.; Strauch, K.; Cachero, T. G.; Day, E. S.; Qian, F.; Cunningham, B.; Fung, A.; Sun, L.; Shipps, G. W.; et al. Small molecule inhibition of the TNF family cytokine CD40 ligand through a subunit fracture mechanism. *ACS Chem Biol* **2011**, *6* (6), 636-647. DOI: 10.1021/cb2000346.

(27) González-Ruiz, D.; Gohlke, H. Targeting protein-protein interactions with small molecules: challenges and perspectives for computational binding epitope detection and ligand finding. *Curr Med Chem* **2006**, *13* (22), 2607-2625. DOI: 10.2174/092986706778201530.

(28) Lau, J. L.; Dunn, M. K. Therapeutic peptides: Historical perspectives, current development trends, and future directions. *Bioorg Med Chem* **2018**, *26* (10), 2700-2707. DOI: 10.1016/j.bmc.2017.06.052.

(29) Hill, T. A.; Shepherd, N. E.; Diness, F.; Fairlie, D. P. Constraining cyclic peptides to mimic protein structure motifs. *Angew Chem Int Ed Engl* **2014**, *53* (48), 13020-13041. DOI: 10.1002/anie.201401058.

(30) Cussol, L.; Mauran-Ambrosino, L.; Buratto, J.; Belorusova, A. Y.; Neuville, M.; Osz, J.; Fribourg, S.; Fremaux, J.; Dolain, C.; Goudreau, S. R.; et al. Structural Basis for α-Helix Mimicry and Inhibition of Protein-Protein Interactions with Oligourea Foldamers. *Angew Chem Int Ed Engl* **2021**, *60* (5), 2296-2303. DOI: 10.1002/anie.202008992.

(31) Kannan, S.; Aronica, P. G. A.; Ng, S.; Gek Lian, D. T.; Frosi, Y.; Chee, S.; Shimin, J.; Yuen, T. Y.; Sadruddin, A.; Kaan, H. Y. K.; et al. Macrocyclization of an all-d linear α-helical peptide imparts cellular permeability. *Chem Sci* **2020**, *11* (21), 5577-5591. DOI: 10.1039/c9sc06383h.

(32) Walensky, L. D.; Bird, G. H. Hydrocarbon-stapled peptides: principles, practice, and progress. *J Med Chem* **2014**, *57* (15), 6275-6288. DOI: 10.1021/jm4011675.

(33) Higueruelo, A. P.; Jubb, H.; Blundell, T. L. Protein-protein interactions as druggable targets: recent technological advances. *Curr Opin Pharmacol* **2013**, *13* (5), 791-796. DOI: 10.1016/j.coph.2013.05.009.

(34) Tisato, V.; Voltan, R.; Gonelli, A.; Secchiero, P.; Zauli, G. MDM2/X inhibitors under clinical evaluation: perspectives for the management of hematological malignancies and pediatric cancer. *J Hematol Oncol* **2017**, *10* (1), 133. DOI: 10.1186/s13045-017-0500-5.

(35) Eyrisch, S.; Helms, V. Transient pockets on protein surfaces involved in protein-protein interaction. *J Med Chem* **2007**, *50* (15), 3457-3464. DOI: 10.1021/jm070095g.

(36) Li, B.; Rong, D.; Wang, Y. Targeting Protein-Protein Interaction with Covalent Small-Molecule Inhibitors. *Curr Top Med Chem* **2019**, *19* (21), 1872-1876. DOI: 10.2174/1568026619666191011163410.

(37) Shin, W. H.; Christoffer, C. W.; Kihara, D. In silico structure-based approaches to discover protein-protein interaction-targeting drugs. *Methods* **2017**, *131*, 22-32. DOI: 10.1016/j.ymeth.2017.08.006.

(38) Milroy, L. G.; Grossmann, T. N.; Hennig, S.; Brunsveld, L.; Ottmann, C. Modulators of protein-protein interactions. *Chem Rev* **2014**, *114* (9), 4695-4748. DOI: 10.1021/cr400698c.

(39) Qiu, Y.; Li, X.; He, X.; Pu, J.; Zhang, J.; Lu, S. Computational methods-guided design of modulators targeting protein-protein interactions (PPIs). *Eur J Med Chem* **2020**, *207*, 112764. DOI: 10.1016/j.ejmech.2020.112764.

(40) Cossar, P. J.; Lewis, P. J.; McCluskey, A. Protein-protein interactions as antibiotic targets: A medicinal chemistry perspective. *Med Res Rev* **2020**, *40* (2), 469-494. DOI: 10.1002/med.21519.

(41) Rao, V. S.; Srinivas, K.; Sujini, G. N.; Kumar, G. N. Protein-protein interaction detection: methods and analysis. *Int J Proteomics* **2014**, *2014*, 147648. DOI: 10.1155/2014/147648.

(42) Lionta, E.; Spyrou, G.; Vassilatis, D. K.; Cournia, Z. Structure-based virtual screening for drug discovery: principles, applications and recent advances. *Curr Top Med Chem* **2014**, *14* (16), 1923-1938. DOI: 10.2174/1568026614666140929124445.

(43) Durrant, J. D.; McCammon, J. A. Molecular dynamics simulations and drug discovery. *BMC Biol* **2011**, *9*, 71. DOI: 10.1186/1741-7007-9-71.

(44) Feng, T.; Barakat, K. Molecular Dynamics Simulation and Prediction of Druggable Binding Sites. *Methods Mol Biol* **2018**, *1762*, 87-103. DOI: 10.1007/978-1-4939-7756-7_6.

(45) Moreira, I. S.; Fernandes, P. A.; Ramos, M. J. Computational alanine scanning mutagenesis--an improved methodological approach. *J Comput Chem* **2007**, *28* (3), 644-654. DOI: 10.1002/jcc.20566 From NLM.

(46) Pedersen, J. T.; Heegaard, N. H. Analysis of protein aggregation in neurodegenerative disease. *Anal Chem* **2013**, *85* (9), 4215-4227. DOI: 10.1021/ac400023c.

(47) Di Maio, R.; Barrett, P. J.; Hoffman, E. K.; Barrett, C. W.; Zharikov, A.; Borah, A.; Hu, X.; McCoy, J.; Chu, C. T.; Burton, E. A.; et al. α-Synuclein binds to TOM20 and inhibits mitochondrial protein import in Parkinson's disease. *Sci Transl Med* **2016**, *8* (342), 342ra378. DOI: 10.1126/scitranslmed.aaf3634.

(48) Li H., R. F., Sinha S., Maiti P., Bitan G. Amyloids and Protein Aggregation–Analytical Methods. *Encyclopedia of analytical chemistry*: 2009; pp 1-32.

(49) Giehm, L.; Lorenzen, N.; Otzen, D. E. Assays for α-synuclein aggregation. *Methods* **2011**, *53* (3), 295-305. DOI: 10.1016/j.ymeth.2010.12.008.

(50) Hudson, S. A.; Ecroyd, H.; Kee, T. W.; Carver, J. A. The thioflavin T fluorescence assay for amyloid fibril detection can be biased by the presence of exogenous compounds. *FEBS J* **2009**, *276* (20), 5960-5972. DOI: 10.1111/j.1742-4658.2009.07307.x.

(51) Gade Malmos, K.; Blancas-Mejia, L. M.; Weber, B.; Buchner, J.; Ramirez-Alvarado, M.; Naiki, H.; Otzen, D. ThT 101: a primer on the use of thioflavin T to investigate amyloid formation. *Amyloid* **2017**, *24* (1), 1-16. DOI: 10.1080/13506129.2017.1304905.

(52) Lorber, B.; Fischer, F.; Bailly, M.; Roy, H.; Kern, D. Protein analysis by dynamic light scattering: methods and techniques for students. *Biochem Mol Biol Educ* **2012**, *40* (6), 372-382. DOI: 10.1002/bmb.20644.

(53) Bose, M.; Mukherjee, P. Potential of Anti-MUC1 Antibodies as a Targeted Therapy for Gastrointestinal Cancers. *Vaccines (Basel)* **2020**, *8* (4). DOI: 10.3390/vaccines8040659.

(54) Nath, S.; Mukherjee, P. MUC1: a multifaceted oncoprotein with a key role in cancer progression. *Trends Mol Med* **2014**, *20* (6), 332-342. DOI: 10.1016/j.molmed.2014.02.007.

(55) Brayman, M.; Thathiah, A.; Carson, D. D. MUC1: a multifunctional cell surface component of reproductive tissue epithelia. *Reprod Biol Endocrinol* **2004**, *2*, 4. DOI: 10.1186/1477-7827-2-4.

(56) Dhar, P.; McAuley, J. The Role of the Cell Surface Mucin MUC1 as a Barrier to Infection and Regulator of Inflammation. *Front Cell Infect Microbiol* **2019**, *9*, 117. DOI: 10.3389/fcimb.2019.00117.

(57) Gao, T.; Cen, Q.; Lei, H. A review on development of MUC1-based cancer vaccine. *Biomed Pharmacother* **2020**, *132*, 110888. DOI: 10.1016/j.biopha.2020.110888.

(58) Beckwith, D. M.; Cudic, M. Tumor-associated O-glycans of MUC1: Carriers of the glyco-code and targets for cancer vaccine design. *Semin Immunol* **2020**, *47*, 101389. DOI: 10.1016/j.smim.2020.101389.

(59) Suzuki, H.; Shoda, J.; Kawamoto, T.; Shinozaki, E.; Miyahara, N.; Hotta, S.; Iizuka, Y.; Nakahara, A.; Tanaka, N.; Yanaka, A.; et al. Expression of MUC1 recognized by monoclonal antibody MY.1E12 is a useful biomarker for tumor aggressiveness of advanced colon carcinoma. *Clin Exp Metastasis* **2004**, *21* (4), 321-329. DOI: 10.1023/b:clin.0000046133.35133.cc.

(60) Hollingsworth, M. A.; Swanson, B. J. Mucins in cancer: protection and control of the cell surface. *Nat Rev Cancer* **2004**, *4* (1), 45-60. DOI: 10.1038/nrc1251.

(61) Pourjafar, M.; Samadi, P.; Saidijam, M. MUC1 antibody-based therapeutics: the promise of cancer immunotherapy. *Immunotherapy* **2020**, *12* (17), 1269-1286. DOI: 10.2217/imt-2020-0019.

(62) Corraliza-Gorjón, I.; Somovilla-Crespo, B.; Santamaria, S.; Garcia-Sanz, J. A.; Kremer, L. New Strategies Using Antibody Combinations to Increase Cancer Treatment Effectiveness. *Front Immunol* **2017**, *8*, 1804. DOI: 10.3389/fimmu.2017.01804.

(63) Curry, J. M.; Thompson, K. J.; Rao, S. G.; Besmer, D. M.; Murphy, A. M.; Grdzelishvili, V. Z.; Ahrens, W. A.; McKillop, I. H.; Sindram, D.; Iannitti, D. A.; et al. The use of a novel MUC1 antibody to identify cancer stem cells and circulating MUC1 in mice and patients with pancreatic cancer. *J Surg Oncol* **2013**, *107* (7), 713-722. DOI: 10.1002/jso.23316.

(64) Moore, L. J.; Roy, L. D.; Zhou, R.; Grover, P.; Wu, S. T.; Curry, J. M.; Dillon, L. M.; Puri, P. M.; Yazdanifar, M.; Puri, R.; et al. Antibody-Guided In Vivo Imaging for Early Detection of Mammary Gland Tumors. *Transl Oncol* **2016**, *9* (4), 295-305. DOI: 10.1016/j.tranon.2016.05.001.

(65) Yonezawa, S.; Kitajima, S.; Higashi, M.; Osako, M.; Horinouchi, M.; Yokoyama, S.; Kitamoto, S.; Yamada, N.; Tamura, Y.; Shimizu, T.; et al. A novel anti-MUC1 antibody against the MUC1 cytoplasmic tail domain: use in sensitive identification of poorly differentiated cells in adenocarcinoma of the stomach. *Gastric Cancer* **2012**, *15* (4), 370-381. DOI: 10.1007/s10120-011-0125-2.

(66) Dian, D.; Janni, W.; Kuhn, C.; Mayr, D.; Karsten, U.; Mylonas, I.; Friese, K.; Jeschke, U. Evaluation of a novel anti-mucin 1 (MUC1) antibody (PankoMab) as a potential diagnostic tool in human ductal breast cancer; comparison with two established antibodies. *Onkologie* **2009**, *32* (5), 238-244. DOI: 10.1159/000209280.

(67) Danielczyk, A.; Stahn, R.; Faulstich, D.; Löffler, A.; Märten, A.; Karsten, U.; Goletz, S. PankoMab: a potent new generation anti-tumour MUC1 antibody. *Cancer Immunol Immunother* **2006**, *55* (11), 1337-1347. DOI: 10.1007/s00262-006-0135-9.

(68) Bose, M.; Mukherjee, P. Microbe-MUC1 Crosstalk in Cancer-Associated Infections. *Trends Mol Med* **2020**, *26* (3), 324-336. DOI: 10.1016/j.molmed.2019.10.003.

(69) Dikic, I. CIN85/CMS family of adaptor molecules. *FEBS Lett* **2002**, *529* (1), 110-115. DOI: 10.1016/s0014-5793(02)03188-5.

(70) Kowanetz, K.; Husnjak, K.; Höller, D.; Kowanetz, M.; Soubeyran, P.; Hirsch, D.; Schmidt, M. H. H.; Pavelic, K.; De Camilli, P.; Randazzo, P. A.; et al. CIN85 associates with multiple effectors controlling intracellular trafficking of epidermal growth factor receptors. *Mol Biol Cell* **2004**, *15* (7), 3155-3166. DOI: 10.1091/mbc.e03-09-0683.

(71) Saksela, K.; Permi, P. SH3 domain ligand binding: What's the consensus and where's the specificity? *FEBS Lett* **2012**, *586* (17), 2609-2614. DOI: 10.1016/j.febslet.2012.04.042.

(72) Oneyama, C.; Nakano, H.; Sharma, S. V. UCS15A, a novel small molecule, SH3 domain-mediated protein-protein interaction blocking drug. *Oncogene* **2002**, *21* (13), 2037-2050. DOI: 10.1038/sj.onc.1205271.

(73) Jozic, D.; Cárdenes, N.; Deribe, Y. L.; Moncalián, G.; Hoeller, D.; Groemping, Y.; Dikic, I.; Rittinger, K.; Bravo, J. Cbl promotes clustering of endocytic adaptor proteins. *Nat Struct Mol Biol* **2005**, *12* (11), 972-979. DOI: 10.1038/nsmb1000.

(74) Larson, S. M.; Davidson, A. R. The identification of conserved interactions within the SH3 domain by alignment of sequences and structures. *Protein Sci* **2000**, *9* (11), 2170-2180. DOI: 10.1110/ps.9.11.2170.

(75) Hashimoto, S.; Hirose, M.; Hashimoto, A.; Morishige, M.; Yamada, A.; Hosaka, H.; Akagi, K.; Ogawa, E.; Oneyama, C.; Agatsuma, T.; et al. Targeting AMAP1 and cortactin binding bearing an atypical src homology 3/proline interface for prevention of breast cancer invasion and metastasis. *Proc Natl Acad Sci U S A* **2006**, *103* (18), 7036-7041. DOI: 10.1073/pnas.0509166103.

(76) Desrochers, G.; Cappadocia, L.; Lussier-Price, M.; Ton, A. T.; Ayoubi, R.; Serohijos, A.; Omichinski, J. G.; Angers, A. Molecular basis of interactions between SH3 domain-containing proteins and the proline-rich region of the ubiquitin ligase Itch. *J Biol Chem* **2017**, *292* (15), 6325-6338. DOI: 10.1074/jbc.M116.754440.

(77) Mayer, B. J. SH3 domains: complexity in moderation. *J Cell Sci* **2001**, *114* (Pt 7), 1253-1263. DOI: 10.1242/jcs.114.7.1253.

(78) Ceregido, M. A.; Garcia-Pino, A.; Ortega-Roldan, J. L.; Casares, S.; López Mayorga, O.; Bravo, J.; van Nuland, N. A.; Azuaga, A. I. Multimeric and differential binding of CIN85/CD2AP with two atypical proline-rich sequences from CD2 and Cbl-b*. *FEBS J* **2013**, *280* (14), 3399-3415. DOI: 10.1111/febs.12333.

(79) Kurakin, A. V.; Wu, S.; Bredesen, D. E. Atypical recognition consensus of CIN85/SETA/Ruk SH3 domains revealed by target-assisted iterative screening. *J Biol Chem* **2003**, *278* (36), 34102-34109. DOI: 10.1074/jbc.M305264200.

(80) Hutchings, N. J.; Clarkson, N.; Chalkley, R.; Barclay, A. N.; Brown, M. H. Linking the T cell surface protein CD2 to the actin-capping protein CAPZ via CMS and CIN85. *J Biol Chem* **2003**, *278* (25), 22396-22403. DOI: 10.1074/jbc.M302540200.

(81) Havrylov, S.; Redowicz, M. J.; Buchman, V. L. Emerging roles of Ruk/CIN85 in vesicle-mediated transport, adhesion, migration and malignancy. *Traffic* **2010**, *11* (6), 721-731. DOI: 10.1111/j.1600-0854.2010.01061.x.

(82) Cascio, S.; Farkas, A. M.; Hughey, R. P.; Finn, O. J. Altered glycosylation of MUC1 influences its association with CIN85: the role of this novel complex in cancer cell invasion and migration. *Oncotarget* **2013**, *4* (10), 1686-1697. DOI: 10.18632/oncotarget.1265.

(83) Ciborowski, P.; Finn, O. J. Non-glycosylated tandem repeats of MUC1 facilitate attachment of breast tumor cells to normal human lung tissue and immobilized extracellular matrix proteins (ECM) in vitro: potential role in metastasis. *Clin Exp Metastasis* **2002**, *19* (4), 339-345. DOI: 10.1023/a:1015590515957.

(84) Dennis, J. W.; Granovsky, M.; Warren, C. E. Glycoprotein glycosylation and cancer progression. *Biochim Biophys Acta* **1999**, *1473* (1), 21-34. DOI: 10.1016/s0304-4165(99)00167-1.

(85) Kohlgraf, K. G.; Gawron, A. J.; Higashi, M.; Meza, J. L.; Burdick, M. D.; Kitajima, S.; Kelly, D. L.; Caffrey, T. C.; Hollingsworth, M. A. Contribution of the MUC1 tandem repeat and cytoplasmic tail to invasive and metastatic properties of a pancreatic cancer cell line. *Cancer Res* **2003**, *63* (16), 5011-5020.

(86) Cascio, S.; Finn, O. J. Complex of MUC1, CIN85 and Cbl in Colon Cancer Progression and Metastasis. *Cancers (Basel)* **2015**, *7* (1), 342-352. DOI: 10.3390/cancers7010342.

(87) Wakui, H.; Tanaka, Y.; Ose, T.; Matsumoto, I.; Kato, K.; Min, Y.; Tachibana, T.; Sato, M.; Naruchi, K.; Martin, F. G.; et al. A straightforward approach to antibodies recognising cancer specific glycopeptidic neoepitopes. *Chem Sci* **2020**, *11* (19), 4999-5006. DOI: 10.1039/d0sc00317d.

(88) Friesner, R. A.; Banks, J. L.; Murphy, R. B.; Halgren, T. A.; Klicic, J. J.; Mainz, D. T.; Repasky, M. P.; Knoll, E. H.; Shelley, M.; Perry, J. K.; et al. Glide: a new approach for rapid, accurate docking and scoring. 1. Method and assessment of docking accuracy. *J Med Chem* **2004**, *47* (7), 1739-1749. DOI: 10.1021/jm0306430.

(89) Halgren, T. A.; Murphy, R. B.; Friesner, R. A.; Beard, H. S.; Frye, L. L.; Pollard, W. T.; Banks, J. L. Glide: a new approach for rapid, accurate docking and scoring. 2. Enrichment factors in database screening. *J Med Chem* **2004**, *47* (7), 1750-1759. DOI: 10.1021/jm030644s.

(90) Bowers, K. J.; Chow, E.; Xu, H.; Dror, R. O.; Eastwood, M. P.; Gregersen, B. A.; Klepeis, J. L.; Kolossvary, I.; Moraes, M. A.; Sacerdoti, F. D.; et al. Scalable algorithms for molecular dynamics simulations on commodity clusters. In Proceedings of the 2006 ACM/IEEE conference on Supercomputing, Tampa, Florida; 2006.

(91) Krüger, D. M.; Gohlke, H. DrugScorePPI webserver: fast and accurate in silico alanine scanning for scoring protein-protein interactions. *Nucleic Acids Res* **2010**, *38* (Web Server issue), W480-486. DOI: 10.1093/nar/gkq471.

(92) Kortemme, T.; Joachimiak, L. A.; Bullock, A. N.; Schuler, A. D.; Stoddard, B. L.; Baker, D. Computational redesign of protein-protein interaction specificity. *Nat Struct Mol Biol* **2004**, *11* (4), 371-379. DOI: 10.1038/nsmb749.

(93) Wolber, G.; Langer, T. LigandScout: 3-D pharmacophores derived from protein-bound ligands and their use as virtual screening filters. *J Chem Inf Model* **2005**, *45* (1), 160-169. DOI: 10.1021/ci049885e.

(94) Wu, K. J.; Lei, P. M.; Liu, H.; Wu, C.; Leung, C. H.; Ma, D. L. Mimicking Strategy for Protein-Protein Interaction Inhibitor Discovery by Virtual Screening. *Molecules* **2019**, *24* (24). DOI: 10.3390/molecules24244428.

(95) Vittorio, S.; Seidel, T.; Garon, A.; Gitto, R.; Langer, T.; De Luca, L. In Silico Identification of Potential Druggable Binding Sites on CIN85 SH3 Domain. *Int J Mol Sci* **2021**, *22* (2). DOI: 10.3390/ijms22020534.

(96) Bhachoo, J.; Beuming, T. Investigating Protein-Peptide Interactions Using the Schrödinger Computational Suite. *Methods Mol Biol* **2017**, *1561*, 235-254. DOI: 10.1007/978-1-4939-6798-8_14.

(97) Sastry, G. M.; Adzhigirey, M.; Day, T.; Annabhimoju, R.; Sherman, W. Protein and ligand preparation: parameters, protocols, and influence on virtual screening enrichments. *J Comput Aided Mol Des* **2013**, *27* (3), 221-234. DOI: 10.1007/s10822-013-9644-8.

(98) Shelley, J. C.; Cholleti, A.; Frye, L. L.; Greenwood, J. R.; Timlin, M. R.; Uchimaya, M. Epik: a software program for pK(a) prediction and protonation state generation for drug-like molecules. *J Comput Aided Mol Des* **2007**, *21* (12), 681-691. DOI: 10.1007/s10822-007-9133-z.

(99) Roos, K.; Wu, C.; Damm, W.; Reboul, M.; Stevenson, J. M.; Lu, C.; Dahlgren, M. K.; Mondal, S.; Chen, W.; Wang, L.; et al. OPLS3e: Extending Force Field Coverage for Drug-Like Small Molecules. *J Chem Theory Comput* **2019**, *15* (3), 1863-1874. DOI: 10.1021/acs.jctc.8b01026.

(100) Mark, P.; Nilsson, L. Structure and Dynamics of the TIP3P, SPC, and SPC/E Water Models at 298 K. *The Journal of Physical Chemistry A* **2001**, *105* (43), 9954-9960.

(101) Genheden, S.; Ryde, U. The MM/PBSA and MM/GBSA methods to estimate ligand-binding affinities. *Expert Opin Drug Discov* **2015**, *10* (5), 449-461. DOI: 10.1517/17460441.2015.1032936.

(102) Beard, H.; Cholleti, A.; Pearlman, D.; Sherman, W.; Loving, K. A. Applying physics-based scoring to calculate free energies of binding for single amino acid mutations in protein-protein complexes. *PLoS One* **2013**, *8* (12), e82849. DOI: 10.1371/journal.pone.0082849.

(103) Chakraborty, A.; Brauer, S.; Diwan, A. Possible therapies of Parkinson's disease: A review. *J Clin Neurosci* **2020**, *75*, 1-4. DOI: 10.1016/j.jocn.2020.03.024.

(104) Cardinale, A.; Calabrese, V.; de Iure, A.; Picconi, B. Alpha-Synuclein as a Prominent Actor in the Inflammatory Synaptopathy of Parkinson's Disease. *Int J Mol Sci* **2021**, *22* (12). DOI: 10.3390/ijms22126517.

(105) Nirale, P.; Paul, A.; Yadav, K. S. Nanoemulsions for targeting the neurodegenerative diseases: Alzheimer's, Parkinson's and Prion's. *Life Sci* **2020**, *245*, 117394. DOI: 10.1016/j.lfs.2020.117394.

(106) Balestrino, R.; Schapira, A. H. V. Parkinson disease. *Eur J Neurol* **2020**, *27* (1), 27-42. DOI: 10.1111/ene.14108.

(107) Dickson, D. W. Parkinson's disease and parkinsonism: neuropathology. *Cold Spring Harb Perspect Med* **2012**, *2* (8). DOI: 10.1101/cshperspect.a009258.

(108) Savitt, D.; Jankovic, J. Targeting α-Synuclein in Parkinson's Disease: Progress Towards the Development of Disease-Modifying Therapeutics. *Drugs* **2019**, *79* (8), 797-810. DOI: 10.1007/s40265-019-01104-1.

(109) Jankovic, J.; Tan, E. K. Parkinson's disease: etiopathogenesis and treatment. *J Neurol Neurosurg Psychiatry* **2020**, *91* (8), 795-808. DOI: 10.1136/jnnp-2019-322338.

(110) Kalia, L. V.; Kalia, S. K.; McLean, P. J.; Lozano, A. M.; Lang, A. E. α-Synuclein oligomers and clinical implications for Parkinson disease. *Ann Neurol* **2013**, *73* (2), 155-169. DOI: 10.1002/ana.23746.

(111) Haddad, F.; Sawalha, M.; Khawaja, Y.; Najjar, A.; Karaman, R. Dopamine and Levodopa Prodrugs for the Treatment of Parkinson's Disease. *Molecules* **2017**, *23* (1), Review. DOI: 10.3390/molecules23010040.

(112) Carrera, I.; Cacabelos, R. Current Drugs and Potential Future Neuroprotective Compounds for Parkinson's Disease. *Current neuropharmacology* **2019**, *17* (3), 295-306, Review. DOI: 10.2174/1570159X17666181127125704.

(113) Stoker, T. B.; Torsney, K. M.; Barker, R. A. Emerging Treatment Approaches for Parkinson's Disease. *Front Neurosci* **2018**, *12*, 693. DOI: 10.3389/fnins.2018.00693.

(114) Borovac, J. A. Side effects of a dopamine agonist therapy for Parkinson's disease: a mini-review of clinical pharmacology. *Yale J Biol Med* **2016**, *89* (1), 37-47.

(115) Save, S. S.; Rachineni, K.; Hosur, R. V.; Choudhary, S. Natural compound safranal driven inhibition and dis-aggregation of α-synuclein fibrils. *Int J Biol Macromol* **2019**, *141*, 585-595. DOI: 10.1016/j.ijbiomac.2019.09.053.

(116) Afitska, K.; Priss, A.; Yushchenko, D. A.; Shvadchak, V. V. Structural Optimization of Inhibitors of α-Synuclein Fibril Growth: Affinity to the Fibril End as a Crucial Factor. *J Mol Biol* **2020**, *432* (4), 967-977. DOI: 10.1016/j.jmb.2019.11.019.

(117) Kyriukha, Y. A.; Afitska, K.; Kurochka, A. S.; Sachan, S.; Galkin, M.; Yushchenko, D. A.; Shvadchak, V. V. alpha-Synuclein Dimers as Potent Inhibitors of Fibrillization. *Journal of medicinal chemistry* **2019**, *62* (22), 10342-10351, Research Support, Non-U.S. Gov't. DOI: 10.1021/acs.jmedchem.9b01400. Serpell, L. C.; Berriman, J.; Jakes, R.; Goedert, M.; Crowther, R. A. Fiber diffraction of synthetic alpha-synuclein filaments shows amyloid-like cross-beta conformation. *Proceedings of the National Academy of Sciences of the United States of America* **2000**, *97* (9), 4897-4902. DOI: 10.1073/pnas.97.9.4897.

(118) Ma, L.; Yang, C.; Zheng, J.; Chen, Y.; Xiao, Y.; Huang, K. Non-polyphenolic natural inhibitors of amyloid aggregation. *European journal of medicinal chemistry* **2020**, *192*, 112197, Review. DOI: 10.1016/j.ejmech.2020.112197.

(119) AlNajjar, Y. T.; Gabr, M.; ElHady, A. K.; Salah, M.; Wilms, G.; Abadi, A. H.; Becker, W.; Abdel-Halim, M.; Engel, M. Discovery of novel 6-hydroxybenzothiazole urea derivatives as dual Dyrk1A/alpha-synuclein aggregation inhibitors with neuroprotective effects. *Eur J Med Chem* **2022**, *227*, 113911. DOI: 10.1016/j.ejmech.2021.113911.

(120) De Miranda, B. R.; Rocha, E. M.; Castro, S. L.; Greenamyre, J. T. Protection from α-Synuclein induced dopaminergic neurodegeneration by overexpression of the mitochondrial import receptor TOM20. *NPJ Parkinsons Dis* **2020**, *6* (1), 38. DOI: 10.1038/s41531-020-00139-6.

(121) Brundin, P.; Melki, R. Prying into the Prion Hypothesis for Parkinson's Disease. *J Neurosci* **2017**, *37* (41), 9808-9818. DOI: 10.1523/JNEUROSCI.1788-16.2017.

(122) Miraglia, F.; Ricci, A.; Rota, L.; Colla, E. Subcellular localization of alpha-synuclein aggregates and their interaction with membranes. *Neural Regen Res* **2018**, *13* (7), 1136-1144. DOI: 10.4103/1673-5374.235013.

(123) Oliveri, V. Toward the discovery and development of effective modulators of α-synuclein amyloid aggregation. *European journal of medicinal chemistry* **2019**, *167*, 10-36. DOI: 10.1016/j.ejmech.2019.01.045.

(124) Rezaeian, N.; Shirvanizadeh, N.; Mohammadi, S.; Nikkhah, M.; Arab, S. S. The inhibitory effects of biomimetically designed peptides on α-synuclein aggregation. *Arch Biochem Biophys* **2017**, *634*, 96-106. DOI: 10.1016/j.abb.2017.09.015.

(125) Recchia, A.; Debetto, P.; Negro, A.; Guidolin, D.; Skaper, S. D.; Giusti, P. Alpha-synuclein and Parkinson's disease. *FASEB J* **2004**, *18* (6), 617-626. DOI: 10.1096/fj.03-0338rev.

(126) Fields, C. R.; Bengoa-Vergniory, N.; Wade-Martins, R. Targeting Alpha-Synuclein as a Therapy for Parkinson's Disease. *Front Mol Neurosci* **2019**, *12*, 299. DOI: 10.3389/fnmol.2019.00299.

(127) Tuttle, M. D.; Comellas, G.; Nieuwkoop, A. J.; Covell, D. J.; Berthold, D. A.; Kloepper, K. D.; Courtney, J. M.; Kim, J. K.; Barclay, A. M.; Kendall, A.; et al. Solid-state NMR structure of a pathogenic fibril of full-length human α-synuclein. *Nat Struct Mol Biol* **2016**, *23* (5), 409-415. DOI: 10.1038/nsmb.3194.

(128) Longhena, F.; Faustini, G.; Brembati, V.; Pizzi, M.; Bellucci, A. The good and bad of therapeutic strategies that directly target α-synuclein. *IUBMB Life* **2020**, *72* (4), 590-600. DOI: 10.1002/iub.2194.

(129) Wong, Y. C.; Krainc, D. α-synuclein toxicity in neurodegeneration: mechanism and therapeutic strategies. *Nat Med* **2017**, *23* (2), 1-13. DOI: 10.1038/nm.4269.

(130) Brundin, P.; Dave, K. D.; Kordower, J. H. Therapeutic approaches to target alpha-synuclein pathology. *Exp Neurol* **2017**, *298* (Pt B), 225-235. DOI: 10.1016/j.expneurol.2017.10.003.

(131) Mittal, S.; Bjørnevik, K.; Im, D. S.; Flierl, A.; Dong, X.; Locascio, J. J.; Abo, K. M.; Long, E.; Jin, M.; Xu, B.; et al. β2-Adrenoreceptor is a regulator of the α-synuclein gene driving risk of Parkinson's disease. *Science* **2017**, *357* (6354), 891-898. DOI: 10.1126/science.aaf3934.

(132) Shihabuddin, L. S.; Brundin, P.; Greenamyre, J. T.; Stephenson, D.; Sardi, S. P. New Frontiers in Parkinson's Disease: From Genetics to the Clinic. *J Neurosci* **2018**, *38* (44), 9375-9382. DOI: 10.1523/JNEUROSCI.1666-18.2018.

(133) Chemerovski-Glikman, M.; Rozentur-Shkop, E.; Richman, M.; Grupi, A.; Getler, A.; Cohen, H. Y.; Shaked, H.; Wallin, C.; Wärmländer, S. K.; Haas, E.; et al. Self-Assembled Cyclic d,l-α-Peptides as Generic Conformational Inhibitors of the α-Synuclein Aggregation and Toxicity: In Vitro and Mechanistic Studies. *Chemistry* **2016**, *22* (40), 14236-14246. DOI: 10.1002/chem.201601830.

(134) Huggins, K. N.; Bisaglia, M.; Bubacco, L.; Tatarek-Nossol, M.; Kapurniotu, A.; Andersen, N. H. Designed hairpin peptides interfere with amyloidogenesis pathways: fibril formation and cytotoxicity inhibition, interception of the preamyloid state. *Biochemistry* **2011**, *50* (38), 8202-8212. DOI: 10.1021/bi200760h.

(135) Di Giovanni, S.; Eleuteri, S.; Paleologou, K. E.; Yin, G.; Zweckstetter, M.; Carrupt, P. A.; Lashuel, H. A. Entacapone and tolcapone, two catechol O-methyltransferase inhibitors, block fibril formation of alpha-synuclein and beta-amyloid and protect against amyloid-induced toxicity. *J Biol Chem* **2010**, *285* (20), 14941-14954. DOI: 10.1074/jbc.M109.080390.

(136) Hong, D. P.; Fink, A. L.; Uversky, V. N. Structural characteristics of alpha-synuclein oligomers stabilized by the flavonoid baicalein. *J Mol Biol* **2008**, *383* (1), 214-223. DOI: 10.1016/j.jmb.2008.08.039.

(137) Muronetz, V. I.; Barinova, K.; Kudryavtseva, S.; Medvedeva, M.; Melnikova, A.; Sevostyanova, I.; Semenyuk, P.; Stroylova, Y.; Sova, M. Natural and Synthetic Derivatives of Hydroxycinnamic Acid Modulating the Pathological Transformation of Amyloidogenic Proteins. *Molecules* **2020**, *25* (20). DOI: 10.3390/molecules25204647.

(138) Medvedeva, M.; Barinova, K.; Melnikova, A.; Semenyuk, P.; Kolmogorov, V.; Gorelkin, P.; Erofeev, A.; Muronetz, V. Naturally occurring cinnamic acid derivatives prevent amyloid transformation of alpha-synuclein. *Biochimie* **2020**, *170*, 128-139. DOI: 10.1016/j.biochi.2020.01.004.

(139) Javed, H.; Nagoor Meeran, M. F.; Azimullah, S.; Adem, A.; Sadek, B.; Ojha, S. K. Plant Extracts and Phytochemicals Targeting alpha-Synuclein Aggregation in Parkinson's Disease Models. *Front Pharmacol* **2018**, *9*, 1555. DOI: 10.3389/fphar.2018.01555.

(140) Ghanem, S. S.; Fayed, H. S.; Zhu, Q.; Lu, J. H.; Vaikath, N. N.; Ponraj, J.; Mansour, S.; El-Agnaf, O. M. A. Natural Alkaloid Compounds as Inhibitors for Alpha-Synuclein Seeded Fibril Formation and Toxicity. *Molecules* **2021**, *26* (12). DOI: 10.3390/molecules26123736.

(141) Fazili, N. A.; Naeem, A. Anti-fibrillation potency of caffeic acid against an antidepressant induced fibrillogenesis of human α-synuclein: Implications for Parkinson's disease. *Biochimie* **2015**, *108*, 178-185. DOI: 10.1016/j.biochi.2014.11.011.

(142) Hong, D. P.; Fink, A. L.; Uversky, V. N. Smoking and Parkinson's disease: does nicotine affect alpha-synuclein fibrillation? *Biochim Biophys Acta* **2009**, *1794* (2), 282-290. DOI: 10.1016/j.bbapap.2008.09.026.

(143) Pena-DIaz, S.; Ventura, S. One ring is sufficient to inhibit α-synuclein aggregation. *Neural Regen Res* **2022**, *17* (3), 508-511. DOI: 10.4103/1673-5374.320973.

(144) Pujols, J.; Pena-Diaz, S.; Conde-Gimenez, M.; Pinheiro, F.; Navarro, S.; Sancho, J.; Ventura, S. High-Throughput Screening Methodology to Identify Alpha-Synuclein Aggregation Inhibitors. *Int J Mol Sci* **2017**, *18* (3). DOI: 10.3390/ijms18030478.

(145) Wagner, J.; Ryazanov, S.; Leonov, A.; Levin, J.; Shi, S.; Schmidt, F.; Prix, C.; Pan-Montojo, F.; Bertsch, U.; Mitteregger-Kretzschmar, G.; et al. Anle138b: a novel oligomer modulator for disease-modifying therapy of neurodegenerative diseases such as prion and Parkinson's disease. *Acta Neuropathol* **2013**, *125* (6), 795-813. DOI: 10.1007/s00401-013-1114-9.

(146) Pujols, J.; Pena-Diaz, S.; Lazaro, D. F.; Peccati, F.; Pinheiro, F.; Gonzalez, D.; Carija, A.; Navarro, S.; Conde-Gimenez, M.; Garcia, J.; et al. Small molecule inhibits alpha-synuclein aggregation, disrupts amyloid fibrils, and prevents degeneration of dopaminergic neurons. *Proc Natl Acad Sci U S A* **2018**, *115* (41), 10481-10486. DOI: 10.1073/pnas.1804198115.

(147) Peña-Díaz, S.; Pujols, J.; Conde-Giménez, M.; Čarija, A.; Dalfo, E.; García, J.; Navarro, S.; Pinheiro, F.; Santos, J.; Salvatella, X.; et al. ZPD-2, a Small Compound That Inhibits α-Synuclein

Amyloid Aggregation and Its Seeded Polymerization. *Front Mol Neurosci* **2019**, *12*, 306. DOI: 10.3389/fnmol.2019.00306.

(148) Pena-Diaz, S.; Pujols, J.; Pinheiro, F.; Santos, J.; Pallares, I.; Navarro, S.; Conde-Gimenez, M.; Garcia, J.; Salvatella, X.; Dalfo, E.; et al. Inhibition of alpha-Synuclein Aggregation and Mature Fibril Disassembling With a Minimalistic Compound, ZPDm. *Front Bioeng Biotechnol* **2020**, *8*, 588947. DOI: 10.3389/fbioe.2020.588947.

(149) Tóth, G.; Neumann, T.; Berthet, A.; Masliah, E.; Spencer, B.; Tao, J.; Jobling, M. F.; Gardai, S. J.; Bertoncini, C. W.; Cremades, N.; et al. Novel Small Molecules Targeting the Intrinsically Disordered Structural Ensemble of α-Synuclein Protect Against Diverse α-Synuclein Mediated Dysfunctions. *Sci Rep* **2019**, *9* (1), 16947. DOI: 10.1038/s41598-019-52598-4.

(150) Vittorio, S.; Adornato, I.; Gitto, R.; Pena-Diaz, S.; Ventura, S.; De Luca, L. Rational design of small molecules able to inhibit alpha-synuclein amyloid aggregation for the treatment of Parkinson's disease. *Journal of enzyme inhibition and medicinal chemistry* **2020**, *35* (1), 1727-1735. DOI: 10.1080/14756366.2020.1816999.

(151) De Luca, L.; Mirabile, S.; Ricci, F.; Adornato, I.; Cacciola, A.; Germanò, M. P.; Gitto, R. Synthesis and biochemical evaluation of 5-(pyridin-4-yl)-3-(alkylsulfanyl)-4H1,2,4-triazol-4-amine-based inhibitors of tyrosinase from Agaricus bisporus. *Arkivoc* **2022**, 155-166. DOI: https://doi.org/10.24820/ark.5550190.p011.677.

(152) Gitto, R.; Vittorio, S.; Bucolo, F.; Peña-Díaz, S.; Siracusa, R.; Cuzzocrea, S.; Ventura, S.; Di Paola, R.; De Luca, L. Discovery of Neuroprotective Agents Based on a 5-(4-Pyridinyl)-1,2,4-triazole Scaffold. *ACS Chem Neurosci* **2022**, *13* (5), 581-586. DOI: 10.1021/acschemneuro.1c00849.

(153) De Luca, L.; Vittorio, S.; Peña-Díaz, S.; Pitasi, G.; Fornt-Suñé, M.; Bucolo, F.; Ventura, S.; Gitto, R. Ligand-Based Discovery of a Small Molecule as Inhibitor of α-Synuclein Amyloid Formation. *Int J Mol Sci* **2022**, *23* (23). DOI: 10.3390/ijms232314844.

(154) Bragina, M. E.; Daina, A.; Perez, M. A. S.; Michielin, O.; Zoete, V. The SwissSimilarity 2021 Web Tool: Novel Chemical Libraries and Additional Methods for an Enhanced Ligand-Based Virtual Screening Experience. *Int J Mol Sci* **2022**, *23* (2). DOI: 10.3390/ijms23020811.

(155) Zoete, V.; Daina, A.; Bovigny, C.; Michielin, O. SwissSimilarity: A Web Tool for Low to Ultra High Throughput Ligand-Based Virtual Screening. *J Chem Inf Model* **2016**, *56* (8), 1399-1404. DOI: 10.1021/acs.jcim.6b00174.

(156) O'Boyle, N. M.; Banck, M.; James, C. A.; Morley, C.; Vandermeersch, T.; Hutchison, G. R. Open Babel: An open chemical toolbox. *J Cheminform* **2011**, *3*, 33. DOI: 10.1186/1758-2946-3-33.

(157) Armstrong, M. S.; Morris, G. M.; Finn, P. W.; Sharma, R.; Moretti, L.; Cooper, R. I.; Richards, W. G. ElectroShape: fast molecular similarity calculations incorporating shape, chirality and electrostatics. *J Comput Aided Mol Des* **2010**, *24* (9), 789-801. DOI: 10.1007/s10822-010-9374-0.

(158) Gladysz, R.; Dos Santos, F. M.; Langenaeker, W.; Thijs, G.; Augustyns, K.; De Winter, H. Spectrophores as one-dimensional descriptors calculated from three-dimensional atomic properties: applications ranging from scaffold hopping to multi-target virtual screening. *J Cheminform* **2018**, *10* (1), 9. DOI: 10.1186/s13321-018-0268-9.

(159) Mahia, A.; Pena-Diaz, S.; Navarro, S.; Jose Galano-Frutos, J.; Pallares, I.; Pujols, J.; Diaz-de-Villegas, M. D.; Galvez, J. A.; Ventura, S.; Sancho, J. Design, synthesis and structure-activity evaluation of novel 2-pyridone-based inhibitors of alpha-synuclein aggregation with potentially improved BBB permeability. *Bioorg Chem* **2021**, *117*, 105472. DOI: 10.1016/j.bioorg.2021.105472. Pena, D. S.; Ventura, S. One ring is sufficient to inhibit alpha-synuclein aggregation. *Neural Regen Res* **2022**, *17* (3), 508-511. DOI: 10.4103/1673-5374.320973.

(160) Guerrero-Ferreira, R.; Taylor, N. M.; Mona, D.; Ringler, P.; Lauer, M. E.; Riek, R.; Britschgi, M.; Stahlberg, H. Cryo-EM structure of alpha-synuclein fibrils. *Elife* **2018**, *7*. DOI: 10.7554/eLife.36402.

(161) Schrodinger, LLC. The PyMOL Molecular Graphics System, Version 1.8. 2015.

(162) Wang, W.; Wang, X.; Gao, W.; Cui, Z.; Zhang, H.; Lu, F.; Liu, F. Ulvan inhibits alpha-synuclein fibrillation and disrupts the mature fibrils: In vitro and in vivo studies. *Int J Biol Macromol* **2022**, *211*, 580-591. DOI: 10.1016/j.ijbiomac.2022.05.045.

(163) Hsieh, C. J.; Ferrie, J. J.; Xu, K.; Lee, I.; Graham, T. J. A.; Tu, Z.; Yu, J.; Dhavale, D.; Kotzbauer, P.; Petersson, E. J.; et al. Alpha Synuclein Fibrils Contain Multiple Binding Sites for Small Molecules. *ACS Chem Neurosci* **2018**, *9* (11), 2521-2527. DOI: 10.1021/acschemneuro.8b00177.

(164) Bian, J.; Liu, Y. Q.; He, J.; Lin, X.; Qiu, C. Y.; Yu, W. B.; Shen, Y.; Zhu, Z. Y.; Ye, D. Y.; Wang, J.; et al. Discovery of styrylaniline derivatives as novel alpha-synuclein aggregates ligands. *Eur J Med Chem* **2021**, *226*, 113887. DOI: 10.1016/j.ejmech.2021.113887.

(165) Pujols, J.; Peña-Díaz, S.; Lázaro, D. F.; Peccati, F.; Pinheiro, F.; González, D.; Carija, A.; Navarro, S.; Conde-Giménez, M.; García, J.; et al. Small molecule inhibits α-synuclein aggregation, disrupts amyloid fibrils, and prevents degeneration of dopaminergic neurons. *Proc Natl Acad Sci U S A* **2018**, *115* (41), 10481-10486. DOI: 10.1073/pnas.1804198115.

(166) Laskowski, R. A.; Macarthur, M. W.; Moss, D. S.; Thornton, J. M. Procheck - a Program to Check the Stereochemical Quality of Protein Structures. *J. Appl. Crystallogr.* **1993**, *26*, 283-291. DOI: Doi 10.1107/S0021889892009944.

(167) Morris, G. M.; Huey, R.; Lindstrom, W.; Sanner, M. F.; Belew, R. K.; Goodsell, D. S.; Olson, A. J. AutoDock4 and AutoDockTools4: Automated docking with selective receptor flexibility. *J Comput Chem* **2009**, *30* (16), 2785-2791. DOI: 10.1002/jcc.21256.

(168) Friesner, R. A.; Murphy, R. B.; Repasky, M. P.; Frye, L. L.; Greenwood, J. R.; Halgren, T. A.; Sanschagrin, P. C.; Mainz, D. T. Extra precision glide: docking and scoring incorporating a model of hydrophobic enclosure for protein-ligand complexes. *J Med Chem* **2006**, *49* (21), 6177-6196. DOI: 10.1021/jm051256o.

(169) Jones, G.; Willett, P.; Glen, R. C.; Leach, A. R.; Taylor, R. Development and validation of a genetic algorithm for flexible docking. *J Mol Biol* **1997**, *267* (3), 727-748. DOI: 10.1006/jmbi.1996.0897.

(170) Bayrak, H.; Demirbas, A.; Demirbas, N.; Karaoglu, S. A. Synthesis of some new 1,2,4-triazoles starting from isonicotinic acid hydrazide and evaluation of their antimicrobial activities. *Eur J Med Chem* **2009**, *44* (11), 4362-4366. DOI: 10.1016/j.ejmech.2009.05.022.

(171) Ledeti, I. V.; Alexa, A. A.; Bercean, V. N. Structural NMR analysis of triazolic compounds derived from isonicotinic acid. Annals of West University of Timisoara, Series of Chemistry 2011; Vol. 20(1), pp 81-86.

(172) Kozakov, D.; Grove, L. E.; Hall, D. R.; Bohnuud, T.; Mottarella, S. E.; Luo, L.; Xia, B.; Beglov, D.; Vajda, S. The FTMap family of web servers for determining and characterizing ligand-binding hot spots of proteins. *Nat Protoc* **2015**, *10* (5), 733-755. DOI: 10.1038/nprot.2015.043.

(173) Halgren, T. New method for fast and accurate binding-site identification and analysis. *Chem Biol Drug Des* **2007**, *69* (2), 146-148. DOI: 10.1111/j.1747-0285.2007.00483.x.

(174) Schmidtke, P.; Le Guilloux, V.; Maupetit, J.; Tufféry, P. fpocket: online tools for protein ensemble pocket detection and tracking. *Nucleic Acids Res* **2010**, *38* (Web Server issue), W582-589. DOI: 10.1093/nar/gkq383.

(175) Le Guilloux, V.; Schmidtke, P.; Tuffery, P. Fpocket: an open source platform for ligand pocket detection. *BMC Bioinformatics* **2009**, *10*, 168. DOI: 10.1186/1471-2105-10-168.

(176) Pedretti, A.; Mazzolari, A.; Gervasoni, S.; Fumagalli, L.; Vistoli, G. The VEGA suite of programs: an versatile platform for cheminformatics and drug design projects. *Bioinformatics* **2021**, *37* (8), 1174-1175. DOI: 10.1093/bioinformatics/btaa774.

(177) Hou, T.; Wang, J.; Li, Y.; Wang, W. Assessing the performance of the MM/PBSA and MM/GBSA methods. 1. The accuracy of binding free energy calculations based on molecular dynamics simulations. *J Chem Inf Model* **2011**, *51* (1), 69-82. DOI: 10.1021/ci100275a.

La borsa di dottorato è stata cofinanziata con risorse del Programma Operativo Complementare Ricerca e Innovazione 2014-2020 (CCI 2014IT16M20P005), Fondo Sociale Europeo, Azione I.1 “Dottorati Innovativi con caratterizzazione Industriale”